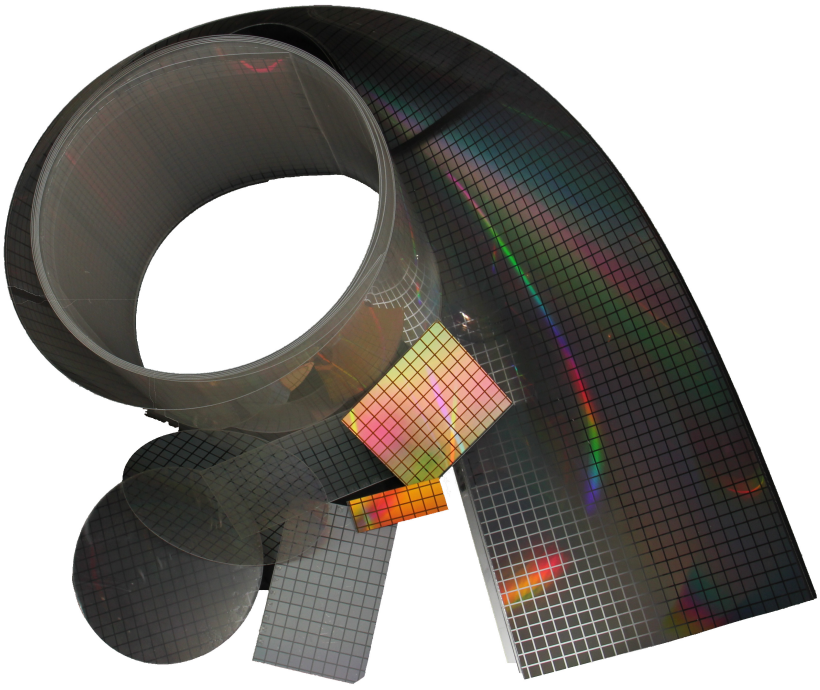

SCIENCE • TECHNOLOGY • RESEARCH HIGHLIGHTS • VISIONS

Dissertation
165

Detection of small molecules and microbial cells by surface-enhanced Raman spectroscopy using roll-to-roll produced substrates

Sanna Uusitalo

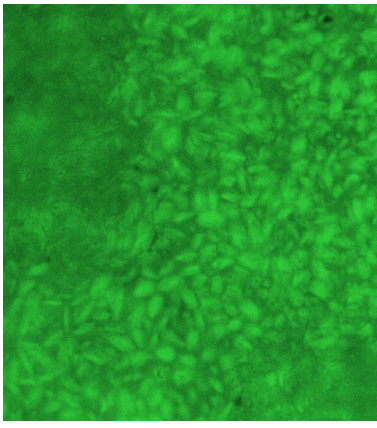

VTT SCIENCE 165

Detection of small molecules and microbial cells by surface-enhanced Raman spectroscopy using roll-to-roll produced substrates

Sanna Uusitalo

VTT Technical Research Centre of Finland Ltd

Information Technology and Electrical Engineering Doctoral Programme
Faculty of Information Technology and Electrical Engineering
University of Oulu

Thesis for the degree of Doctor of Science in Technology to be presented with due permission for public examination and criticism in Auditorium IT115, at the University of Oulu, on the 24th of November at 12 o'clock noon.

ISBN 978-951-38-8577-9 (Soft back ed.)
ISBN 978-951-38-8576-2 (URL: http://www.vttresearch.com/impact/publications)

VTT Science 165

ISSN-L 2242-119X
ISSN 2242-119X (Print)
ISSN 2242-1203 (Online)
http://urn.fi/URN:ISBN:978-951-38-8576-2

JULKAISIJA – UTGIVARE – PUBLISHER

Teknologian tutkimuskeskus VTT Oy
PL 1000 (Tekniikantie 4 A, Espoo)
02044 VTT
Puh. 020 722 111, faksi 020 722 7001

Teknologiska forskningscentralen VTT Ab
PB 1000 (Teknikvägen 4 A, Esbo)
FI-02044 VTT
Tfn +358 20 722 111, telefax +358 20 722 7001

VTT Technical Research Centre of Finland Ltd
P.O. Box 1000 (Tekniikantie 4 A, Espoo)
FI-02044 VTT, Finland
Tel. +358 20 722 111, fax +358 20 722 7001

Cover image: Noora Heinilehto

Juvenes Print, Tampere 2017

Preface

This thesis is based on research carried out at VTT Technical Research Centre of Finland Ltd during 2014–2016. The work has been supported by University of Oulu Graduate School and Infotech Oulu Doctoral Program through 2-year PhD research grant for years 2014–2015. Part of the work has been carried out in an Academy of Finland project M-SPEC (Grant No. 284907) and Tekes project FMA. Tauno Tönning foundation and Jenny and Antti Wihuri foundation have granted financial support for finalising the dissertation, and I thank both foundations for their support.

I am very grateful for my patient Professor Emeritus Risto Myllylä (University of Oulu) and my supervisors Docent Jussi Hiltunen (VTT) and Docent Matti Kinnunen (University of Oulu). Especially I would like to thank Jussi for his graceful style of correcting my errors and my misunderstandings, and the never-failing belief that we will get the job done and reach the day of dissertation. I would like to thank my follow-up group, Professor Kristiina Takkinen (VTT), Professor Jukka Hast (VTT) and Docent Alexey Popov (University of Oulu), for the discussions and the support. Professors Jiří Homola and Harri Lipsanen are greatly acknowledged for the comprehensive peer-review of the thesis manuscript. Additionally I would like to thank Professor Pentti Karioja (VTT) for the ground work and support in the research field of R2R fabrication of optical polymer structures.

I wish to thank all of my co-authors and co-workers for their contribution and expertise. The support given by Jarno Petäjä (VTT), Anna-Liisa Välimaa (Luke), Martin Kögler (University of Berlin), Ville Kontturi (NanoComp), Samuli Siitonen (Nanocomp), Yury Ryabchikov (P.N. Lebedev Physical Institute of Russian Academy of Sciences) and Arja Laitila (VTT) is especially appreciated. I am also grateful for the support shown by Dr Leena Hakalahti (VTT), Dr Jussi Paakkari (VTT), Professor Harri Kopola (VTT) and Dr Arto Maaninen (VTT).

I would like to thank all the colleagues at VTT who have given me help, advice and support during this process. Special thanks goes to Annukka Kokkonen and Marika Kurkinen, who have encouraged me in my occasional moments of despair, and rejoiced the breakthroughs with a glass of wine. I would also like to thank my friends, especially Anthi, Julia and Laura, for distracting me time to time with movies and other get-togethers.

This project co-existed with another huge project, building of our house. I wish to thank my husband Marko for carrying the main responsibility over the house project, and giving me the opportunity to divide myself between the projects. A big thanks goes also to my parents-in-law for helping out a lot and to my family for all the support. I have two amazing boys Jaro and Aleksi, who are the reason for living. I love you all, now and forever.

Oulu, October 2017

Sanna Uusitalo

Academic dissertation

Supervisors

Professor Emeritus Risto Myllylä
University of Oulu
Faculty of Information Technology and Electrical Engineering
P.O. Box 4500
90014 University of Oulu, Finland

Dr. Jussi Hiltunen
VTT Technical Research Centre of Finland Ltd
P.O. Box 1100
FI-90571 Oulu, Finland

Dr. Matti Kinnunen
University of Oulu
Faculty of Information Technology and Electrical Engineering
P.O. Box 4500
90014 University of Oulu, Finland

Reviewers

Professor Jiří Homola
Charles University
Institute of Photonics and Electronics ASCR
Chaberská 57, 182 51 Prague 8, Czech Republic

Professor Harri Lipsanen
Aalto University
Department of Electronics and Nanoengineering
PO Box 13500, FI-00076 Aalto, Finland

Opponents

Professor Jukka Lekkala
Tampere University of Technology
Faculty of Biomedical Sciences and Engineering
PL 527, 33101 Tampere, Finland

Professor Harri Lipsanen
Aalto University
Department of Electronics and Nanoengineering
PO Box 13500, FI-00076 Aalto, Finland

List of publications

This thesis is based on the following original publications, which are referred to in the text as I–IV. The publications are reproduced with kind permission from the publishers.

I Uusitalo S., Hiltunen J., Karioja P., Siitonen S., Kontturi V., Myllylä R., Kinnunen M. and Meglinski I. (2015). *Performance and flow dynamics studies of polymeric optofluidic SERS sensors*, Journal of the European Optical Society – Rapid publications, 10, DOI information: 10.2971/jeos.2015.15043.

II Uusitalo S., Kögler M., Välimaa A.-L., Popov A., Ryabchikov Y., Kontturi V., Siitonen S., Petäjä J., Virtanen T., Laitinen R., Kinnunen M., Meglinski I., Kabashin A., Bunker A., Viitala T. and Hiltunen J. (2016). *Detection of Listeria innocua on roll-to-roll produced SERS substrates with gold nanoparticles*, RSC Advances, 6(67), 62981–62989, DOI information: 10.1039/C6RA08313G.

III Uusitalo S., Kögler M., Välimaa A.-L., Petäjä J., Kontturi V., Siitonen S., Laitinen R., Kinnunen M., Viitala T. and Hiltunen J. (2017). *Stability optimization of microbial surface-enhanced Raman spectroscopy detection with immunomagnetic separation beads*. Optical Engineering, 56(3), 037102, DOI information: 10.1117/1.OE.56.3.037102.

IV Uusitalo S., Popov A., Ryabchikov Y. V., Bibikova O., Alakomi H.-L., Juvonen R., Kontturi V., Siitonen S., Kabashin A., Meglinski I., Hiltunen J. and Laitila A. (2017). *Surface-enhanced Raman spectroscopy for identification and discrimination of beverage spoilage yeasts using patterned substrates and gold nanoparticles.* Journal of Food Engineering, 212, 47–54, DOI information: 10.1016/j.jfoodeng.2017. 05.007.

Author's contributions

The author of the thesis carried out most of the experimental work concerning the SERS chip integration, SERS experiments and data analysis. The author prepared all of the manuscripts with help from co-authors.

Paper I: Performance and flow dynamics studies of polymeric optofluidic SERS sensors

The author performed SERS chip integration, SERS experiments and data analysis, and prepared the manuscript. Co-authors fabricated the SERS substrates with roll-to-roll UV-imprint replication equipment.

Paper II: Detection of *Listeria innocua* on roll-to-roll produced SERS substrates with gold nanoparticles

The author performed SERS chip integration. The author performed the SERS experiments with 785 nm excitation with help from co-authors. The author performed data analysis, and prepared the manuscript. Co-authors performed the IMS bead separation, bacterial cultivation, nanoparticle synthesis and reference measurements with time-gated Raman. Co-authors fabricated the SERS substrates with roll-to-roll UV-imprint replication equipment.

Paper III: Stability optimization of microbial surface-enhanced Raman spectroscopy detection with immunomagnetic separation beads

The author performed SERS chip integration, SERS experiments, data analysis, and prepared the manuscript. Co-authors performed the IMS bead separation, bacterial cultivation and nanoparticle synthesis. Co-authors fabricated the SERS substrates with roll-to-roll UV-imprint replication equipment.

Paper IV: Surface enhanced Raman spectroscopy for identification and discrimination of the beverage spoilage yeasts with patterned substrates and gold nanoparticles

The author performed SERS chip integration, the SERS experiments, data analysis, and prepared the manuscript. Co-authors performed the yeast cultivations and gold-silicon nanoparticle fabrication. Co-authors fabricated the SERS substrates with roll-to-roll UV-imprint replication equipment.

Contents

List of abbreviations

Ag	silver
AgNP	silver nanoparticle
Al	aluminium
Au	gold
AuNP	gold nanoparticle
AuSi NC	gold-silicon nanocomposite
Cu	copper
CW	continuous wave
C-C	carbon-carbon
-CH	carbon-hydrogen group
$-CH_2$	carbon-dihydrogen group
$-CH_3$	carbon-trihydrogen group
C-N	carbon-nitrogen
C-S	carbon-sulphur
CE	chemical enhancement
CCD	charge-coupled device
CFU	colony-forming units
DI	de-ionized
DNA	deoxyribonucleic acid
CTD	charge transfer device
EBL	electron beam lithography
EM	electromagnetic
H_2O	water
HOMO	highest occupied molecular orbital
IMS	immuno-magnetic separation
IUPAC	International union of pure and applied chemistry
LEE	*Listeria* express enrichment

LSPR	localised surface plasmon resonance
LUMO	lowest unoccupied molecular orbital
NAG	N-acetyl D-glucose amine
-NH	nitrogen-hydrogen group
NIL	nanoimprint lithography
NIR	near-infra-red
NP	nanoparticle
PBS	phosphate-buffered saline
PCR	polymerase chain reaction
PDMS	polydimethylsiloxane
PFU	particle-forming units
PMMA	poly(methyl methacrylate)
PVP	polyvinylpyrrolidone
R2R	roll-to-roll
R6G	rhodamine 6G
SEM	scanning electron microscopy
SERS	surface-enhanced Raman scattering
Si	silicon
SPR	surface plasmon resonance
TEM	transmission electron microscopy
UV	ultra-violet

List of symbols

E	electric field strength
E_0	vibrational amplitude
ΔE	change of energy
h	Planck constant
ν_0	frequency of incident light
ν_k	frequency after molecular vibration
ν_m	change of frequency caused by molecule vibration
$\tilde{\nu}$	wavenumber
$\Delta\tilde{\nu}$	change of wavenumber
λ	wavelength
c	velocity of light
t	time
P	electric dipole moment
α	polarizability
α_0	polarizability at equilibrium
q	nuclear displacement
q_0	amplitude of vibration
$(\partial\alpha/\partial q)_0$	rate of change of polarizability
ω_p	plasma frequency
n	electron density
m_{eff}	effective mass
e	charge of an electron
ε_0	permittivity of free space
$\vec{E}(\nu_0)$	oscillating electromagnetic field of light
$\overrightarrow{E_{tot}}(\nu_0)$	total electric field
$\overrightarrow{E_{ind}}(\nu_0)$	induced electric field component
$F_E(\nu_0)$	Field enhancement

F_{SERS} *(0)*	enhancement factor of molecules in contact with metal
g_0	variable for dielectric properties of metal
$\widetilde{\varepsilon_r}(v_0)$	dielectric constant
n_{solv}	refractive index of surrounding medium
$\vec{E}_{Ra,ind}$	secondary electric field component
a_0	colloid radius
d	distance from surface of the metal

1. Introduction

1.1 Motivation

Optical biosensing is a diverse and evolving research field aiming towards simplified and high sensitivity diagnostic tools for the detection of biological and chemical analytes in environmental monitoring, medical analysis, food safety and national security. Often the methods used for analyte sensing require complex procedures, lab scale equipment and trained personnel. Label-free sensing is attracting interest since it does not require additional molecules and labelling steps, which complicate the detection. There are several technologies available for label-free optical sensing, including interferometry[1–6], resonant-cavity sensing[7–9], photonic crystal detection[6,10–12], surface plasmon resonance (SPR)[13–15] and surface-enhanced Raman scattering (SERS)[6,16–18]. SERS is a special type of Raman spectroscopy, in which irregular or patterned metal substrates or metal nanocolloids of different shapes and sizes can be used for signal enhancement. Enhancement can be achieved through the use of noble metals, for example gold or silver, to trigger localised surface plasmons. When the localised surface plasmons resonate with the incident light, the scattered Raman signal grows in intensity. SERS can have high detection sensitivity, in some cases even in the range of only a few molecules.[19–21] Using SERS, biological analytes can be identified through the spectrum of scattered light, in which the intensity of the signal as a function of Raman shifted wavelength reveals information concerning the composition of the molecules forming the analyte. Thus the chemical structure of the analyte provides a specific fingerprint spectrum which can be used in identification of the analyte, whether it is a small molecule or a biological cell containing different organic molecules.

SERS has been widely studied for the past 30 years. The number of publications has increased exponentially since 2000.[16,22] Although many methods have been developed for the fabrication of different SERS substrates, SERS detection has not yet become a common analysis tool outside its use in research laboratories. There are several reasons behind the slow adoption of SERS into common use in central laboratories and in the field. One important aspect, especially with bioanalytes, is the requirement for disposable analysis chips. Multi-use chips give rise to a higher risk of cross contamination and false positive results, and the chips require thorough cleaning steps after use. The conventional ways of fabricating structured SERS substrates [23–34], such as spin-coating, dip coating, chemical vapour deposition, electrochemical synthesis, electron beam lithography and etching, are not ideal for manufacturing single use chips in terms of throughput volume or cost. The fabricated sensor areas are often small and the fabrication methods are difficult to transfer to the high volume production required for truly disposable sensor chips. The focus of the SERS substrate development has thus shifted towards the study of different methods for low cost fabrication, such as soft lithography[35].

The objective of this study was to develop a simplified and affordable method for label-free detection of biological analytes using disposable SERS substrates.

The suitability of the method for rhodamine 6G (R6G) and microbial cell detection was studied. Our approach is based on roll-to-roll (R2R) fabrication of structured SERS substrates on polymer webs in large scale by applying soft lithography in which patterns are imprinted and cured with ultra-violet (UV) exposure.[36] A hybrid detection method was developed, combining the use of these structured SERS substrates and gold nanoparticles for additional SERS signal enhancement.

1.2 Theory of Raman spectroscopy

1.2.1 Inelastic scattering of photons

Raman spectroscopy is based on inelastic scattering of photons from the subject of interest, which is a significantly weaker phenomenon than elastic Rayleigh scattering of light[37]. In Raman scattering, a fraction of incident photons scatters in such a way that the energy of the scattered photons differs from that of the incident photons. The energy difference is equal to the transition energy between the two vibrational states of the molecule which scatters the photon, as can be seen in Figure 1. This phenomenon was first discovered by the Indian scientist C. V. Raman in 1928 and it became known as the Raman effect.[38] When the photons scatter inelastically, they experience a frequency shift. When the frequency of the scattered light is lower than the incident frequency of the photon, the molecule remains in a higher vibrational excited state. This state is called Stokes scattering. Anti-Stokes scattering refers to an opposite situation in which the frequency of the scattered light increases and the molecule drops into a lower vibrational state. Since in ambient temperature the molecules mainly exist in ground state, from which they can be lifted into higher states, the Stokes scattering is more probable than anti-Stokes scattering. Thus the applications in Raman spectroscopy are mainly focused on Stokes scattering.[38]

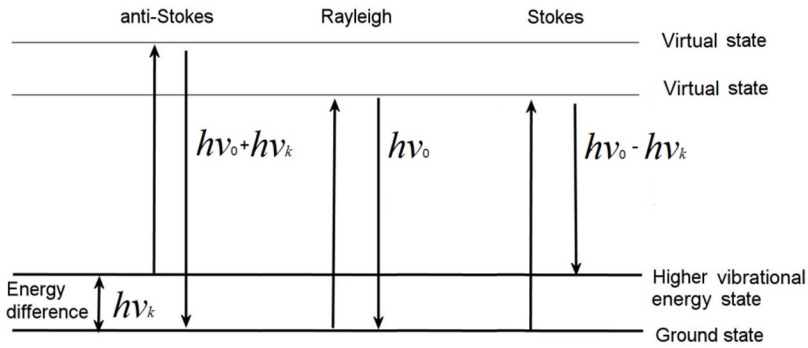

Figure 1. A diagram showing the energy states of elastic Rayleigh scattering and inelastic anti-Stokes and Stokes Raman scattering, where h is the Planck constant, v_0 is the frequency of the incident light and v_k is the frequency difference after molecular vibration.

When a molecule interacts with an electromagnetic field of a photon as depicted in Figure 1, the energy transfer must satisfy Bohr's frequency condition, in which the energy difference ΔE of two quantized states is[37]

$$\Delta E = hv_k = h\frac{c}{\lambda_k} = hc\tilde{v}, \qquad (1)$$

in which c is the velocity of light. Thus the wavenumber $\tilde{v}$ is proportional to the energy difference ΔE divided by the constant hc:

$$\tilde{v} = \frac{1}{hc}\Delta E. \qquad (2)$$

The relation of wavenumber to the transition energy has been utilised in vibrational spectroscopy in which the detected vibrational lines are depicted as a function of change of the wavenumber $\Delta\tilde{v}$ instead of as a function of change in frequency. The intensities of the lines are proportional to the likelihood of the transitions caused by photons. The relationship between the vibrational frequencies and the molecular structure leads to distinguishable Raman spectra for each molecule.

1.2.2 Polarizability and dipole moments in molecules

A molecule is a three-dimensional structure with chemical bonds and a varying electron cloud surrounding the molecule. The bonds of the molecule allow it to have vibrational states occurring from stretching and bending of bonds. These molecular vibrations cause photons to scatter or absorb depending on the nature of the vibration. If a bond vibration changes the net dipole moment of the molecule, the molecule absorbs energy at infrared wavelengths. A molecular dipole exists when the molecule consists of atoms having non-uniform positive and negative charges

giving the molecule a local positive and a negative pole. These polar molecules can absorb photons and they experience a net change on the dipole moment

$$\partial\mu/\partial q \text{ , where} \quad (3)$$

$\partial\mu$ is the change in net dipole moment and ∂q is the change in nuclear displacement due to bond vibration.

Raman scattering on the other hand is excited when the molecule has vibrational bonds, but the dipole moment vectors of the vibration will cancel each other out and the net dipole moment change will be zero. Thus it undergoes a polarizability change without an effect on the net dipole:

$$\partial\alpha/\partial q, \text{ where} \quad (4)$$

$\partial\alpha$ is the change in polarizability and ∂q is the change in nuclear displacement due to bond vibration.

The origin of Raman scattering can be explained by classical electromagnetic theory. A simple way to observe the relationship between electric dipole moment, the change in polarizability and the Raman scattering is to consider the photon-induced electric dipole moment in a diatomic molecule. The electric field strength *E* of the incident photons as a function of time is

$$E = E_0 \cos(2\pi v_0 t), \quad (5)$$

where E_0 is the vibrational amplitude, v_0 is the frequency of the incident photon and t is time. For a simple situation with a diatomic molecule the incident light induces an electric dipole moment P

$$P = \alpha E = \alpha E_0 \cos(2\pi v_0 t), \quad (6)$$

in which α is a proportionality constant called polarizability. If the molecule vibrates with frequency v_m, the nuclear displacement q is expressed as

$$q = q_0 \cos(2\pi v_m t), \quad (7)$$

where q_0 is the amplitude of vibration. If the vibration has a low amplitude, the polarizability α is a linear function of q and can be written as

$$\alpha = \alpha_0 + \left(\frac{\partial\alpha}{\partial q}\right)_0 q + \cdots, \quad (8)$$

where α_0 is the polarizability at equilibrium and $\left(\partial\alpha/\partial q\right)_0$ is the rate of change of polarizability evaluated at equilibrium.

Combining the equations (4) to (6) we can express the electric dipole moment P as

$$P = \alpha E_0 \cos(2\pi v_0 t) = \alpha_0 E_0 \cos(2\pi v_0 t) + \left(\frac{\partial \alpha}{\partial q}\right)_0 q E_0 \cos(2\pi v_0 t)$$

$$= \alpha_0 E_0 \cos(2\pi v_0 t) + \left(\frac{\partial \alpha}{\partial q}\right)_0 q_0 E_0 \cos(2\pi v_0 t) \cos(2\pi v_m t)$$

$$= \alpha_0 E_0 \cos(2\pi v_0 t) + \tfrac{1}{2}\left(\frac{\partial \alpha}{\partial q}\right)_0 q_0 E_0 [\cos(2\pi(v_0 + v_m)t) + \cos(2\pi(v_0 - v_m)t)].^{37} \quad (9)$$

The first term defines Rayleigh scattering which is radiated with frequency v_0; the second and third terms define anti-Stokes $(v_0 + v_m)$ and Stokes $(v_0 - v_m)$ Raman scattering, respectively. Similarly, it is possible to deduce the electric dipole moment *P* for more complex polyatomic molecules. However, the calculation will be long and complex, as all the nuclei of the polyatomic molecule perform their own harmonic oscillations, which need to be expressed as a superposition of independent vibrations. From the relationship deduced for the diatomic molecule, we can see that if the rate of change of polarizability is zero $\left(\partial\alpha/\partial q\right)$ = 0, the vibration does not produce Raman scattering and the molecule is not Raman active. Thus in order for a molecule to be Raman active, its polarizability must change during the vibration.

The change in polarizability occurs as the molecule undergoes a distortion in which the positively charged nuclei are drawn towards the negative pole and the electrons are drawn towards the positive pole.[37] This is easily understood when considering triatomic molecules such as carbon disulphide CS_2 depicted in Figure 2. A symmetrical stretch changes the polarization of the molecule and causes photons to Raman scatter, exciting only weak or non-existent infrared absorption. When the molecule experiences an asymmetric or a bending mode, there is a dipole change and the molecule experiences infrared absorption with weak or non-existent Raman scattering.[37,39]

Vibration	Symmetric	Asymmetric	Bending
	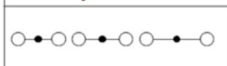	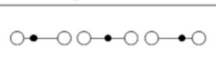	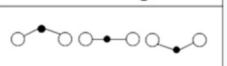
Dipole moment $\partial\mu/\partial q$	± ± ±	+ − ± − +	+ − ± − +
	$\partial\mu/\partial q = 0$	$\partial\mu/\partial q \neq 0$	$\partial\mu/\partial q \neq 0$
Polarizability $\left(\partial\alpha/\partial q\right)_0$			
	$\left(\partial\alpha/\partial q\right)_0 \neq 0$	$\left(\partial\alpha/\partial q\right)_0 = 0$	$\left(\partial\alpha/\partial q\right)_0 = 0$
Excited state	Raman scattering	Infra-red absorption	Infra-red absorption

Figure 2. Dipole moment and polarizability change in carbon disulphide CS_2, along with the effect on the infra-red and Raman detection.[39,40]

The strength of bonds between atoms of the molecule and the weight of the atoms have an effect on the required transition energy: the stronger the bonds the higher the frequency of the vibrational line, and the heavier the atoms the lower the frequency. Thus strong bonds and light atoms will give higher frequencies of vibration and heavy atoms and weak bonds will give lower ones.[39]

1.3 Theory of Surface-enhanced Raman spectroscopy (SERS)

1.3.1 Origin of the SERS enhancement

Raman scattering is an inherently weak phenomenon and it requires a large sample volume for reliable analyte recognition. Such a volume can be difficult to achieve in many fields of diagnostic sensing. Forty years ago it was accidentally discovered that the Raman process can be greatly enhanced by a phenomenon in which a molecule is adsorbed onto the surface of a patterned metal layer or metal nanoparticle.[41,42] Enhancement is due to both long range electromagnetic (EM) enhancement and short range chemical enhancement (CE). The main origin of the SERS enhancement is believed to come from EM enhancement. The mechanism is based on the interaction of light with surface plasmons of the metal and it can yield enhancements between factors of 10^4 and 10^8. The plasmon resonance excitation occurs when incident light interacts with free conduction electrons of metal. The CE mechanism on the other hand is caused by the enhancement in effective polarizability due to phenomena such as an electronic resonance process, in which a charge is transferred between the lowest unoccupied molecular orbital (LUMO), the Fermi level of the metal substrate and the highest occupied molecular orbital (HOMO) of the molecule as shown in Figure 3. The charge transfer caused by the incident laser excitation is only possible if the difference between the Fermi level of the metal and the HOMO and LUMO energy levels of the molecule are matched by the laser energy.

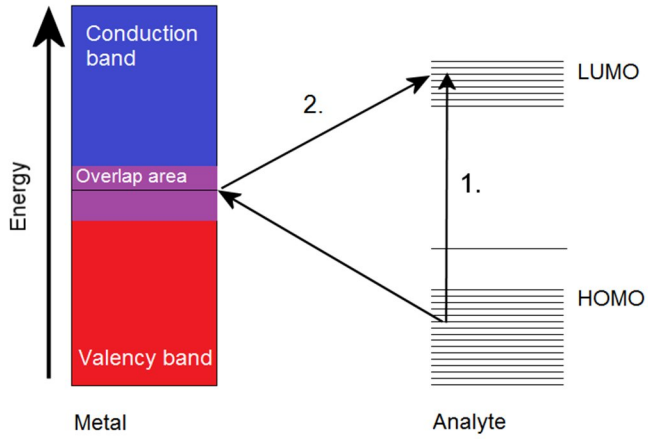

Figure 3. A depiction of the principle of the charge transfer in chemical enhancement. The laser energy can either be in direct resonance with the energy needed for electron transition with metal-analyte complex (1.) or benefit from indirect coupling (2.) via an electron transition through the metal.[22]

The CE enhancement can affect the Raman peak intensity and it can also shift peak positions, but the enhancement factor is substantially smaller, 10-100, compared to the EM enhancement. Although the contribution of CE effect to SERS is smaller, it is of interest as it could enable surface plasmon enhanced photochemical reactions.[17,43–46]

1.3.2 Electromagnetic field enhancement of the surface-enhanced Raman

The electromagnetic enhancement occurs when electrons of metal encounter a time-dependent force caused by the changing electromagnetic field of the light. This results in an oscillation of electrons. The oscillating conduction electrons have a characteristic frequency called plasma frequency[17]

$$\omega_p = \sqrt{\frac{ne^2}{m_{eff}\varepsilon_0}}, \qquad (10)$$

in which n is the density of the electrons, m_{eff} is the effective mass denoting the ease of motion of the electrons in response to the electromagnetic field, e is the charge of an electron and ε_0 is the permittivity of free space. The electron motion has a resonance frequency which changes in response to the driving force of the incident field. If the frequency of incident light is above the plasma frequency, usually in the ultraviolet range, the electrons will not oscillate. The light is either transmitted or absorbed. If the frequency of light is below the plasma frequency, electrons oscillate and a strong light reflection is caused. The dielectric constant of metal dictates

whether the metal electrons are able to oscillate at the frequency of incident light. If the shape of the metal is restricted to small colloid forms or thin metal layers, the oscillations exist at the metal surface and create resonating charge waves. The excitation causes a collective oscillation of conduction electrons in the metal.[17]

The size of the metal particle has an effect on the scattering efficiency of the particle. If the particle is small, less than 15 nm in diameter, the oscillating energy is quickly converted into heat through electron-electron surface scattering. Larger particles have a reduced electron-electron scattering and the energy of the plasmons is re-radiated. Thus the larger particles scatter the light more effectively and have a stronger scattering cross-section. Because metal nanostructures with LSPRs have local fields, bringing the structures into the near vicinity of each other causes the local fields to overlap. This can lead to a growth of the total field, with an additional enhancement factor of 10 to 10^4 when the particles aggregate. The critical gap distance for the EM coupling is approximately the diameter of a single particle.[17,45] Additional field enhancement increases SERS detection sensitivity, but it can make the SERS enhancement unpredictable.

Classical electromagnetic theory can be used to explain the field enhancement of the surface-enhanced Raman. When spherical colloids have a size much smaller than the wavelength of incident light, the oscillating electromagnetic field $\vec{E}_0(v_0)$ of light induces an electric dipole moment in the colloid and excites surface plasmons on the surface of the colloid. This leads to an additional electric field component $\vec{E}_{ind}(v_0)$ in the near field of the colloid, which increases both the excitation and emission rates of the Raman process due to the increase in the local-mode density of the field.[38,44] The principle of the enhancement is expressed in Figure 4.

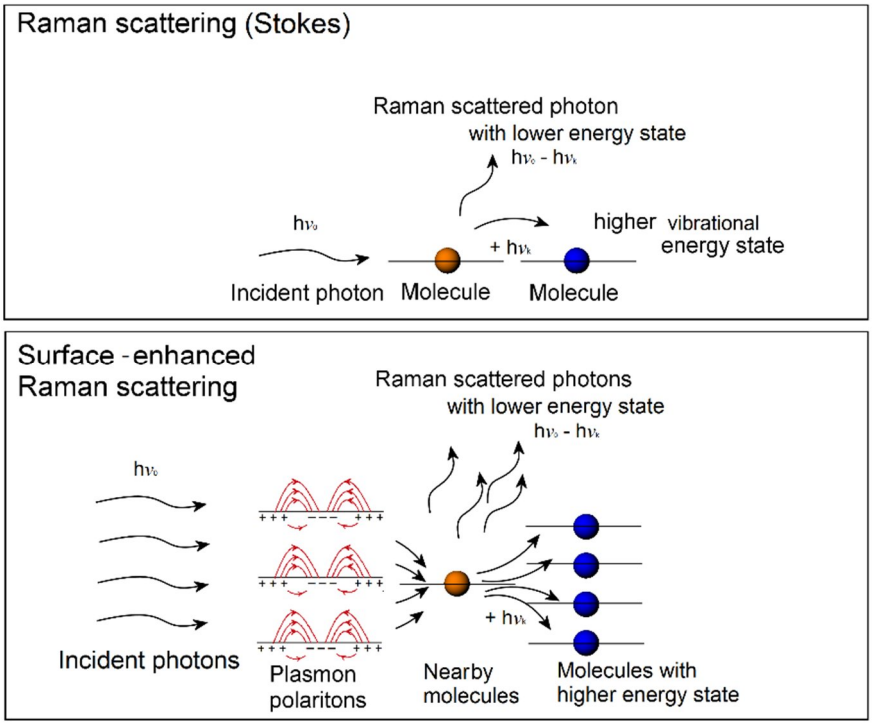

Figure 4. Schematic of Raman excitation and SERS enhancement through quantum states of photons and plasmon polaritons.[44]

The total electric field with frequency v_0 can be expressed as:[38]

$$\vec{E}_{tot}(v_0) = \vec{E}_0(v_0) + \vec{E}_{ind}(v_0). \quad (11)$$

Thus the enhancement of the local field can be expressed as:

$$F_{Loc}(v_0) = \frac{|\vec{E}_0(v_0)+\vec{E}_{ind}(v_0)|}{|\vec{E}_0(v_0)|}, \quad (12)$$

The molecules located close to the spherical metal colloids are excited by the total electric field $\vec{E}_{tot}(v_0)$. In the case in which the resonance condition applies for the incident light with frequency v_0, the condition also holds true for the re-radiated light with shifted frequencies $v_0 \pm v_k$. The electromagnetic field of the re-radiated light induces an additional secondary field component $\vec{E}_{Rad,ind}(v_0 \pm v_k)$ in the metal colloid, adding to the total electromagnetic field.

Thus the total SERS enhancement consists of initial local field enhancement and radiation enhancement from re-emission, and the SERS enhancement factor for a single molecule can be expressed as

$$SMEF \approx F_{Loc}(v_0) \cdot F_{Rad}(v_0 \pm v_k)\,, \qquad (13)$$

where F_{Loc} is local field enhancement and F_{Rad} is directional radiation enhancement. It is possible to compute F_{Loc} by solving the electromagnetic problem, but estimating F_{Rad} is challenging as the electromagnetic problem would need to be solved with dipolar emission, which leads to challenges with regard to numerical and theoretical solving. However, it is possible to approximate the SERS enhancement with an assumption of

$$F_{Loc}(v_0) \approx F_{Rad}(v_0 \pm v_k), \qquad (14)$$

because both local field and radiation enhancement have the same physical origin. The resonances are qualitatively similar for both mechanisms, although they might have differences in the coupling.[22] The intensity of the local field is proportional to the square of electromagnetic field amplitude[22,47]:

$$LFI \propto |F|^2. \qquad (15)$$

Thus the SERS enhancement of the Raman intensity can be expressed as:

$$LFI_{SERS}(v_0 \pm v_k) = |F_{Loc}|^2 \cdot |F_{Rad}|^2 \approx |F_{Loc}|^4 \quad (16)$$

In this situation a field enhancement F_{Loc} with a factor of 10 results in intensity growth of the surface-enhanced Raman scattering with a factor of 10^4. This approximation is justifiable for particles which are clearly smaller than the wavelength and thus the shape and size do not affect the end result. With larger particles, the enhancement depends on both shape and size and, especially with large spherical and ellipsoidal particles, causes the maximum enhancement wavelength to red-shift. This is also the case with aggregated colloids.[38]

1.3.3 Plasmonic field decay

SERS does not require the molecules to have direct contact with metal, but the plasmonic field decays with growing distance between the molecule and the metal. For spherical colloids the decrease can be calculated from[38]

$$F_{SERS}(d) = F_{SERS}(0) \cdot \left(\frac{a_0}{a_0+d}\right)^2, \qquad (17)$$

where $F_{SERS(0)}$ is the enhancement factor of molecules in contact with metal, a_0 is the colloid radius and d is the distance from the surface of the metal. With biological molecules, the distance dependence can be important. This holds true especially with silver (Ag) colloids, which are toxic to biological cells. Ag colloids need a biocompatible coating in order to protect the biological analytes from the oxidising

effect of the Ag molecules. This increases the distance between the analyte and the metal. If the coating thickness is less than 5nm, the enhancement is still strong enough for SERS detection. A biocompatible coating or an antibody capture layer on top of the SERS structure also prohibits use of the chemical SERS effect, as the analytes are not in direct contact with the metal surface. Therefore CE may have only limited importance in SERS detection of biological analytes.[38]

2. SERS substrates and colloids in microbial cell detection

2.1 SERS substrates and colloids

Nanoparticles have been widely studied for several application areas, as they exhibit interesting physical and chemical properties which differ from those of bulk material made with the same composition.[48] In SERS the used metal and the composition, size and shape of the particles all have an effect on the field enhancement factor and on the resonance excitation wavelength. Ag, Au and copper (Cu) particles have their resonance excitation in the visible and near infra-red wavelength area, which is convenient for use. The majority of studies use Ag and Au particles as enhancers. Other metals such as aluminium (Al) have also been studied with SERS, but they require resonant excitation in the UV range.[49] Novel materials such as semiconductors, quantum dots and graphene have also been investigated as SERS enhancers, but they involve purely chemical enhancement without an increase in EM field and thus they rarely achieve high enhancement factors[50–54]. The shape of the colloids can vary from spherical[55–61], ellipsoidal[62], rods and wires[62–65], triangles and pyramids[66,67], cubes[68,69] and stars[70–72] to nanocrystals[21] and nanoshells[73,74]. Some of the typical nanoparticle shapes are presented in Figure 5.

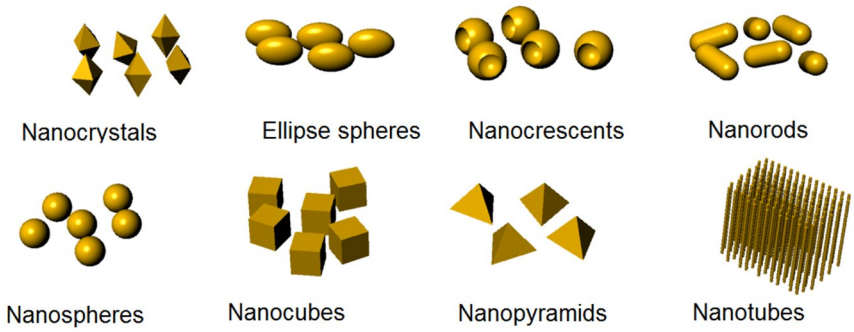

Figure 5. A depiction of different nanoparticles shapes used as SERS enhancers.

The optimal plasmon resonance frequencies can be shifted by the shape and size of the particles.[75] Larger particles, especially with elliptical shape, experience a red-shift and have their biggest enhancement factors at near infra-red excitation wavelengths. It is widely accepted that single molecule detection by SERS requires either an aggregation of nanocolloids which create hot spot areas with intense electromagnetic field,[20,61] or formation of fractal structures on planar surfaces[76]. The molecules in the studies are often highly Raman active, such as dyes, and they need to be in the hot spots where they experience very high enhancement factors

around 10^{11}. Although aggregation of colloids offers sensitive detection, it has both repeatability problems and practical issues, because the aggregation demands for nanoparticle synthesis and incubation steps. The highest field enhancements occur in the gaps between colloids, and preparing substrates with colloid cover before applying the sample may prohibit the entrance of the molecules into the hot spot pockets.[77,78] Thus the aggregation requires incubation of samples with the colloids before the detection. In addition, many larger biological analytes such as whole cells may not fit at all in such a pocket, as the optimal pocket size is under 10 nm.[79] With the fractal surfaces, Raman intensity distributions are inhomogeneous and ''hypersensitive'' to the polarization and wavelength of excitation light.[43,80] The poor reproducibility of the hotspots in randomly aggregated colloids and fractal structure formations is a major problem, as it makes the quantification of SERS more difficult.[78]

The development of different planar SERS substrates attempts to reduce the repeatability issues of the colloids through periodicity of the nanostructures on top of the substrates. The control over the pattern geometry, a repeatable enhancement factor and ease of use make planar substrates very attractive. The substrates have a varying degree of plasmon coupling, which depends strongly on the shape and size of the nanostructures. The control over nanostructure geometry makes it possible to model the effect of the shape and size of the structures on the plasmon resonance frequency and enhancement factor, and thus quantify the SERS response in the design phase.[78] Common patterning methods include addition of nanocolloids to the surface[33,34,81–84], electron beam lithography (EBL)[29,30], conventional lithographic patterning[85–87], nano-lithographic patterning such as nanosphere lithography and UV- or heat cured nanoimprinting[23,26,88], fractal or metal island thin film growth[24,27] and self alignment[28,34]. Some of the common SERS substrates are presented in Figure 6.

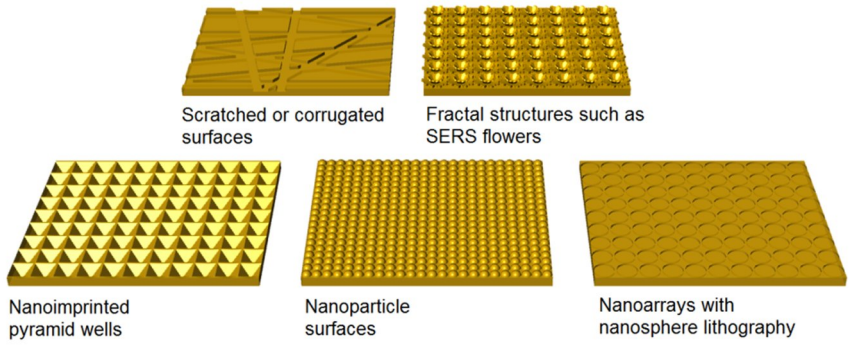

Figure 6. A schematic of the common SERS substrates.

The substrate type can have a strong effect on the SERS enhancement ability of the patterned surface. In general, the SERS enhancement varies between factors of 10^5 and 10^9. The enhancement factors for different substrate types are listed in

Table 1. The SERS substrate with inverted pyramid pattern applied in this research has been shown to reach an SERS enhancement factor of 10^7 with benzenethiol as an analyte.[36]

Table 1. Different SERS substrates and their SERS enhancement factors.

Substrate type	Analyte	Wavelength	SERS EF	Reference
Ag coated EBL patterned PMMA on quartz	R6G	488 nm	10^5	[30]
Au Nanoparticle Aggregate substrate	R6G	785 nm	10^7	[82]
Au Nanosphere lithography patterned substrate	4,4'-bipyridine	785 nm	10^5 - 10^9	[23],[88]
Au coated inverted pyramid pattern by UV-nanoimprint lithography	Benzenethiol	785 nm	10^7	[36]
Au coated EBL patterned inverted pyramid pattern	Benzenethiol	785 nm	10^9	[36]

Low cost single-use SERS sensors are required for mass fabrication of the structured SERS surfaces. Thus it is necessary to consider the applicability of the presented methods for industrial high volume production. The high end fabrication processes such as EBL produce highly ordered SERS substrates with exceptional control over periodic nanoscale SERS arrays with precise shape.[31,32,35,36] However these methods are not compatible with the production of large area sensor surfaces due to high cost and slow and complex fabrication processes. Scratching or corrugating planar metal surfaces can be feasible with continuous production, but the surfaces are random and thus the SERS detection faces challenges with acquiring repeatable signal levels. Additionally, the gold layer undergoing the scratch or corrugation process must be thick in order to avoid exposing the underlying web material. Especially polymer and paper web materials are active Raman scatterers. If exposed, they can create strong background disturbance in SERS detection. Thick gold layers, on the other hand, increase the expense of the production. There are fabrication methods applying SERS active nanoparticle coatings in large scale by dispensing nanoparticle inks on polymer or paper webs. However, these surfaces encounter challenges similar to those faced by corrugated surfaces, due to the randomly positioned and aggregated nanoparticles and possible disturbance from the underlying web. An alternative method for fabrication is UV nanoimprinting. UV nano-imprinting is a soft lithography method which produces ordered nanostructures, but unlike conventional lithography it is robust and affordable. The method is adaptable to rapid and cost-effective fabrication with high yields. It is easy to perform, requires low-cost equipment and can provide high-resolution nano-scale features down to sub-10 nm. The lithography is performed by pressing a mould onto a UV-sensitive coating with simultaneous UV light curing. The process takes place at room temperature and does not require high pressure

during the imprinting process. The surface is made SERS active by covering the entire area with a thin metal coating by evaporation. Thus the surface does not encounter SERS disturbance from the carrier web materials.

2.2 Detection of R6G molecules and microbial cells

The success of SERS detection of sample analytes depends on several factors. The result will be affected by whether or not the analyte is a strong or weak Raman scatterer with the used excitation wavelength[89]. Another affecting factor, especially when using colloids as a SERS enhancer, is the charge of the analyte[22]. Electrostatic repulsion can block the adsorption between a nanoparticle and a molecule in a case in which the molecule and the nanoparticle are similarly charged. This can lead to weak SERS enhancement. On the other hand if the colloids and the molecules are oppositely charged, a strong adsorption can enhance the SERS excitation.[22] When using a SERS substrate, the size of the analyte can affect the recorded signal strength. As depicted in Figure 7 the analyte size and pyramid well diameter affect how the plasmonic structures extend around the analyte. This has an effect on the enhancement level. Molecular analytes, with a diameter around 1 nm – 100 nm, are small enough to easily fit inside the pyramid wells, experiencing a three dimensional plasmon coupling from the surrounding structure. In the case of microbial cells, e.g. bacteria, with a diameter around 1µm, can only partly enter the wells and yeast cells, of diameter around 4-6 µm, experience only the plasmon coupling generated by the top of the well structures. This also has the consequence that only part of the cell surface area will be detected by the substrate. The majority of studies of biological cell detection using SERS have been conducted with nanoparticles which can surround the cells from all directions and thus generate a stronger SERS excitation.

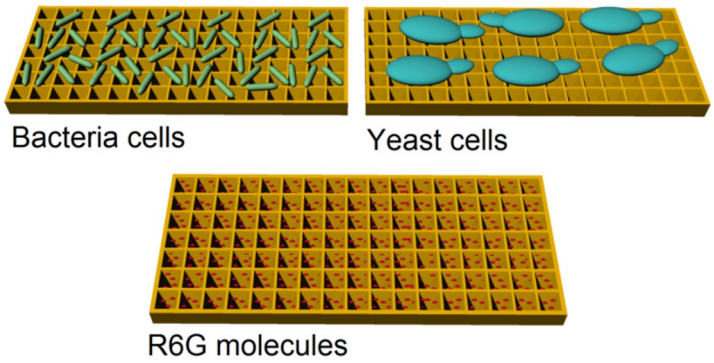

Figure 7. The difference between the alignment of the molecules and biological cells on the pyramid wells of the SERS substrate.

The interest in using SERS detection with biological cells is due to several factors. SERS is label-free, requires short detection times, can be quite sensitive and is not disturbed by the water content of the cells. The conventional methods for detecting microbial cells, i.e. culturing, counting methods and serological classification, are very reliable, but they are also laborious and time consuming. Other methods developed for faster detection, such as polymerase chain reaction (PCR) and immunological identification, typically still require 48 hours to complete the analysis.[90–92] The first detection of whole bacterial cells with SERS was conducted with incubated silver nanoparticles and *Escherichia coli* cells in 1998.[93] Since then several different bacterial species, strains and spores have been identified by SERS.[94–97] Most studies have used Au or Ag colloids as SERS enhancers. The particles are commonly attached either on the outer cell wall of the bacteria by external coating or adsoption,[98–101] or inside the bacterial cell by in-situ synthesis[93,102]. Typically the bacteria are measured by averaging over a larger volume of bacteria, achieving detection limits such as 10^3 CFU/ml to 10^5 CFU/ml[101,103], but there are also studies using optical tweezers[104] or confocal microscopy which have claimed the detection of single cells or less than 10 cells [105–108]. In addition to bacterial cells, SERS detection has also been applied for other biological cells such as yeast cells, fungi, mammalian cells and tissues[109–113]. One subject of interest in microbial detection by SERS is food and beverage quality control. The presence of only a few cells of specific bacteria or spoilage yeast at any stage of the manufacturing process may result in quality defects that can be dangerous to the consumer or spoil the taste of the products[92,114,115]. Despite many advances in controlling microbiological risks in food and beverage production, the global nature of modern trade, the use of new raw materials, novel processing technologies and the growing demand for minimally processed fresh-like products all create new challenges for manufacturers to ensure product safety and stability.

Thus, there is an interest to develop new methods such as SERS detection for the effective control and detection of harmful microbes.

Silver is the commonly used metal in SERS detection of microbes,[94–96] due to the high field enhancement of silver colloids. Especially when in aqueous solutions, silver releases toxic silver ions which can damage the cells under investigation. The rapid oxidation of the silver diminishes the field enhancement factor of the used AgNPs or the Ag substrates.[116] This can lead to poor repeatability of the detection and prohibit storing the silver SERS enhancers for longer time periods. Using gold is preferable for microbe detection in real applications, as it is biocompatible and has less issues with material stability.[117,118] There is no need for a polymer capping to protect the microbial cells, and it can easily be modified with thiol groups. In the case of biological cell detection, gold has one more benefit as it can be excited at NIR wavelengths. This reduces the auto-fluorescence issues generated by the microbes and reduces thermal damage to the cells through lower absorption when compared to the visible wavelengths.

3. Materials and methods

In the work described in this thesis, polymer microfluidic circuits (PAPER I) and sample wells (PAPER II–PAPER IV) were integrated on SERS substrates in order to bring the sample analytes to the SERS detection areas. Immunomagnetic separation beads were used for concentration of the bacterial cells (PAPER II–III). The details of the Raman spectroscopy, R2R fabrication of SERS substrates, characterisation of gold nanoparticles and integration of microfluidic circuits and hydrophobic sample wells are described in this section.

3.1 Raman instruments coupled with a microscope

In Raman spectroscopy the spectra can be recorded from samples having different physical states such as solid, liquid or vapour state[119]. The samples can be bulk, microscopic or molecule layers. Water can be used as the sample solvent as it is ideal due to the weak Raman scattering cross section of water molecules. The spectral recording of Raman scattering is based on laser excitation of the sample with monochromatic light and detection of the back scattered light with detectors such as charge-coupled device (CCD)[119]. Generally, Raman scattering can be recorded over a range of 10–4000 cm^{-1}, but with organic molecules the Raman active vibrations occur after 400 cm^{-1}. Filtering is used to isolate a single laser beam and to separate the weak Raman lines from high intensity Rayleigh scattering.[120]

In these experiments, the SERS spectral recording was made using Raman instruments (BaySpec Nomadic (San Jose, USA) and an in-house built Raman detector) with 785 nm wavelength continuous wave diode lasers coupled with an optical microscope (Olympus BX-51). The samples were optically focused to the surface of the SERS substrate patterns, or to the microbial cells on top of SERS substrates. The used excitation laser power ranged from 10 mW with thermally dried samples to 40 mW with samples in aqueous solutions. 20 X, 40 X and 50 X magnifying objective lenses were used to excite the samples locally. A picture of the in-house built Raman device coupled with the Olympus microscope is presented in Figure 8.

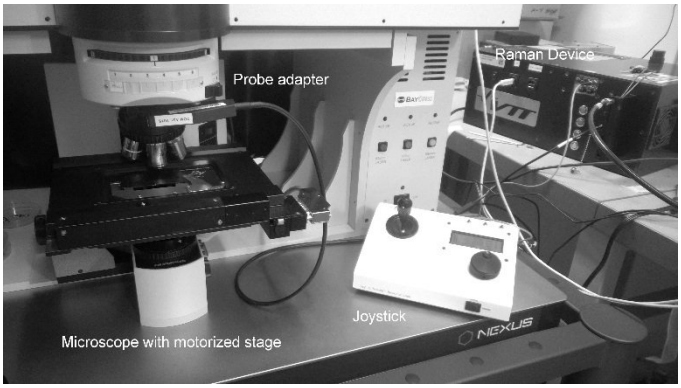

Figure 8. The in-house built Raman device has been coupled with the Olympus microscope by using a probe adapter.

3.2 Fabrication of the SERS sensor chips

3.2.1 R2R fabrication of the SERS substrates

The aim of this study was to detect small molecules and microbial cells with an inexpensive and structured SERS surface. The SERS surface chosen for the study consisted of an array of inverted square pyramid wells. A pyramid is a highly compatible shape for UV nanoimprinting due to its drafted edges. Imprinting is based on moulding shapes into a polymer material. It is prone to challenges with reproduction of shapes during the mould release, if the edges are too vertical. Additionally the pyramid wells of the SERS surface have been shown to provide reproducible SERS signals with a good SERS enhancement factor.[36] The SERS patterns were imprinted on top of a poly(methyl methacrylate) (PMMA) polymer sheet with UV-nanoimprint lithography using roll-to-roll equipment as shown in Figure 9.

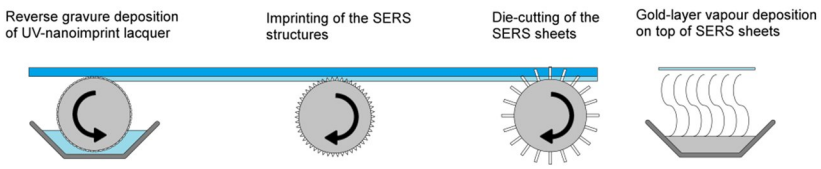

Figure 9. A schematic picture of the R2R fabrication of the SERS substrates. (PAPER III)

Reverse gravure technique was used for coating a PMMA polymer web with a UV-curable lacquer. The lacquer layer was patterned by pressing indentations into the lacquer by relief structures of an embossing reel with simultaneous UV-light curing through the transparent polymer web. The patterned sheets were then die-cut into smaller sensor chips and a 240 nm thick gold layer was added by evaporation. The produced polymer webs and die-cut sheets before and after gold deposition are presented in Figure 10.

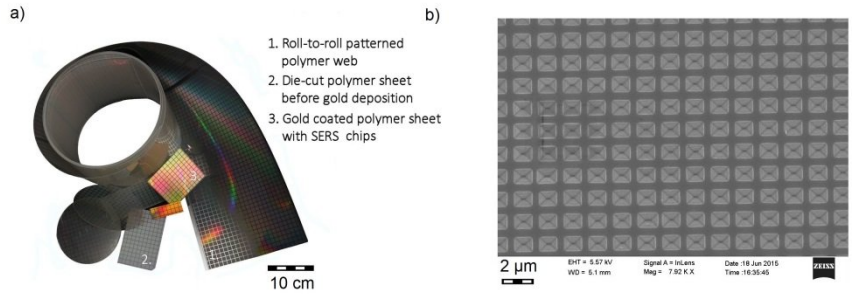

Figure 10. a) A picture of the R2R fabricated SERS structures before and after vapour deposition of gold (PAPER II); b) an SEM picture of the polymer SERS substrate.

The polymer patterning of SERS substrates with R2R lines transferred the fabrication from lab scale into industrial scale with high production volumes. This enables the production of larger sensor surface areas, which can easily be cut into smaller SERS substrates. This SERS platform is applicable for low cost production and is thus practical for one-time use, which reduces the contamination issues often encountered in the detection of biological analytes.

3.2.2 Integration of sample handling reservoirs

There are two typical ways to bring the sample analytes to the surface of the SERS substrates. A common way, especially with molecule detection, is to dip the SERS substrate into the solution containing the analytes and then wait until the analytes diffuse near the surface and adsorb.[121] The diffusion of the analytes is however a slow process, and without convective force or help from gravity only a small fraction of the molecules adsorbs to the surface. The second way involves bringing the analyte solution on top of the substrate inside sample reservoirs by fluidic channels or sample wells. Microfluidic channels enable flowing sample solution on chip in a controlled way, the chip can be washed between samples and the samples can be accumulated on the sensor surface by analyte capture.

The integration of SERS substrates with microfluidic channels enables the fabrication of disposable optofluidic polymer SERS biosensors. In optofluidic

sensors the detection of analytes from the bulk sample relies on transport of the analytes to the detection area and to the detection surface. Since the concentration of the analytes in the sample solution is typically low and the diffusion of the molecules is slow, the used detection method must be sensitive in order to detect and quantify the molecules. In this study, microfluidic circuits for detection of R6G molecules in flow were integrated on top of the SERS substrates by adhesion. The shape of the fluidic channel was cut by a cutting plotter CraftRobo Pro S into a 220 µm thick double-sided 3M adhesive. The circuit had an oval detection chamber having 2 µl sample volume with 400 µm wide inlet/outlet channels leading into the chamber. The circuit was lidded with a high optical clarity polyolefin diagnostic adhesive (3M 9795R). A roll laminator (Yosan S.A., Spain) was used for the layer assembly. A picture of the assembled chip is shown in Figure 11 a).

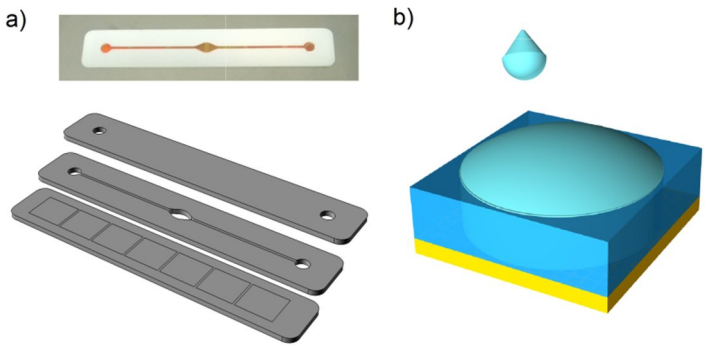

Figure 11. a) A picture of the microfluidic SERS sensor chip with integrated polymer layers (PAPER I), b) Depiction of the hydrophobic sample accumulation in an integrated sample well.

The concentration of the biological cells into the detection zone with microfluidic channels can be challenging. Another way to concentrate sample analytes is by utilising hydrophobic surfaces and structures. The hydrophobic systems are needed to constrain the droplet from spreading over a wide area on top of the hydrophilic gold surface. Such spreading would scatter the analytes and cause a weaker SERS signal. Especially with samples having low concentrations of analytes, the concentration of analytes can be crucial for reaching sufficiently high detection sensitivities. In order to stop the spreading, several different schemes for confining the sample drying by super hydrophobic surfaces have been reported[121–123], but it would be difficult if not impossible to join these structures with the patterned SERS substrate. A simple solution for constraining the sample into a smaller area could be the integration of simple sample wells cut into polymer adhesives as depicted in Figure 11 b), but it is not trivial which materials are used as the sample well walls. Too hydrophilic materials would allow for the sample to retreat by capillary forces into the corners of the wells and dry unevenly. After testing several materials, thin

polydimethylsiloxane (PDMS) sheets were chosen for the well construction. PDMS had high enough hydrophobicity to allow the droplet to dry evenly inside the relatively large sample wells with diameter ranging from 1 mm to 2 mm. A depiction of the sample procedure with bacterial cells dried inside the PDMS wells on top of SERS substrate with gold nanoparticles is presented in Figure 12. Wells were fabricated from 0.5–1 mm thick PDMS sheets (Wacker, Elastosil) and biopsy punchers were used to cut wells into the sheets prior to bonding the wells to the SERS substrate by physical adsorption. A hand lamination roller was used for ensuring good contact. Oxygen plasma treatment was applied before bonding with 1 min 200 W prior to detection of yeast cells.

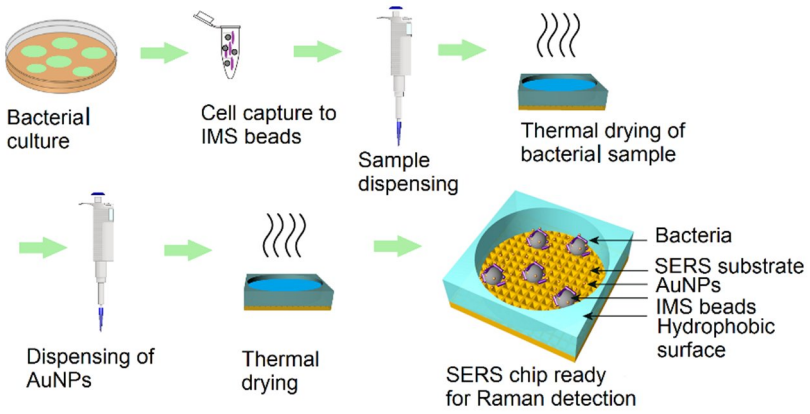

Figure 12. A picture depicting the sample procedure from bacterial culture to the SERS detection of bacterial cells with a Raman microscope.

3.3 Microbial cell capture with immunomagnetic separation beads

Recording of complex SERS spectra for bacterial species often requires that the detection is performed using suspensions with high concentration[102,124]. When the detected concentrations are low, such as 10^5 CFU/ml or lower, the intensities of the detected Raman peaks often diminish and many of the peaks disappear from the spectrum. As different cells commonly have very similar SERS spectra, an incomplete spectrum makes it difficult to identify the specific bacterial cells from other bacterial species, other microbes and from the sample media background. The detection of the recorded bacterial cell spectra can be developed for low bacterial cell levels by using pathogen-capture proteins for the identification of the cells, while utilising SERS for the detection[125]. One way to identify the cells is to use an antibody layer bound to the SERS substrate, as reported by Grow et al.[126]

Although the cells can be successfully detected, the antibodies prohibit the direct contact of cells with the substrate and create a separation distance which weakens

the SERS signal.[127] Thus, this approach with planar SERS substrates can face challenges with sensitivity. Another possibility for capturing bacteria is the use of immuno-magnetic separation beads to bind the bacterial cells[128,129]. In this study, the *Listeria innocua* ATCC 33090 cells were captured by using a commercially available Dynabeads® anti-Listeria (Life Technologies (Invitrogen) 71006) IMS separation kit. Prior to the IMS separation the *L. innocua* was cultivated in Listeria Express Enrichment (LEE) Broth. The concentration was analyzed spectrophotometrically and diluted into a concentration series in LEE Broth. The IMS beads with bacteria were re-suspended into washing buffer for the SERS detection. Before SERS detection the sample was dried into the hydrophobic PDMS well on top of the polymer SERS substrate with the gold nanoparticles. Figure 13 shows a SEM image of the IMS beads thermally dried on top of SERS substrate.

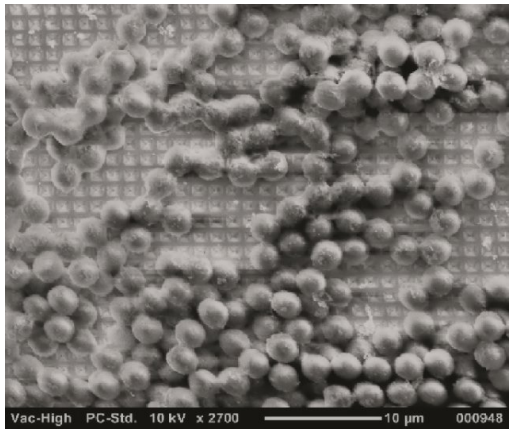

Figure 13. SEM image of the IMS beads thermally dried on top of the SERS substrate (PAPER II).

3.4 Yeast cell cultivation

The yeasts used in the study, *Wickerhamomyces anomalus* VTT C-02470 (C470), *Brettanomyces bruxellensis* VTT C-05796 (C796) and *Rhodotorula mucilaginosa* VTT C-89179 (C179), were all isolated from beverage production by VTT personnel (http://culturecollection.vtt.fi). The yeast strains were taken from the culture collection and grown on yeast-malt extract agar, YM-agar (Difco Laboratories, Detroit, USA) at 25 °C for 2-4 days. Yeast cells were added in 0.9% physiological saline buffer by using inoculating loops for sampling and precision scales for setting the ratio of yeast mass and the saline. *W. anomalus* concentration used with nanoparticle and power study was $8 \cdot 10^7$ cells/ml. The concentrations of *W. anomalus, B. bruxellensis* and *R. mucilaginosa* yeast suspensions were $4 \cdot 10^7$ cells/ml during the final spectral acquisition with gold-silicon composite nanoparticles (AuSi NC). 4 µl volume of each yeast suspension was dispensed

inside sample wells on top of the SERS substrates and dried at 30°C as can be seen from the pictures displayed in Figure 14.

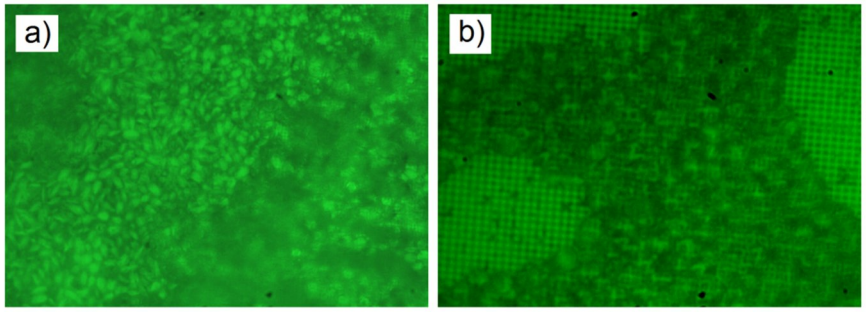

Figure 14. Microscope images (Olympus BX-51) of yeast cells dried on top of SERS substrate with AuNPs a) recorded with 20 X magnification and b) recorded with 40 X magnification. Image colours have been adjusted to green for better visual clarity.

3.5 Characterisation of the nanoparticles and SERS substrates

The characteristics of several nanoparticles with different size, shape and composition both in experimental state and as commercially available were studied by using scanning electron microscopy (SEM) with a JCM-5000 (JEOL, Japan), transmission electron microscopy (TEM) with an LEO 912 Ω EFTEM (Zeiss, Germany) and visible to near infrared (VIS-NIR) spectroscopy (Optronic Laboratories, USA). The SERS substrate patterns shown in Figure 15 were recorded with SEM.

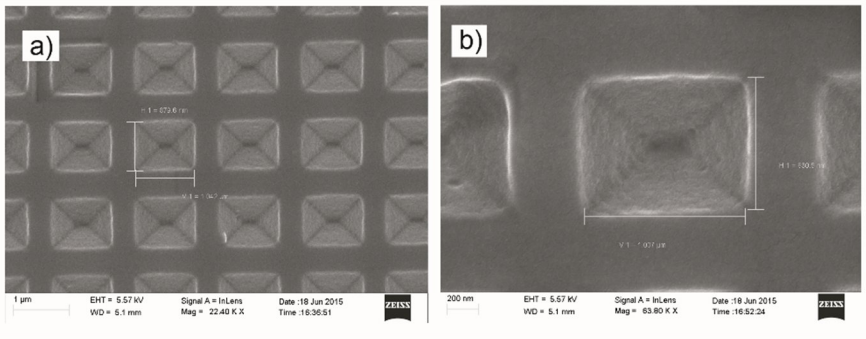

Figure 15. SEM images of the R2R fabricated SERS substrates (PAPER I).

3.5.1 Scanning electron microscopy

Scanning electron microscopy is based on image construction from electron-sample interactions rather than the photon-sample interactions used in conventional visible-light microscopes. Because of the diffraction of light, conventional microscopes have a theoretical limit of resolution of 200–250 nm with white light illumination. High end SEM devices can reach a resolution from 1 nm to 2 nm[130]. To produce the image, electrons are generated with a heated filament and accelerated through lenses and apertures to form a focused electron beam. The sample is mounted on a stage and the electron beam is swept over the sample surface. The secondary electrons, reflected and back scattered initial electrons are detected and they render a highly magnified image of the sample surface. In addition to the higher magnification and higher resolution, the SEM also has a large depth of field, creating images with a three dimensional effect. In order to obtain a clear SEM image of the sample, the reflection of the sample can be enhanced with a metal coating.[131,132]

3.5.2 Transmission electron microscopy

Transmission electron microscopy (TEM) is similarly based on detection of electrons, but in TEM the electrons are transmitted through the sample specimen and they interact with the sample as they pass through. TEM samples therefore need to be thin in order to pass some of the electrons through. At smaller TEM magnifications, as is the case with the metal colloids and IMS beads, the image contrast is produced by the absorption of electrons in the sample, due to the thickness and composition of the sample material. After transmission the image generated by electrons is magnified by electromagnetic fields.[132,133]

3.5.3 Light absorption spectroscopy

Absorbance spectroscopy or spectrophotometry is based on measuring the amount of light absorbed by the sample upon laser excitation. The sample can be a gas, a liquid or a solid. The used wavelength generally ranges from 190 nm to 1000 nm, and the sample is typically at room temperature.[134] The absorbed energy is usually dissipated as heat after collisions between the excited molecule and the other molecules before the excited molecule returns to ground state. In some cases, the excited energy is dissipated as photon emission. In spectrophotometry, absorption is mainly due to the possible spatial distributions of the electrons, and to a lesser extent to the various modes of vibration of the molecule through the stretching and bending of covalent bonds. Thus spectrophotometry can only give an indication of the best resonance wavelengths for the Raman scattering.

3.6 Experimental setups

3.6.1 R6G molecule detection

The compatibility of polymer microfluidic channels for small analyte detection with SERS was studied by filling the integrated chip shown in Figure 11 with R6G samples, deionised H_2O serving as a reference. Reduced pressure was used for transporting the samples from 2 ml vials to the SERS sensor chips with a Nexus 3000 syringe pump. A picture of the flow actuation is shown in Figure 16.

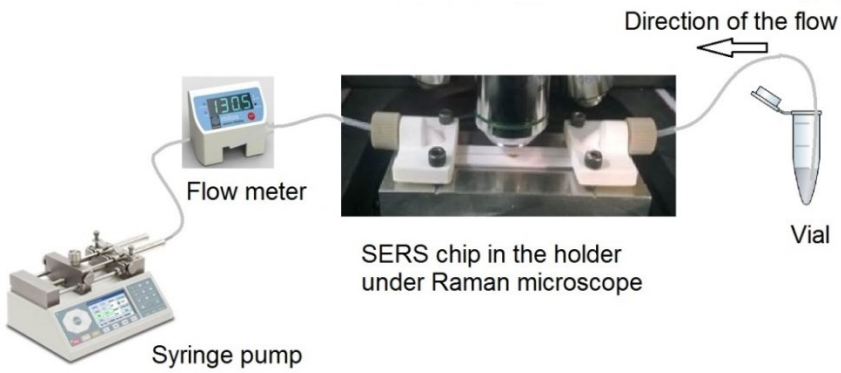

Figure 16. The setup for R6G detection on polymer microfluidic channels (PAPER I).

The Raman microscope was focused through the polyolefin lid before each Raman spectrum acquisition.

3.6.2 Microbial cell detection

Detection of microbial cells in liquid samples requires a close proximity of the cells and the SERS enhancers. Additionally, both the cells and the SERS active agents need to be within the focus depth of the Raman instrument. Detecting microbial cells floating free in the solution can show low SERS enhancement, because most cells are outside the best focus of the detection system. Furthermore, the reproducibility and stability can be affected by micro-currents, generated by the evaporation of the liquid, moving the light weight cells near droplet edges.[135] This phenomenon is known as the coffee stain effect. The flow of cells to the edges of the droplet can be suppressed by the use of heavier IMS beads, which have higher stability with respect to their location. A magnetic field created by a neodymium magnet under the SERS sensor chip was used to accumulate paramagnetic IMS beads on the surface of the SERS substrate. Figure 17 depicts a situation in which the *L. innocua* ATCC 33090 cells are migrating to the SERS substrate due to the magnetic field generated by the external magnet.

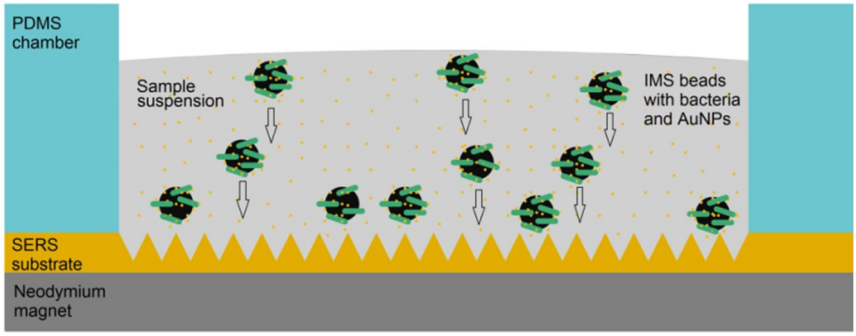

Figure 17. A schematic of a magnetic field created by an external magnet pulling the paramagnetic IMS beads on the surface of the SERS substrate. The arrows show the direction of the IMS bead migration (PAPER III).

4. Results and discussion

In this thesis, the detection of small molecules and microbial cells was studied with disposable SERS substrates and gold nanoparticles using integrated polymer sample reservoirs for sample control. The results of the experiments presented in PAPER I – PAPER IV are described in this section.

4.1 Small molecule detection

4.1.1 R6G molecule detection with integrated microfluidic circuits

In order for SERS to become more common in the detection of molecules and microbes, an SERS sensor should attain high sensitivity, ease of use and the possibility for low cost per chip through industrial scale production. The conventional fabrication of silicon-based sensors can be transferred to industrial scale, but the requirement for disposability and large detection surfaces drives the cost of the sensor so high that single use would be relatively expensive. The ease of use sets additional requirements for the sample handling. For the SERS sensor to succeed, disposable sample reservoirs need to be integrated to the SERS substrates. There are studies reporting methods for low cost fabrication of SERS substrates, such as inkjet printing of nanoparticles, patterning of PDMS with soft lithography and sputtering of nanoparticle surfaces on polymer, but they have only rarely focused on a sensor with integrated sample reservoirs.

In order to study the compatibility of SERS and optofluidic sensing of small analytes, we integrated R2R UV-imprinted polymer SERS substrates with adhesive-based microfluidic parts. The concept of the chip has been presented in Section 3.2.2. The whole sensor is polymer-based, with an addition of the evaporated thin gold layer. This sensor can be patterned in industrial scale with low material costs. The functionality of the integrated SERS sensor was studied with R6G as a model analyte. The chip was first filled with DI water acting as a reference medium with consecutive 1 mM R6G sample intake. The flow setup with pump-inflicted pressure was presented in Section 3.6.1. The Raman spectra were detected using image-mapping on top of the patterned SERS substrate and smooth gold area as the Raman reference. The Raman spectra with subtracted water background are presented in Figure 18 a) and b) with linear and logarithmic y-axis scales. The distinctive peaks for R6G appear in the Raman shift area of 1100 cm^{-1} to 1800 cm^{-1}.

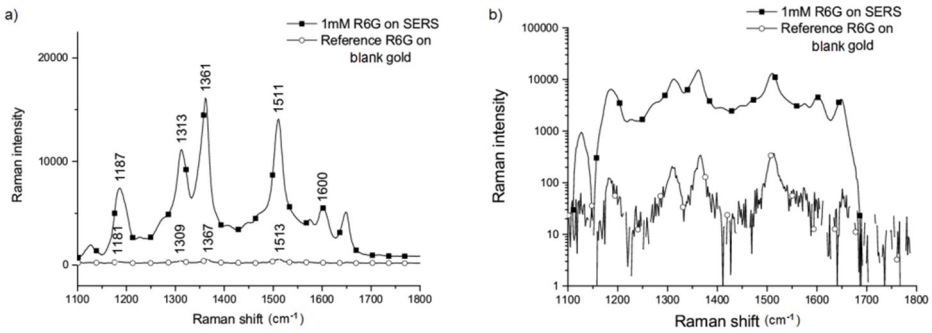

Figure 18. a) Raman spectra for 1mM R6G sample on top of SERS substrate and smooth gold. b) The detected spectra presented in logarithmic scale (PAPER I).

The collection of SERS scattering after laser excitation through a microscope objective is dependent on the depth of focus of the system. The misalignment of the focus was studied in order to determine the effect of focus alignment drift on the signal intensities between trials. The laser beam was misaligned by focusing the system to the bulk sample above the SERS substrate. As can be seen from the results in Figure 19, raising the focus level above the SERS substrate affects the signal level. This confirms that the signal is surface enhanced rather than a conventional Raman surface. However, the level drops only to half with 100 µm misalignment and thus smaller alignment drifts such as 5 - 10 µm do not change the levels dramatically.

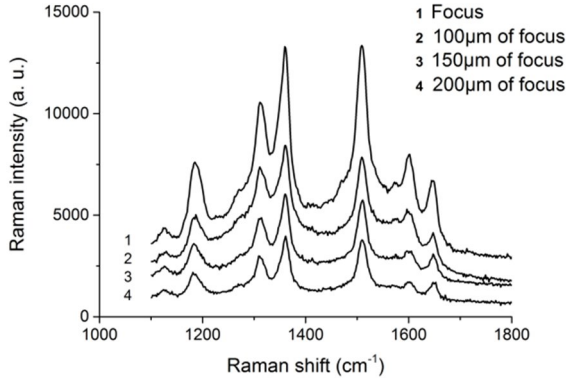

Figure 19. The effect of misalignment of laser beam focus on the signal levels of 1 mM R6G (PAPER I).

Polymer microfluidic circuits require a polymer lid between the SERS substrate and the collection of the Raman scattering. Because polymers are Raman active, the lid could disturb the SERS signal of the analytes in the channel. In order to

demonstrate the effect of the polyolefin lid, the SERS response was measured with diluted 10 µM and 100 µM R6G solutions. The polyolefin reference and the Raman spectra for R6G samples are shown in Figure 20 a). Figure 20 b) shows the 10 µM and 100 µM R6G spectra with polyolefin reference subtracted. The results show that the polyolefin lid induces low Raman peaks. However, the effect of the lid can be minimized by subtracting the reference spectrum from the R6G spectrums.

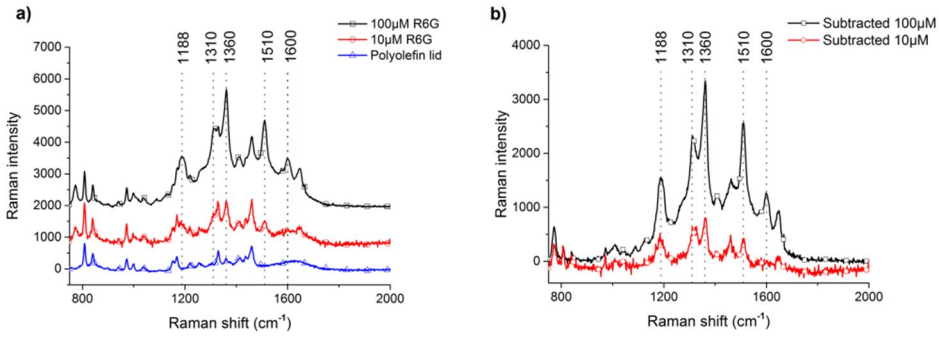

Figure 20. a) The Raman spectra of R6G solutions compared to the polyolefin reference (785nm laser, 40 mW power, 20 X objective and 30 s integration time) b) The Raman spectra of R6G solutions with polyolefin reference subtracted. (PAPER I)

The integrated microfluidic circuit permits the use of continuous flow, and thus repeated sample and washing steps were used to study the dynamic abilities of the sensor. With a planar optical sensing surface, the flow in a microchannel can have a strong influence on the recorded signal. When the flow of the liquid is produced by pump-inflicted pressure, the sample molecules arriving in the detection area need to be in the near vicinity of the plasmonic surface in order to be detected. The excited SERS signal originates from the sample molecules adsorbed onto the detection surface. In smooth microfluidic channels the theoretical Reynold's number is 10 or below, with a flow velocity range from 25 µl/min to 1000 µl/min, indicating laminar flow.[136] The flow profile of the pressure-driven liquid with laminar flow in a microfluidic channel is parabolic, meaning that the fluid has the highest velocity gradient in the middle of the channel, and the velocity decreases as the observation point moves nearer to the walls.

The forces between transport of a molecule in the flow depend on the original placement of the molecule in the channel: in the middle, the convection (drift) is the dominant force behind the transport, whereas in the region between the wall and the middle convection and diffusion both have a role, and in the near vicinity of the channel walls, molecules are transferred by diffusion. Since the flow velocity approaches zero near the walls, transport of the sample molecules by convection is negligible. The region is called the diffusion boundary layer. The molecule transport has an effect on the signal construction through two phenomena: insufficient molecule transport and slow diffusion in the boundary layer. In mass transport

limited flow, transport of analytes to the sensor surface is so slow that the available binding sites do not fill as fast as they could, because of the lack of molecules in the vicinity of the surface, and the signal rise times are delayed. Whereas insufficient molecule transport causes analyte depletion, the transport by diffusion in the boundary layer delays the signal rise due to slow molecule transfer. As a net effect, the molecules adsorbing to the sensor surface are detected with a delay when compared to detection of the molecules in the main flow by other methods such as fluorescence. The effect is dependent on the flow rate of the bulk flow, as the effect of transport limitation decreases when flow rate increases. High enough flow rates can transfer the molecules to the surface at the same velocity as the bulk flow, and the measured signal reflects binding kinetics. Too high flow rates cause new limitations due to the reaction kinetics of the analyte binding. This kinetic limitation occurs when the binding rates are slow and bulk flow velocity is high. The analytes are transported over the detection zone so rapidly that very few of them have enough time to bind to the surface.

In this study, adsorption to the SERS surface occurred through van der Wall's forces by physisorption. The effects of the flow dynamics on the optical SERS signal in the integrated SERS sensor were studied with continuous flow and 0.5 mM R6G solution in DI H_2O. The fluid flow velocity was varied from 25 to 1000 µl/min. A similar study was reported previously by Hüttner et al. with a glass slide-based optofluidic SERS chip using R6G molecules in ethanol with preceding and subsequent pure ethanol cycles[137]. In our experiment, we focused more on the dynamics of the optical signal response to the used flow velocity than on the relation between sample concentration and signal intensity, as Hüttner et al. reported. In order to observe the net effect of diffusive molecule transport and mass transport limitation to the SERS signal, the convective transport of the molecules by the bulk flow was measured by fluorescence microscopy and the arrival of the molecules at the detection surface with SERS. The signal increase on SERS surface was detected without a dissociation phase, because the binding strength of R6G molecules to the gold surface was strong and the detected signal did not decrease to the original level during washing. A cleaning step was carried out by oxygen plasma etching (5 min 300 W) between the flow runs. Baseline tilt of the Raman spectrum was removed with linear fitting. Peak intensity for the main R6G peaks (1188 cm^{-1}, 1310 cm^{-1}, 1360 cm^{-1}, 1510 cm^{-1} and 1600 cm^{-1}) was calculated and averaged from 5 pixels. Change of the peak intensity as a function of time was calculated. Results of the measured signals were normalized and the average signal of 5 repeated measurements was calculated. The recorded average fluorescence and SERS signals for the measured flow velocities are depicted in Figure 21 a) and b) as a function of time.

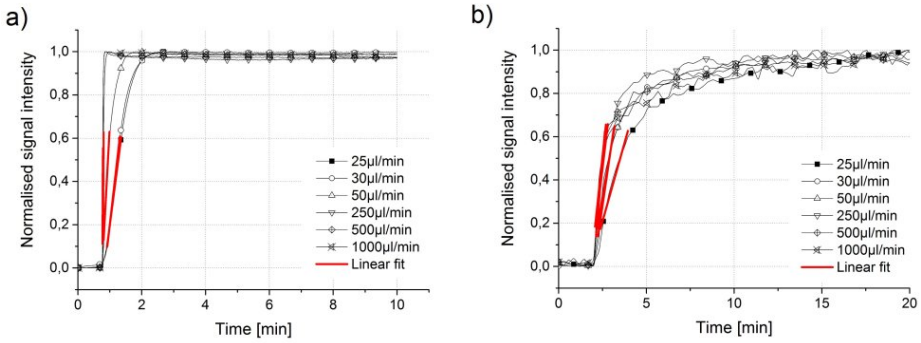

Figure 21. a) Fluorescence intensity as a function of time; b) SERS intensity as a function of time. A linear function was fitted for the rising edge of signals. (PAPER I)

Analysis of the signal rise times was made by fitting linear functions on the rising edge of the fluorescence and SERS signals for the range of 10- 60% of the maximal signal intensity. Figure 22 a) shows the comparison of the SERS signal rise times and the fluorescence signal rise times. It is evident that the detected SERS signal rise is slower than the fluorescence signal rise of the R6G with all velocities in the study. The lag between the arrival of R6G molecules in the detection chamber by convective flow and the diffusion and adsorption of R6G molecules on the SERS substrate is approximately 40 seconds, as depicted in Figure 22 b). As predicted, the lag time grows with slower flow velocities. This is due to insufficient molecular transport to the diffusion boundary layer. The lag time settles for velocities higher than 200 µl/min and the dynamics of the diffusion and surface adsorption become constant. When planning SERS studies with bioanalyte samples and capture proteins on the SERS surface, the influence of increasing mass transport limitation with flow velocities less than 50 µl/min must be taken into account.

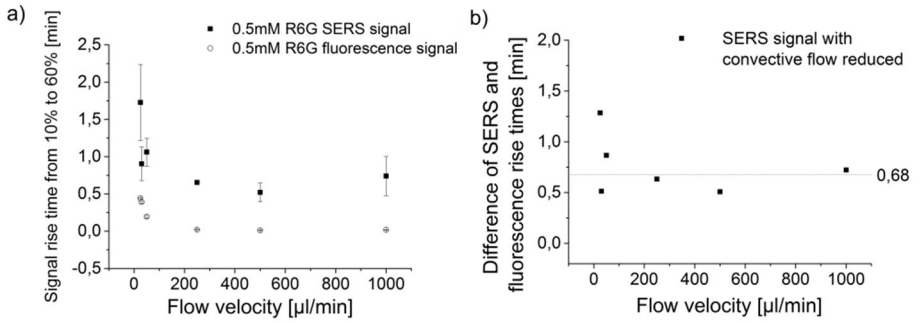

Figure 22. a) The rise times for the SERS signal and the fluorescence signal intensity; b) The lag time in signal rise between the SERS and the fluorescence signal. (PAPER I)

4.1.2 Hybrid SERS detection of R6G molecules

Using hydrophobic structures for sample confinement can assist in analyte accumulation to achieve enhanced signal intensity. Drying a sample on top of SERS substrate inside a hydrophobic sample well has the advantage of quick and easy accumulation without the need for a cover lid disturbing the recorded analyte spectra. Hydrophobic PDMS sample wells were integrated on top of SERS substrate as described in Section 3.2.2, to study the detection of thermally dried model analyte R6G. Although the SERS substrate was shown to have an enhancement factor of 10^7 in a study with benzyl mercaptan ($C_6H_5CH_2SH$) test molecules[36], the detection of microbial cells has a final requirement for detection of very low cell counts on the scale of 10–10^4, which can be difficult to achieve using only SERS substrates. A commercial SERS substrate (Klarite) similar to the polymer fabricated substrate was used in the detection of *Bacillus* endospores and viruses, but the spores had a rather high concentration as they were grown for 7 days prior to detection[138] and the virus concentration was 10^6–10^7 PFU/ml[139]. In order to enhance the detection sensitivity with polymer substrates, a hybrid detection method combining SERS substrate with gold nanoparticle plasmonic enhancement was studied by drying 100 µM R6G sample on top of the SERS substrate with subsequent drying of commercial 150 nm AuNPs in citrate buffer. The recorded spectra for SERS substrate detection, AuNP detection on top of a silicon wafer and hybrid detection are presented in Figure 23 a). From Figure 23 b) it can be seen that the hybrid method increases the Raman peak intensity on average 21-fold when compared to the Raman intensity of the AuNP and SERS substrate detection alone. Hybrid detection also increased the complexity of the spectra.

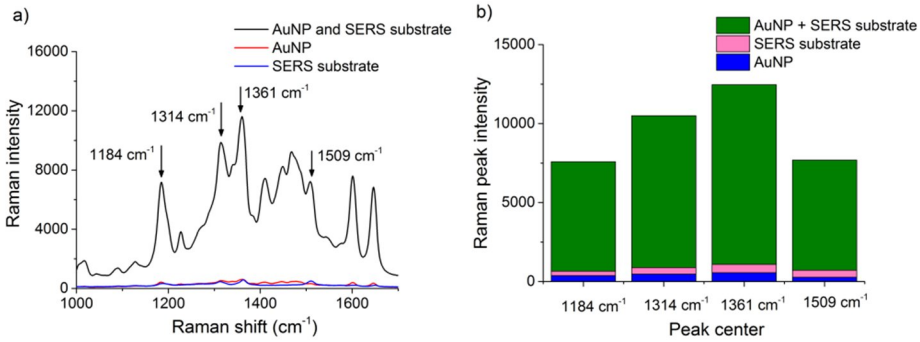

Figure 23. a) The recorded SERS spectra of 100 µM R6G sample detected with SERS substrates, AuNPs and a hybrid method. b) Comparison of the Raman peak heights detected with the hybrid method, SERS substrates and AuNPs.

4.2 SERS detection of bacterial cells with IMS capture

Detection of microbial cells with the hybrid method differs from the situation presented in Figure 23. The distance between SERS substrate, gold nanoparticles and R6G molecules is smaller than the distance in the case of cell detection. The smaller distance allows for the local plasmonic enhancement fields to couple more effectively. In addition, the small size of the molecules allows them to fit inside the pyramid wells and to experience a 3D plasmonic field. As depicted in Figure 7 in Section 2.2, microbial cells cannot fit inside the 1 µm pyramid wells and the size difference affects the plasmonic field coupling. In this section the hybrid detection method is applied to bacterial cells.

4.2.1 Optimisation of hybrid SERS detection of bacterial cells

The main objective of bacterial detection with the hybrid method was to develop a simplified and affordable label-free detection of *Listeria* strains using polymer SERS substrates. *Listeria innocua* was chosen as a model strain representing the food pathogen *Listeria monocytogenes*. *Listeria monocytogenes* is difficult to control in food production, as it tolerates a wide range of temperature and pH conditions. It is the most common bacteria causing food poisoning and has a relatively high fatality rate ranging from 20% to 30%[92]. Typically, different Listeria strains have been identified by the SERS method from highly concentrated samples, mostly in the range of 10^7–10^{10} CFU/ml. The effect of the hybrid detection on the *L. innocua* SERS response was studied with three different AuNPs, one set of small laser ablated ultrapure AuNPs and 2 sets of synthesized AuNPs with different average diameters. The ultrapure AuNPs lack the residuals of non-reacted reagents, by-products, ions and surfactants often present in particle synthesis, and thus they could show better biocompatibility with bacterial cells than the synthesized AuNPs. The chemically synthesized AuNPs were chosen in order to observe the effect of shape and size on the hybrid detection of bacteria.

The diameter and shape of the AuNPs were recorded with transmission electron microscopy (TEM) using a LEO 912 OMEGA (Zeiss, Germany). The TEM images are presented in Figure 24 with the corresponding size distributions and the UV-VIS spectra of the AuNP. A fitting was applied to the size histograms with Gaussian function in order to identify the median size of the AuNPs. The median diameter of the small ultrapure particles was approximately 50 nm. The medium sized synthesized AuNPs had a median diameter of 60 nm, with occasional large particles of 90 nm. The larger synthesized AuNPs had 85 nm median diameter and a rod-like shape. From the VIS-NIR spectra in Figure 24 g), it can be seen how the absorption resonance shifts in the direction of the excitation wavelength (785 nm) as the median size of the particles increases.

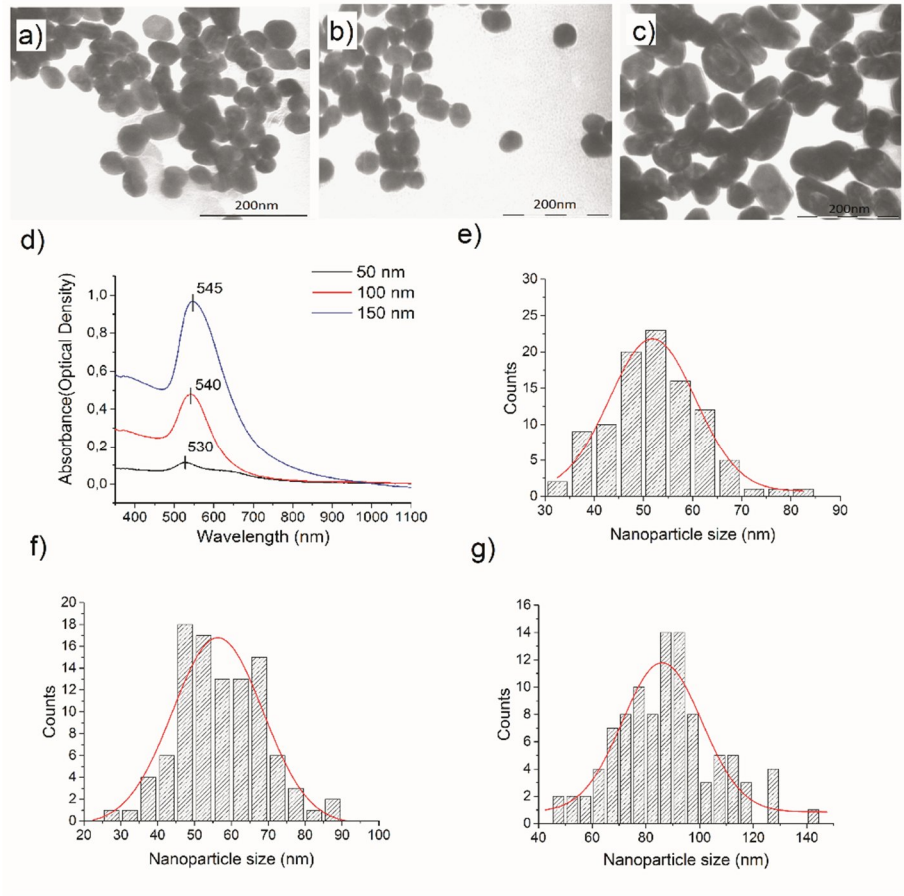

Figure 24. TEM images of the different AuNPs: a) small ultrapure, b) medium and c) large synthesized AuNPs, respectively. d) Corresponding VIS-NIR spectra for the AuNPs. Size distribution histograms calculated from AuNP TEM images with Gaussian fit for e) small, f) medium and g) large AuNPs. (PAPER II)

The enhancement ability of the hybrid detection with different AuNPs was studied by dispensing 5 µl of bacterial sample and 2 µl of each AuNP solution into duplicate PDMS wells integrated on top of the polymer SERS substrate. The recorded SERS spectra are presented in Figure 25 a). The average intensity of the main Raman peak, 737 cm^{-1}, of the *L. innocua* detected with the AuNPs is presented in Figure 25 b). From the graph it can be seen that the synthesized AuNPs showed the highest enhancement for a bacterial concentration of 5×10^5 CFU/ml. However, as the larger synthesized AuNPs had the maximum absorption of their UV-VIS spectra closer to 785 nm excitation wavelength and provided more consistent spectra, they were chosen as the best candidate for hybrid bacterial detection. The results presented in Figure 25 show that larger particles enhance the signal more than

small ones in bacterial detection. The AuNP fabrication by physical ablation did not benefit the detection by counterweighting the advantage of the size and the shape of the particles.

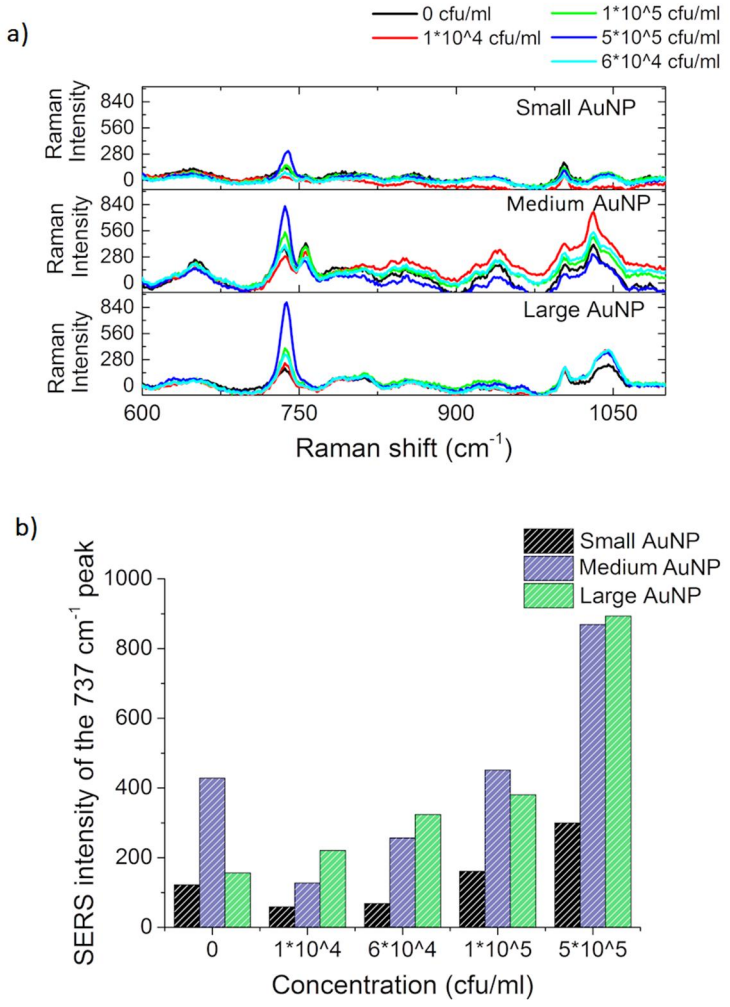

Figure 25. a) A concentration series of the IMS-bound *L. innocua* ATCC 33090 with different AuNPs on top of polymer SERS substrate. The results are an average of 18 measurement points. b) SERS intensity of the *L. innocua* peak at 737 cm^{-1} for a cell concentration series with AuNPs on top of the polymer SERS substrate. (PAPER II)

4.2.2 SERS signal enhancement with bacterial cell capture beads

Detecting the SERS signal of bacterial cells in food matrix is challenging, as the food produces complex Raman spectra and disturbs the detection. In order to separate the bacterial cells from the growth media and to concentrate them for detection, IMS beads described in Section 3.3 can be used. With SERS detection, the IMS beads are often removed before detection or used as part of a customised sandwich assay with SERS labels. To simplify the detection, *L. innocua* cells were bound into commercial anti-*Listeria* Dynabeads and the bacterial spectra were detected with the cells bound to the beads. Figure 26 a) shows a comparison of the SERS detection of *L. innocua* cells with and without IMS beads. The bead capture accumulates the cells around the bead and the effect of the accumulation strengthens the detected SERS intensity. The signal intensity with beads was found to be 20-fold stronger than the signal intensity recorded without the beads.

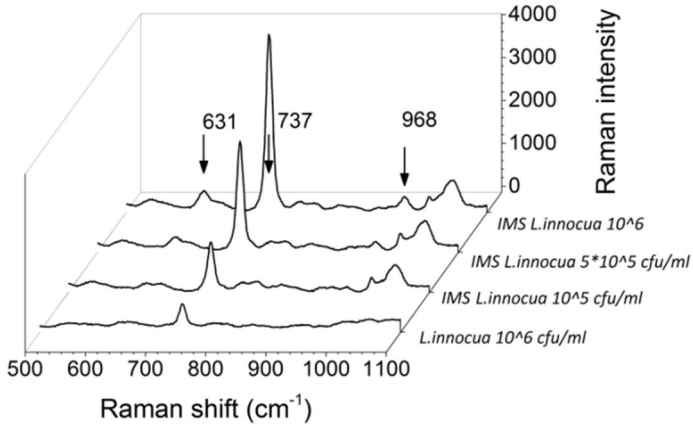

Figure 26. The effect of IMS capture on the *L. innocua* ATCC 33090 SERS signal intensity with synthesized AuNPs and polymer SERS substrate. (PAPER II)

In order to observe the effect of the hybrid detection on the SERS enhancement, *L. innocua* cells captured with IMS beads were excited on top of silicon wafer with AuNPs and on top of SERS substrate with and without AuNPs. The results of the study are presented in Figure 27. The hybrid detection combining AuNPs and the SERS substrate showed over 20-fold higher signal intensity than the SERS substrate and gold nanoparticles alone. When the nanoparticle enhancement is compared to the hybrid method with bacterial cell detection, the intensity has tripled. Because the bacterial cells are large compared to the pyramid wells, they do not experience 3D enhancement as the R6G molecules do, and the advantage of the hybrid detection is smaller.

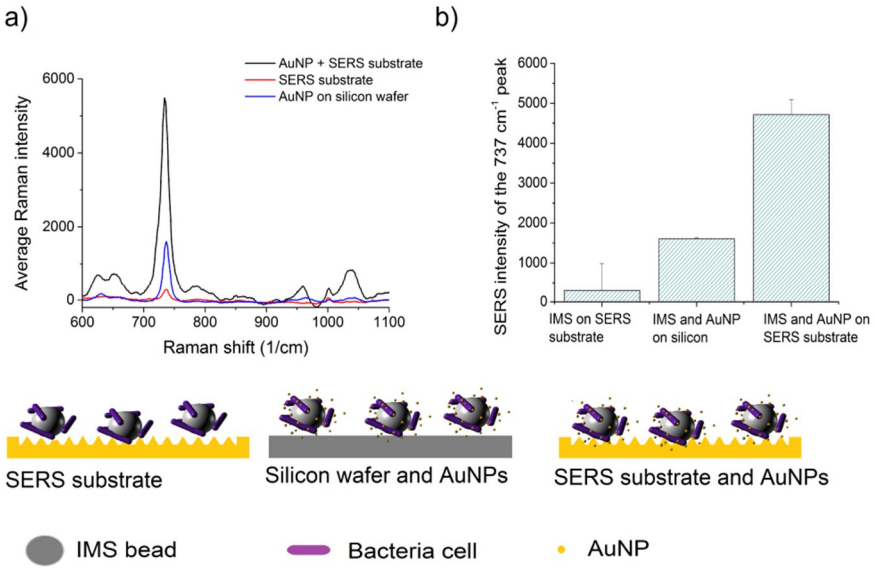

Figure 27. a) IMS bound $1 \cdot 10^7$ CFU/ml *L. innocua* ATCC 33090 sample on top of polymer SERS substrate, on top of a silicon wafer with large synthesized AuNPs, and on top of polymer SERS substrate with large synthesized AuNPs. b) SERS signal intensity for the main *L. innocua* 737 cm^{-1} peak. (PAPER II)

In order to study the *L. innocua* specific Raman bands, bacterial samples were dispensed inside the hydrophobic PDMS sample wells without thermal drying and the SERS spectra were recorded by using 40 mW laser power and 20 X magnification. The assumption was that the cells in liquid would undergo less thermal stress during the SERS excitation and that the complexity of spectra would be less affected than with the dried samples. Figure 28 a) shows the average SERS spectra of 3 bacterial concentrations. 9 Raman bands originated from the bacterial cells, and it can be seen that rest of the peaks in the spectra were caused by the salts from the sample buffer and residuals of culture media. When comparing the LEE broth and 0 CFU/ml sample shown in the graph in Figure 28 b), many of the non-bacterial peaks appear to originate from traces of the LEE broth.

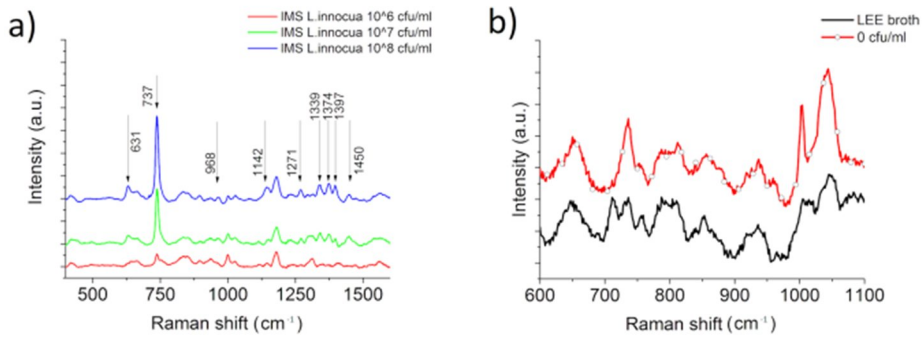

Figure 28 a) SERS spectra of *L. innocua* ATCC 33090 samples with large synthesized AuNPs on top of polymer SERS substrate with IMS bead capture. b) Comparison of the SERS signals for the cultivation media, i.e. LEE broth, and the 0 CFU/ml sample. (PAPER II)

4.2.3 Band assignments for *L. innocua* Raman peaks

The recorded *L. innocua* specific Raman bands are listed in Table 2 with tentative assignments listed according to literature references. For the main Raman peak of 737 cm^{-1}, several different assignments are listed in publications, including a glycosidic ring, adenine or CH_2 rocking[135]. Assuming that the bacterial cells are intact during the detection, the presence of adenine on the surface of a gram-positive bacterial cell would be unlikely. The outer wall structure of *Listeria spp.* has a thick peptidoglycan structure rich in N-acetyl D-glucoseamine (NAG), and thus it would be logical that the origin of the peak would be a glycosidic ring mode of NAG rather than adenine.[135,140] The Raman bands in the range of 1300–1400 cm^{-1} are interesting because none of the three have been recorded with *L. innocua* or *L. monocytogenes* in previous studies. A line 1331 cm^{-1} associated with CH_2 deformation was recorded with *Listeria* samples by Luo et al.[135]. This line is near the recorded line 1339 cm^{-1}. The shift of the line could be related to the use of silver colloids instead of gold and a custom Raman instrument. Another possibility for the association could be amide III, as proposed in an *E. coli* study by Vohník et al.[141], or it could be related to the aromatic amino acids tyrosine and tryptophan, as suggested by Harz et al.[97] Harz et al. also proposed a listing for a band near to the second line 1374 cm^{-1}, which was associated with DNA. The last line of the group 1397 cm^{-1} could be related to symmetric deformation of CH_3 group, which has been reported for *E. coli.*[142,143]

Table 2. The nine Raman bands recorded for *L. innocua* ATCC 33090.

Detected lines	Raman shift (cm^{-1})	Tentative assignments	Reference
631	627/620	Phenylalanine (skeletal)	Luo, Lin 2008[135] [135], Maquelin et al. 2002[144]
737	732	glycosidic ring mode of D-glucoseamine (NAG), adenine or CH_2 rocking	Luo, Lin 2008[135], Cui et al. 2015[145]
968	955	C-N stretching	Vohník et al. 1998[141]
1142	1134/1130	C-N and C-C stretch (carbohydrates)	Fan, Hu 2011[142], Chen et al 2015[124]
1271	1230-1295	Amide III	Liu, Chen 2007[146], Lu, Al-Qadiri 2011[147], Maquelin et al. 2002[144]
1339	1334/1339/1338	Deformation CH/Amide III/ signature of adenosine; monophosphate and guanosine monophosphate, aromatic amino acids tyrosine and tryptophan	Maquelin et al. 2000[148] Vohník et al. 1998[141] Harz, Rösch, Popp 2008[97]
1374	1371	DNA	Harz, Rösch, Popp 2008[97]
1397	1392/1398	Symmetric deformation of CH_3 groups	Fan, Hu 2011[142] Al-Qadiri, Lin 2008[143]
1450	1453	CH_2 deformation (lipids)	Fan, Hu 2011[142], Cui et al. 2015[145]

When comparing the *L. innocua* Raman bands reported in publications, the SERS spectra differ between different studies. Liu et al., among others, speculated that this could be related to differences in bacterial growth conditions such as the cultivation media and incubation temperature, or to the SERS parameters such as excitation wavelength of the laser or the SERS enhancer metal.[146,140] In order to test this hypothesis, the SERS spectra of *L. innocua* were recorded with two laser excitation wavelengths and two SERS enhancers and the results were compared to a literature reference[135]. Figure 29 shows the *L. innocua* spectra for 3 different SERS conditions. First the bacterial spectra were recorded using hybrid detection with gold colloids on top of polymer SERS substrate and 785 nm continuous wave (CW) laser excitation. In the second case, the same sample was detected on top of a glass slide with silver colloids and pulsed laser excitation at a different wavelength of 532 nm. The results are generally in agreement. They are also in agreement with the third case published by Luo et al., employing silver colloids using 785 nm CW laser excitation. In addition Kairyte et al.[149] used silver colloids with 1064 nm excitation, with a similar outcome. According to this comparison there is no connection between the variations in spectra and the SERS enhancer metal (silver/gold) or the excitation wavelength.

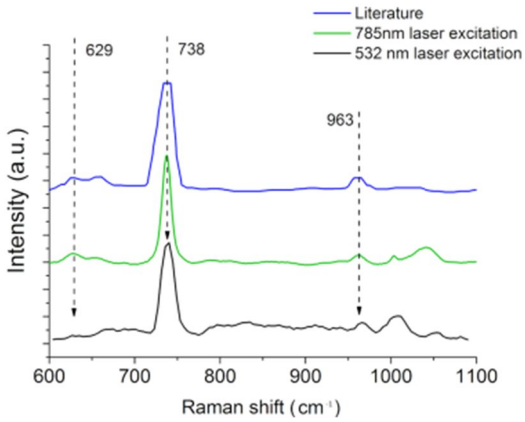

Figure 29. A comparison of three *L. innocua* SERS spectra: the literature reference borrowed from a publication by Luo et al. (2008) measured with CW 785 nm laser with silver colloid enhancers[135]; the spectra of IMS bound *L. innocua* recorded by using a hybrid detection method with CW 785 nm laser excitation; and by using silver colloid enhancers and pulsed 532 nm laser excitation. (PAPER II)

4.2.4 Improvement in the sensitivity of bacterial detection with sample concentration

Thermal drying of the sample on top of SERS substrate concentrated the samples, allowing more bacterial cells to be excited inside the laser beam area, and lowered the detection limit when compared to liquid samples. However, when using 20 X magnification the detection limit was around 10^5 CFU/ml. To further lower the detection limit, the power of the laser was manually tuned down to 10 mW from the earlier 40 mW and the magnification was changed to 40 X. Lower laser power allowed the use of 40 X magnification without burning the dried specimen during the measurement procedure. With dried samples, there is an issue of media traces and buffer salts blocking parts of the bacterial samples, and the sample density was reduced by using larger sample wells. Figure 30 a) shows the decline of the main Raman peak with decreasing cell concentration. In the results, the Raman intensities of the spectra were normalised by the background peak at 787 cm^{-1}. The intensity of the main *L. innocua* peak as a function of cell concentration is presented in Figure 30 b) on a logarithmic scale with an exponential fit. For the concentration range below 10^5 CFU/ml, the relation between intensity and concentration was found to be linear. The lowest limit of detection needs to be considered through the deviation of the background signal generated by the sample matrix, because the blank 0 CFU/ml sample exhibits a signal at 737 cm^{-1}.

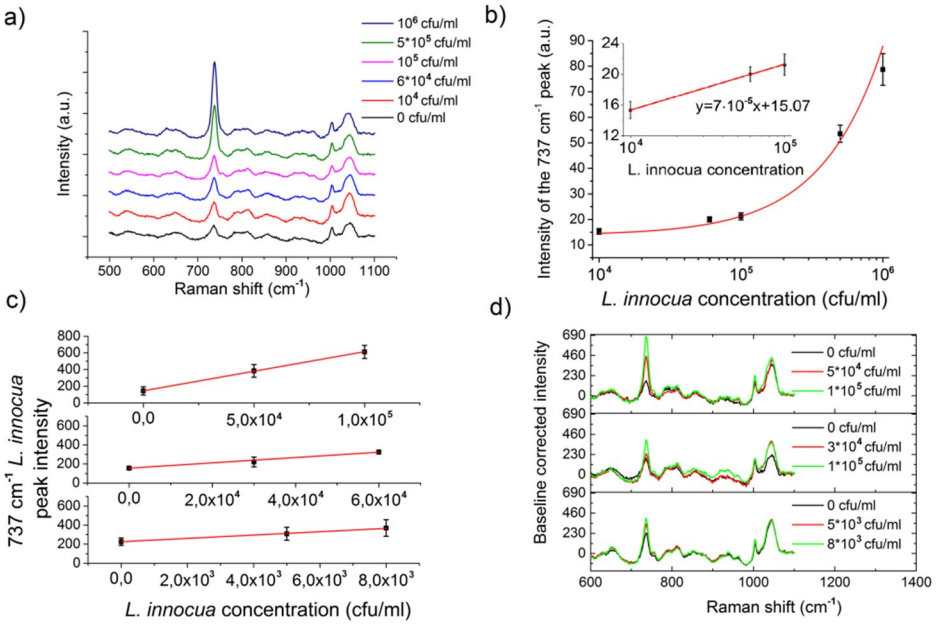

Figure 30. a) *L. innocua* concentration series for the determination of limit of detection. b) An exponential function was fitted on the concentration series shown in logarithmic scale. Additionally, a linear fit was made for the low concentrations. c) Comparison of the 737 cm^{-1} peak intensity for different concentration series of *L. innocua* ATCC 33090. d) Comparison of three of the concentration series. All figures are a mean of 9 measurement points with mean absolute deviations. (PAPER II)

For determination of the lowest limit of detection, a definition provided by International Union of Pure and Applied chemistry, IUPAC, was applied. According to the definition, the limit of detection (*LOD*) is defined as the lowest concentration detected with reasonable certainty, and it can be derived from

$$LOD = k \cdot s_{bi} \cdot S, \tag{18}$$

where s_{bi} is the standard deviation of the blank samples, k = 3 is a factor for confidence level provided by IUPAC and S is the slope of the calibration curve. S can be defined as a ratio of the concentration change Δc and the Raman intensity response ΔI:

$$S = \Delta c / \Delta I.^{150} \tag{19}$$

By determining S from the linear fit shown in Figure 30 b), the *LOD* was calculated to be $1.4 \cdot 10^4$ CFU/ml. The result can be confirmed by inspecting the concentration series displayed in Figure 30 c) and d), where the deviations of the concentrations

below 10^4 CFU/ml coincide with the deviations of the average blank samples. Thus the samples with lower concentrations cannot reliably be detected. With this detection limit the estimated detection time including pre-cultivation[151] (6 hours) for 10^4 CFU/ml cell concentration, IMS capture (15 minutes), sample preparations on SERS chip (15 minutes), SERS detection (10 minutes) and data handling (5 minutes) is estimated to be 7 hours. Thus the hybrid SERS detection method with *Listeria* specific IMS capture reduces the time needed for detection by 41 hours when compared to the current official ISO 11290-1:1996/amd.1:2004 method.

4.2.5 The effect of capture beads on bacterial cell detection in liquids

The detection process could be developed further by utilizing the magnetic nature of the IMS beads on the SERS substrate. Because detection of microbial cells in liquid samples is highly dependent on the cells being in the near vicinity of the SERS enhancers and surfaces and both the cells and the SERS active agents being within the focus depth of the detection system[152], accumulation of the cells into the detection spot is of critical importance. Furthermore, when detecting a sample droplet, micro-currents generated by evaporation of the liquid and shrinkage of the droplet can cause repeatability issues.[135] The evaporation, enhanced by heat of the focused laser-beam, causes micro-currents to move the cells towards the edges of the droplet, where the signal can grow significantly higher than in the middle of the droplet. This phenomenon is related to the coffee stain effect. Thus the use of heavier objects, such as IMS beads to bind the cells, could have positive effects on the spatial and temporal stability of cell detection with liquid samples and SERS.

The stability of the SERS signal for three cases, as a droplet on a surface without and with IMS bead capture and confined in a PDMS well, are presented in Figure 31 a)–c), respectively. By using IMS bead capture the large average deviation, 44%, of the main Raman peak at 737 cm^{-1} shown in Figure 31 a) in a case without IMS beads can be reduced to 13%. This could enable semi-quantitative detection due to the improved signal stability and repeatability. But there are also other factors affecting the detection of SERS signal from a droplet. Dispensing a droplet with a constant shape and a similar footprint repetitively can be challenging, and the lens-like shape of the droplet can affect the correct focus depth and the signal capture of the scattered Raman photons. By confining the sample droplet into a hydrophobic sample well, the repeatability of the detection can be increased. The result in Figure 31 c) shows that the average deviation can be decreased with integrated sample wells.

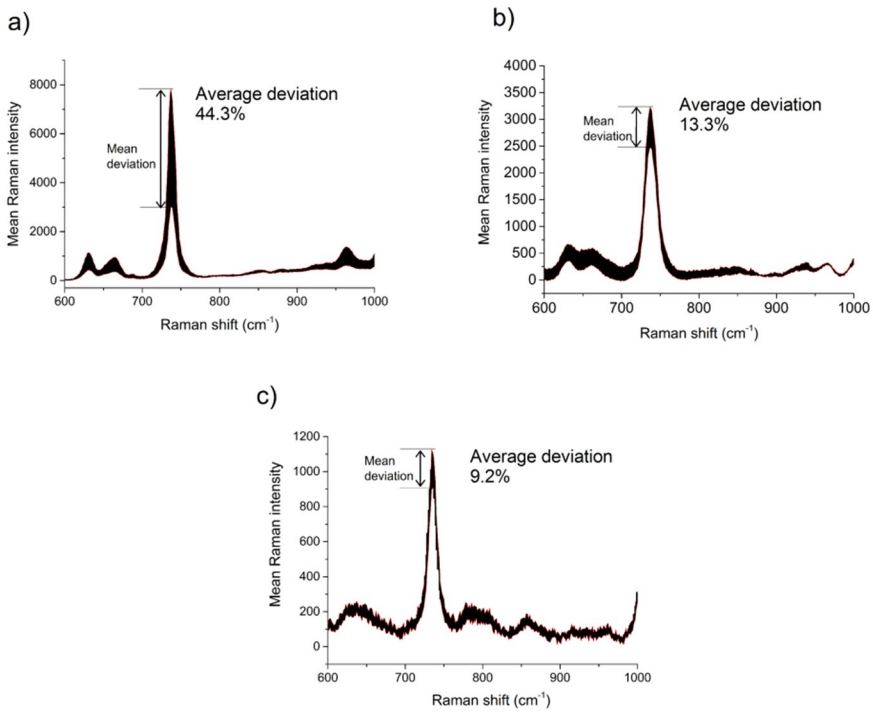

Figure 31. Average deviation of *L. innocua* spectrum recorded with gold colloids and SERS substrate from a) a 6 µl droplet of 10^9 CFU/ml *L. innocua,* b) a 6 µl droplet of 10^8 CFU/ml *L. innocua* with IMS bead capture and c) 10^6 CFU/ml *L. innocua* bound to IMS beads inside a PDMS well. (PAPER III)

The effect of time on the migration of the IMS bead bound bacterial cells to the SERS substrate by gravity was studied for 3 cell concentrations. Figure 32 shows the temporal growth of the SERS signal of the main Raman peak, 737 cm^{-1}, as a function of time. The bead accumulation is evident even after 20 minutes of waiting time. During this waiting time, the IMS beads slowly accumulate to the SERS substrate and to the focus depth of the Raman system. The migration of the beads adds temporal variance to the signal and delays recording of the maximal signal intensity. The intensity relation of 10^6–10^8 CFU/ml bacterial concentrations detected after a 10 minute waiting time are presented in Figure 32 a)–d).

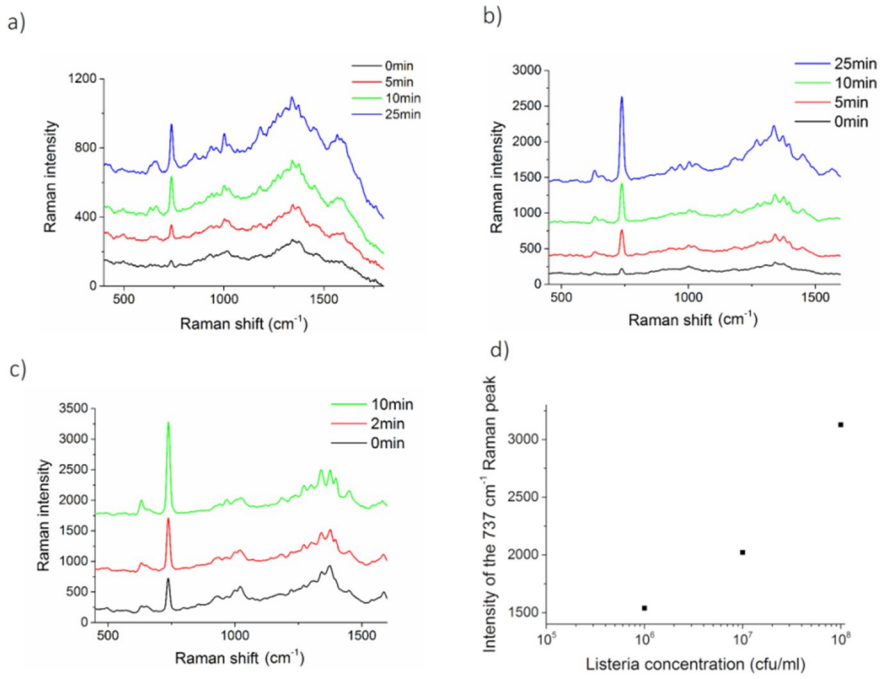

Figure 32. SERS signal growth of IMS-captured *L. innocua* cells with different concentrations as a function of time. The slow migration of the heavy IMS beads to the surface of polymer SERS substrate increases the signal intensity of a) 10^6 CFU/ml *L. innocua* sample, b) 10^7 CFU/ml *L. innocua* sample and c) 10^8 CFU/ml *L. innocua* sample. d) Relation of the intensity of the main Raman peak at 737 cm^{-1} as a function of sample concentration after 10 minutes of migration. The spectra were smoothed with a Savitsky-Golay function. (PAPER III)

The migration of beads to the SERS substrate can be accelerated by employing the paramagnetic property of the IMS beads. A neodymium magnet was placed under the SERS substrate prior to sample dispensing. Figure 33 shows how the magnetic field enhances the bead migration.

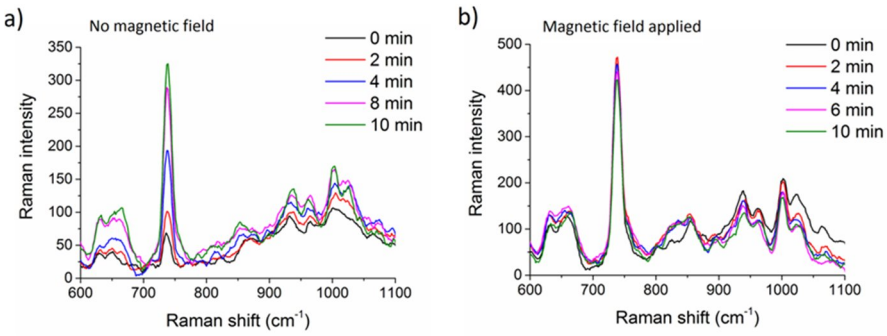

Figure 33. SERS signal of IMS-bound *L. innocua* samples a) without and b) with a neodymium magnet placed underneath the SERS chip. The neodymium magnet placed underneath the SERS chip clearly forces the beads to accumulate faster to the bottom of the hydrophobic sample well. Sample concentration: 10^6 CFU/ml. A Savitsky-Golay function was used for spectrum smoothing. (PAPER III)

The increase of signal intensity reaches saturation point within 2 minutes of sample dispensing. The results for the increase of the SERS signal intensity as a function of time with and without magnetic field are presented in Figure 34. After the highest signal intensity is reached, the signal intensity changes only 4.9%. The decline of the signal after 2 minutes is attributed to local heating of the detection spot and to the degrading effect of the local heating on the bacterial cells. Without the magnetic field, the signal does not reach the saturation point during the 10 minute trial and grows steadily at a constant rate of 2.5%/minute. The results of the study show how the IMS beads can reduce both the temporal and spatial signal deviation, and concentrate the bacterial cells evenly into the focus depth and into the focal point of the laser beam.

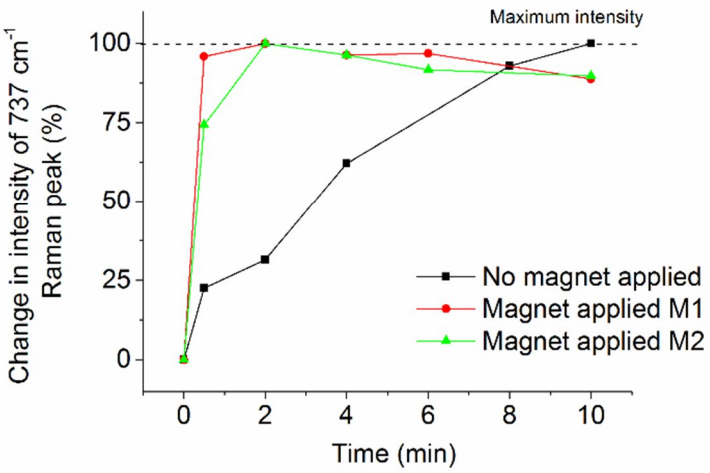

Figure 34. Change in the SERS signal intensity of *L. innocua* samples as a function of time, recorded with and without a magnetic field. Sample concentration was 10^6 CFU/ml. (PAPER III)

4.3 Yeast cell discrimination with SERS detection

Spoilage yeasts are an expensive problem for the beverage industry, due to off-flavours caused by the metabolic end products of yeast cells[153–155]. Although certain yeasts are obviously needed in the brewing process and they can have an important role in forming the specific taste of the beverage[115,156], others can spoil the final product. Sometimes the spoilage is evident as exploding cans or as a cloudy, re-fermented appearance, but often it is only observable in the taste of the product, as it takes up to 10 000 cells/ml to change the appearance of the drink. The presence of a few cells of a specific spoilage yeast at any stage of the manufacturing process can cause quality defects that are perceptible to the consumer. In the beverage industry, microbiological quality is controlled by plate cultivation techniques, which are laborious and last typically 5–7 days. Plating rarely distinguishes between spoilage and harmless strains and requires DNA sequencing or morphological and physiological testing to identify the organisms[153–155,157]. SERS could be a suitable identification method for yeasts, as it enables rapid detection, has the possibility for multiple simultaneous analyses and is not prone to the contamination of samples by other microbes or DNA in the laboratory[114].

Detection of yeast with SERS substrates alone can be difficult, because yeasts are relatively large organisms, having a diameter from 4 to 10 µm. The SERS signal excitation is limited to the area of the yeast in the near vicinity of the SERS surface, thus extending only on one side of the yeast cell. As a consequence, in studies

reported previously the yeast cells are detected by using metal nanoparticles adsorbed around the yeast cell. Several research groups have studied the detection of yeasts by SERS[25,158–161]. The research has mainly focused on characterization of different yeasts with suspensions of silver colloids incubated with the cells by focusing on single cells or small clusters of cells with highly magnifying optics[112,158,159,161–163]. Syamala et al. discussed the difficulty of obtaining repeatable SERS spectra with silver colloids incubation, as the adsorption of colloids to the proteins of the cell wall is affected by several factors such as the flexibility/mobility, accessibility, polarity and the exposed protein surface[161]. *Saccharomyces cerevisiae* has been the most commonly used yeast in SERS research. Of the beverage spoilage species, Rodriguez et al. have studied the Raman signals of wine spoilage yeasts including *Saccharomyces cerevisiae, Zygosaccharomyces bailii* and *Brettanomyces bruxellensis (B. bruxellensis)*, but the study was not able to detect complex SERS spectra with multiple Raman bands for different yeast species[114].

In this study three yeasts, including two beverage spoilage yeasts *Wickerhamomyces anomalus (W. anomalus)* and *B. bruxellensis*, and a control yeast, *Rhodotorula mucilaginosa (R. mucilaginosa)*, were detected with a hybrid detection method. Nanoparticle incubation with yeast cells before detection was avoided, in order to record spectra with less variance due to differing colloid adsorption. The beverage spoilage yeasts, *W. anomalus* and *B. bruxellensis,* are of interest as they produce volatile compounds which cause off-flavours in wines, beers and soft drinks[164]. *Brettanomyces bruxellensis,* also known as *Dekkera bruxellensis*, can produce acetate-esters which develop an acetic taste in beers and undesirable flavours in soft drinks.[165] *Rhodotorula mucilaginosa* is used as a control yeast for testing the hygiene of the manufacturing facilities. It produces red/pink coloured carotenoids, which cause a characteristic pink appearance[166], and it has not been associated with spoilage of the final products[167].

4.3.1 Optimisation of hybrid SERS detection of yeast cells

Yeast detection with the hybrid method was developed by analysing the suitability of different nanoparticles for the signal enhancement of 100 µM R6G solution and yeasts with the hybrid detection. The palette of NPs included star-shaped AuNPs, commercially available AuNPs and gold-silicon nanocomposite (AuSi NCs) particles. The size and shape of the nanoparticles was studied with light spectroscopy and transmission electron microscopy (TEM) imaging. TEM imaging showed that the NPs of the study had a spherical basic shape as shown in Figure 35 a)–g). Figure 35 a) shows how star-shaped AuNPs have additional sharp spikes, which can create SERS hotspots. The AuSi NCs shown in Figure 35 b) have a few larger particles in the midst of the small ones.

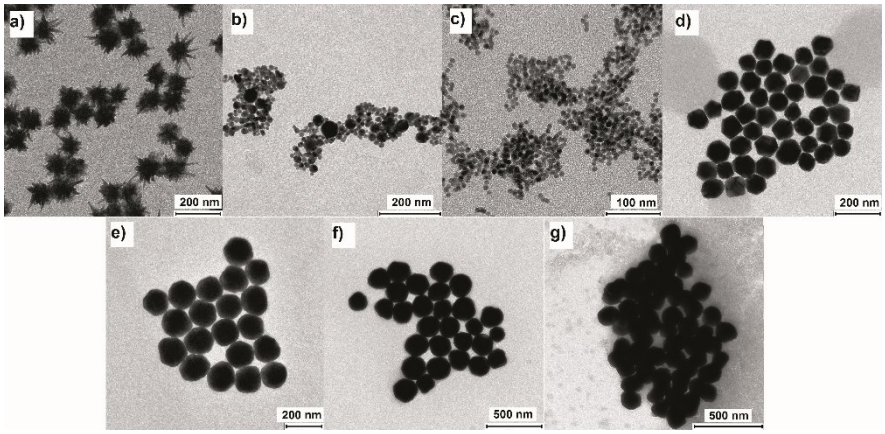

Figure 35. TEM images of the nanoparticles including a) Star AuNPs with an average diameter of 79 nm with spikes excluded, b) AuSi NCs with an average diameter of 16 nm, c) 10 nm AuNPs in citrate buffer, d) 80 nm AuNPs in citrate buffer, e) 150 nm AuNPs in citrate buffer, f) 200 nm AuNPs in citrate buffer and g) 150 nm AuNPs in PBS buffer. (PAPER IV)

The light absorbance was used as an indication of the best excitation resonance wavelength band for SERS. According to the VIS-NIR spectra shown in Figure 36, star AuNPs and 200 nm AuNPs in citrate buffer absorb best at 785 nm wavelength, whereas the smallest particles have lowest absorbance at this wavelength.

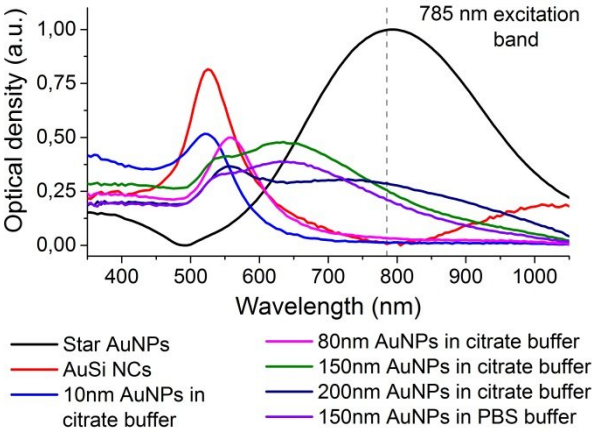

Figure 36. The resonance maxima for the analysed nanoparticles recorded with light absorption spectroscopy in the VIS-NIR range. (PAPER IV)

The SERS enhancement with hybrid detection was first studied by detecting Raman active R6G molecules. Figure 37 shows the comparison of SERS intensities of 100 µM R6G detected with different nanoparticles on top of SERS substrate. The results show how the 150 nm and 200 nm spherical AuNPs show the highest R6G peaks. The highest intensity was recorded with 150 nm AuNPs in PBS, but the peaks have a high background, possibly originating from the PBS buffer. As a high background can overflow the signal of the microbial cells, PBS buffer does not appear to be suitable for yeast detection with the hybrid method. The star AuNPs, with the best light absorbance, do not exceed the other AuNPs as SERS enhancers. They show similar signal intensity to that of the 80 nm particles. This could be related to the surface properties of the star AuNPs, which have polymer PVP ligands on their surface. The results also reveal the good enhancement ability of the small AuSi NCs. Although much smaller in size (16 nm), they show similar enhancement ability to that of the 80 nm particles. This could be related to the bare surface of the AuSi NCs allowing excellent contact of the particles with sample molecules. The 10 nm particles did not enhance the signal with SERS substrate. From the results, we can see that the AuNP buffer can affect the detection and that the citrate buffer is preferential to the PBS buffer.

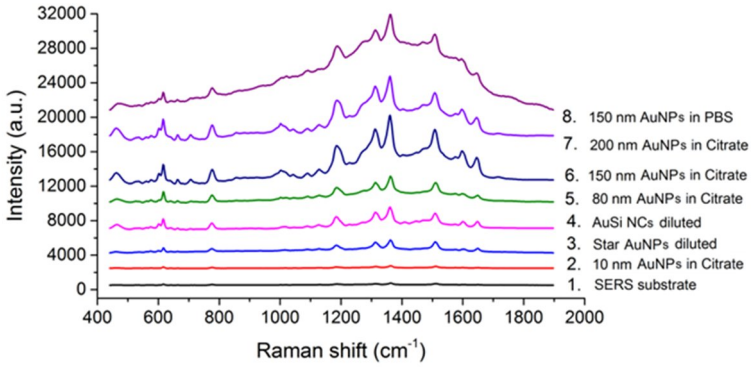

Figure 37. R6G SERS spectra recorded with hybrid detection adding sample and nanoparticles on top of SERS substrate. The results were averaged from 30 measurement points recorded from duplicate samples. (PAPER IV)

4.3.2 Detection of *W. anomalus* with a hybrid SERS method

In SERS detection the heat of the laser power can damage the biological cells under detection even at NIR wavelengths[113,160]. The amount of local heating also depends on the state of the sample, either dried or in liquid form. As the nanoparticle incubation can affect the detected spectra, the aim of this study was to detect the cells in thermally dried state with NIR excitation wavelength and low excitation power in order to avoid causing excess thermal damage to the cells. The SERS

spectra for *W. anomalus* with different laser powers and integration times were recorded to study the relationship between the energy used and SERS spectra construction. Figure 38 a) shows the relationship of the average intensity of the main Raman peak 738 cm^{-1} to the used laser power. Low laser power requires a long integration time to distinguish characteristic peaks for the yeast. On the other hand, 20 mW and 34 mW laser power begin to degenerate the cells, and the characteristic Raman peaks such as the peaks at 738 cm^{-1} and 967 cm^{-1} are becoming weaker, as can be seen in Figure 38 b). The main Raman peak 738 cm^{-1} is not visible any more with 34 mW power. 12 mW power shows the highest peak intensity with a suitably fast 30 s integration time.

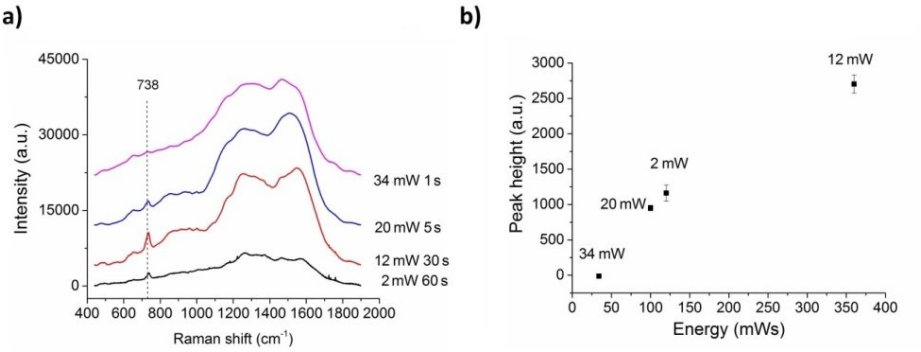

Figure 38. a) SERS spectra of *W. anomalus* detected with hybrid detection and different laser powers and integration times. b) The peak height for the Raman peak 738 cm^{-1} as a function of energy. The hybrid detection was performed using 150 nm AuNPs in citrate buffer on top of SERS substrate and the average result was calculated from 15 points measured per laser power. (PAPER IV)

The detected *W. anomalus* spectrum is assumed to originate from the yeast cells of the sample, but this requires additional confirmation as the culture medium can excite peaks at the same wavelength range as the yeast cells. To confirm the origin of the peaks, the effect of yeast cell concentration on the SERS signal was recorded with 150 nm AuNPs in citrate buffer. The graphs in Figure 39 a) show how the Raman peak intensity grows with higher sample concentration. Figure 39 b) shows the SERS spectra of the $3 \cdot 10^8$ cells/ml sample and the spectra of the buffer (0.9% physiological saline) solution. From the results, it can be concluded that the peaks originated from the yeast.

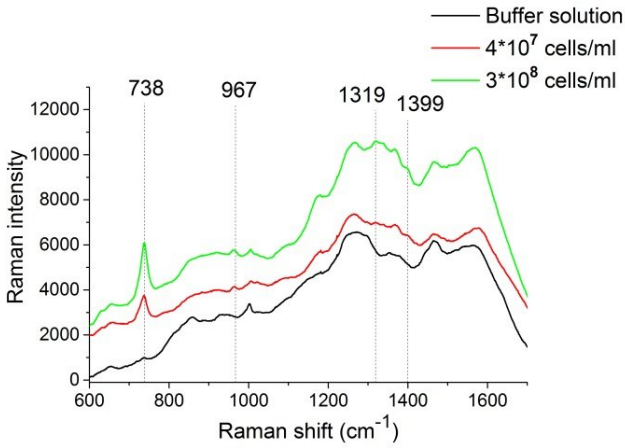

Figure 39. a) SERS spectra detected with a hybrid detection method for *W. anomalus* with two cell concentrations and a sample containing the sample matrix (0.9% physiological saline and AuNPs in citrate buffer). The average SERS spectra were calculated from 30 points measured from duplicate samples using 12 mW power and 30 s integration time. (PAPER IV)

4.3.3 Optimisation of the hybrid SERS method for *W. anomalus*

The hybrid detection was used to detect *W. anomalus* spectra using 10 mW excitation laser power and a reduced integration time of 15 s to ensure minimal thermal damage to the yeast cells. The SERS response recorded with different nanoparticles can be seen in Figure 40. The SERS substrate alone or with 10 nm particles cannot enhance the Raman scattering enough to form a SERS spectrum on its own with 10^7 cells/ml samples. Similarly, the star AuNPs show low signal intensity without characteristic peaks. This result is contradictory to the R6G molecule detection, in which star AuNPs showed a clear signal similar to the 80 nm particles. A possible reason for this could be the PVP coverage of the star AuNPs. The PVP surface appears to have a stronger influence on microbial cells than the R6G molecules and thus the contact of the nanoparticles with the yeast cells is hindered and the Raman signal is suppressed.

The 80 nm, 150 nm and 200 nm nanoparticles in citrate buffer show a 738 cm^{-1} peak for *W. anomalus*. The SERS spectrum of 150 nm AuNPs is more distinct than the spectra of 80 nm or 200 nm AuNPs. The higher absorption seen in light absorbance for 200 nm particles does not produce a higher SERS intensity with yeast samples. The AuNP buffer affects the SERS spectra as the PBS buffer of 150 nm particles prevents the yeast detection. This could be due to the Raman signal of the PBS salts. By replacing the PBS with DI water (Raman neutral medium), the background signal is less disturbing, but the intensity of the detected spectra is still lower than that recorded with similar AuNPs in citrate buffer. AuSi NCs show a better compatibility with SERS detection of yeast than they do with R6G detection. The

spectrum detected with AuSi NCs shows the lowest background signal for *W. anomalus,* and in this respect could be well suited for yeast detection.

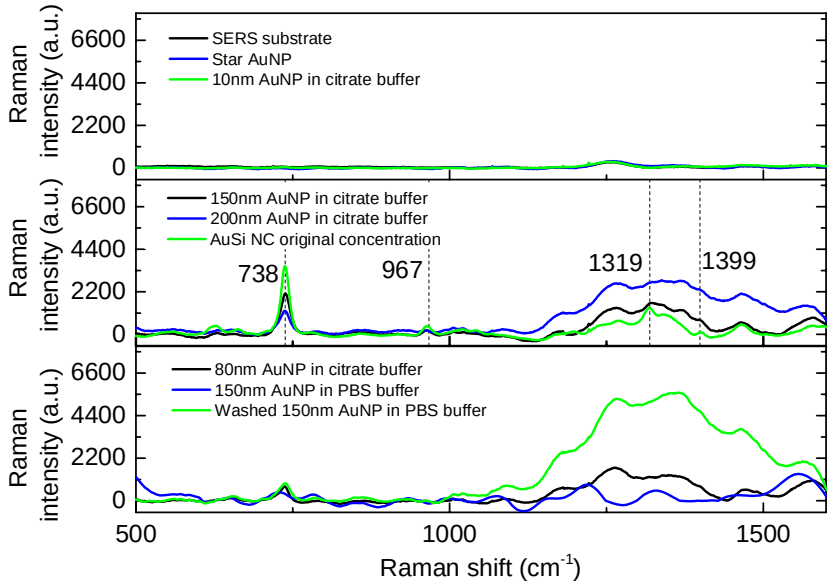

Figure 40. SERS spectra of *W. anomalus* detected using hybrid detection with different nanoparticles. The average SERS spectra were calculated from 30 points measured from triplicate samples. (PAPER IV)

The sensitivity of the SERS spectra of *W. anomalus* was enhanced by increasing the NP concentration. The concentration was doubled by concentrating the particles of 1 ml AuNP solution to the bottom of a vial by centrifuging and removing 500 µl of the supernatant. The effect of the higher NP concentration on the SERS signal construction is presented in Figure 41. A double increase in nanoparticle concentration increases the intensity of *W. anomalus* SERS signal by a factor of 3.1. The signal increase is 1.5 times the amount of added SERS enhancers. The high increase could be due to large numbers of AuNP molecules attaching to the single yeast cell wall in the near vicinity of each other, creating areas of higher electromagnetic field intensity. Furthermore, higher concentration in the AuNP liquid before dispensing can cause nanoparticle aggregation, which in turn increases the signal intensity.[168,169]

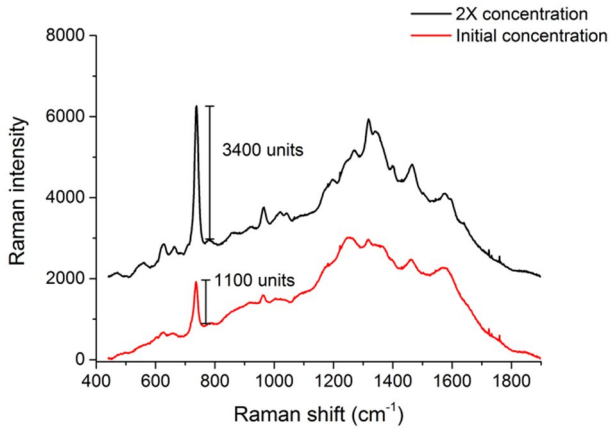

Figure 41. SERS spectra of two *W. anomalus* samples in 0.9% physiological saline recorded with hybrid detection using AuSiNCs. The SERS spectra were averaged from 30 measurements recorded from triplicate samples using 30 s integration time. (PAPER IV)

4.3.4 SERS detection and discrimination of different yeast strains

The SERS spectra of *W. anomalus*, *B. bruxellensis* and *R. mucilaginosa* were detected with hybrid detection using the concentrated AuSi NCs. The yeast spectra were detected from thermally dried samples with subsequent addition of AuSi NC. Figure 42 shows the recorded SERS spectra with the buffer solution reference. Several Raman bands can be distinguished for each yeast. The control yeast *R. mucilaginosa* showed 7 characteristic bands, whereas the spoilage yeasts *W. anomalus* and *B. bruxellensis* showed 4 peaks. The buffer SERS spectrum has been subtracted from the spectra of the yeasts.

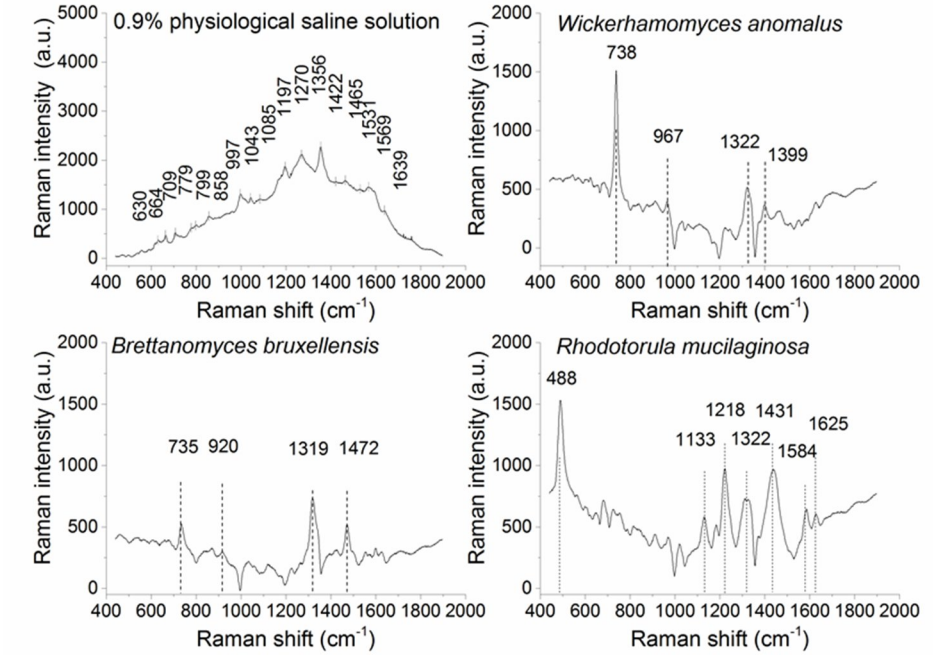

Figure 42. Hybrid detection with AuSi NCs and polymer SERS substrate of a) 0.9% physiological saline, b) *W. anomalus,* c) *B. bruxellensis* and d) *R. mucilaginosa*. The SERS spectra are an average of 30 points measured from triplicate samples. The baseline of yeast spectra was subtracted. (PAPER IV)

The recorded Raman bands from the spectra of Figure 42 are presented in Table 3. The yeast cell wall contains 25% helical b(1–3) and b(1–6)-D-glucans, 25% oligomannans, 20% protein, 10% lipids, and some chitin. The proteins of the wall are mainly mannoprotein complexes[162]. The *W. anomalus* Raman spectra, with four characteristic peaks at 738 cm^{-1}, 967 cm^{-1}, 1322 cm^{-1} and 1399 cm^{-1}, have not been studied previously. The possible band assignments are related to C-S bond and C-N stretch, and to protein and lipid bands. The SERS spectra of *W. anomalus* have features similar to those of *Candida albicans* spectra[162]. The spectra of *B. bruxellensis* had Raman bands at 735 cm^{-1}, 920 cm^{-1}, 1319 cm^{-1} and 1472 cm^{-1} Raman shifts. Although the bands for *W. anomalus* and *B. bruxellensis* were in similar regions, they were slightly shifted. The band assignments for *B. bruxellensis* are related to sugars, proteins and lipids. The Raman bands of *R. mucilaginosa* can be compared to the peaks reported earlier with Raman microimaging[113,170] and SERS active silver coated glass fibre tips[160]. The detected bands for *R. mucilaginosa* originate from polysaccharides, lipids and hemoproteins. The cell wall structures responsible for the recorded peaks are listed next to the band assignments[170].

The characteristic Raman bands 1001 cm^{-1}, 1151 cm^{-1} and 1508 cm^{-1}, described in previous studies of *R. mucilaginosa* carotenoids[160], do not show in the recorded

spectra. This could be due to the fact that the NIR excitation does not match the carotenoid absorption spectrum. Although NIR can be preferable with microbial cells due to reduced thermal damage when compared to the SERS detection with visible wavelengths, NIR suppresses carotenoid bands, as can be seen from one study with *Micrococcus luteus* cells[113]. Although the carotenoid peaks are absent, *R. mucilaginosa* excites Raman peaks which can be used for yeast discrimination.

Table 3. Raman band assignments according to a study by Sayin et al. [162] for the detected yeasts *W. anomalus, B. bruxellensis and R. mucilaginosa* and a reference biomolecule listing for *R. mucilaginosa* by Pacia et al[170].

Raman band	***W. anomalus***	***B. bruxellensis***	***R. mucilaginosa***	***Study by* Pacia et al** [170]
488			Polysaccharides	Outside detection range
735/ 738	Adenine from flavin, C–S, N-acetyl-D-glucosamine	Adenine from flavin, C–S, N-acetyl-D-glucosamine		
920		Glucose		
967	C-N stretch			
1133			Lipid	Hemoprotein, cell wall
1218			Amide III	Hemoprotein, cell wall
1319/ 1322	C-H bend protein	C-H bend protein	C-H bend protein	Lipid or hemoprotein, cell wall
1399	CH_2 bend (protein, lipid)			
1431			CH_2 bend (protein, lipid)	Lipid, cell wall
1472		CH_2 bend (protein, lipid)		
1584			N-H, C-H bend, C=C stretch	Lipid, cell wall
1625			Tyrosine, tryptophan	Hemoprotein, cell wall

The results of this study show that the hybrid detection method can be used for discrimination of *W. anomalus*, *B. bruxellensis* and *R. mucilaginosa.* The recorded Raman spectra contain peaks which are clearly shifted from each other. The yeasts were detected from relatively high concentrations (10^7 cells/ml) in 0.9% physiological saline, but the method could be implemented for detection of lower cell counts by utilising chemometric data analysis[171,172] and additional cell accumulation methods such as filtration[173].

4.4 Future work

The current SERS detection of biomolecules and microbial cells requires bulky laboratory Raman apparatus commonly attached to a microscope for the excitation and recording of the signal. This restricts the use of SERS detection in the field, especially in harsh environments. Although with conventional Raman detection there are many hand held devices on the market, a compact module for SERS detection has hitherto been lacking. This situation might change in the near future, as a new SERS detection module was recently launched with a line of compatible single use SERS substrates[174]. These substrates have been fabricated with nanoimprinting technology and are thus similar to the substrates studied in this thesis. The detection of samples in the device requires drying of the sample for the SERS analysis, but as shown in this thesis, that is not necessarily a problem for microbial cell detection. In future, this type of devices can change SERS from a laboratory research tool to a more flexible in-field diagnostic tool. However, the efficiency of the signal collection, level of the dark current and the overall device performance with analytes, which are weaker Raman scatterers even with SERS enhancement, limit the fields which can utilise the on-field SERS.

In future, the hybrid detection method could be tested with integrated SERS modules for microbial cell detection. This would indicate whether the low analyte levels required in environmental monitoring and food diagnostics are achievable with the new portable SERS modules. Another path towards easily operated SERS devices would be the fabrication of single use sensors which integrate a disposable substrate with disposable microfluidic circuits. This would require extensive screening for materials which have a minimal impact on the Raman signal, either through non-scattering composition or the ability to produce thin material layers causing minimal disruption of the spectra. Although in this study it was possible to discriminate 3 yeasts from each other, the positive identification of microbial cells grown in different conditions can be challenging. In practice, SERS often requires a supplementary method for the cell identification. An interesting study for the future would be the detection of microbial cells with a sandwich assay combining IMS bead binding and gold nanoparticles with antibody coating. It would be beneficial if the gold nanoparticle surface were covered with short capture proteins such as fab-fragments or nanopods in order to shorten the distance between the cell surface and the SERS enhancer. This arrangement with a short incubation step, possibly inside a microfluidic circuit, could enhance the detected SERS signal and make the SERS detection applicable in many areas needing biological sensing.

5. Summary

In this thesis, R2R patterned SERS substrates were integrated with microfluidic sample handling systems and hydrophobic sample chambers for molecule and microbial cell detection. The aim of the work was to develop a sensitive SERS detection method utilising an integrated sensor platform meeting the criteria for a disposable low cost device with the possibility for high throughput manufacturing. The suitability of a new hybrid SERS detection method was studied with R6G molecules and microbes by combining nanoparticles with polymer SERS substrates.

The R6G molecules were used for the validation of a polymer adhesive based fluidic circuit integrated with patterned polymer SERS substrate. The effect of the polyolefin lid on the R6G signal was minimised by reference spectra subtraction. The detection of SERS signal of the R6G molecules was compared to the detection of R6G molecules by conventional fluorescence detection. The study showed that the migration and adsorption of analyte molecules to the SERS sensor surface from the bulk flow caused over 40 seconds delay for the detection of the R6G. A flow of less than 50 µl/min velocity caused mass transport limitation and created an analyte depletion zone near the sensor surface. The presented fabrication method for the microfluidic SERS chip shows potential for production of disposable strips for analytical applications.

The polymer substrates with hydrophobic sample wells were applied for bacterial cell detection with the hybrid method combining the SERS substrates with gold nanoparticle enhancement. The suitability of several nanoparticle types was analysed for *Listeria innocua* detection. The results of this study provide new insights into Listeria diagnostics. The cell concentration using immuno-magnetic separation beads proved to be beneficial, due to enhancement of the signal intensity by a factor of 10. The use of thin hydrophobic PDMS wells for sample preparation enabled controlled sample deposition and reduced the signal intensity deviation. The limit of *L. innocua* detection was determined to be in the range of ~10^4 CFU/ml, shown for the first time for label-free gold enhanced SERS. In addition, the spatial and temporal stability of SERS detection of bacterial cells in liquid was studied with IMS bead capture and hydrophobic sample wells. The IMS bead capture of cells improved the spatial signal stability by 35% when the bacterial cells were placed into a confined area of the sample well. The temporal stability was affected by gravity-assisted concentration of the IMS beads inside the sample well. Sample stabilization took 10-20 minutes to reach saturation with gravity-assisted migration. However, by using a magnetic field as an IMS bead attractor, the saturation time for sample stabilization was reduced to less than 2 minutes. Besides producing reproducible and more reliable SERS results, this method enables quicker and more straightforward laboratory testing.

The detection of three yeast strains, *W. anomalus, B. bruxellensis and R. mucilaginosa,* was studied using the hybrid detection method. The study revealed that thermally dried yeast cells can be clearly discriminated with near-infrared

excitation without the need for chemometric calculations. The hybrid detection with different AuNPs showed that the effect of the AuNP buffer on the acquired SERS spectra can cause overflow of the Raman lines. It is not trivial which buffers are used in biological cell detection using SERS. In addition, when detecting microbial cells, the surface coatings of the AuNPs, such as the PVP cover of the star nanoparticles, can critically decrease the SERS enhancement efficacy. 150 nm spherical gold nanoparticles in citrate buffer and ultrapure composite nanoparticles were best suited for the SERS detection of yeasts. AuSi composite particles were used for detection of *W. anomalus, B. bruxellensis and R. mucilaginosa* and distinctive spectra were recorded. The developed SERS detection method provides a simple and straightforward yeast discrimination tool, in particular for the food and beverage industry.

The results discussed in this thesis offer different methods for the construction of a polymer-based SERS optofluidic sensor chip. The sensor can be used for the detection of small molecules adsorbed to the surface or for detection of microbial cells bound with capture beads. Since the sensor has low cost and is suitable for single use, it shows promise as a tool for analyte detection in environmental monitoring, security and food safety.

References

1. S. Aikio et al., “Disposable (bio)chemical integrated optical waveguide sensors implemented on roll-to-roll produced platforms,” RSC Adv. **6**(56), 50414–50422, Royal Society of Chemistry (2016) [doi:10.1039/C6RA07320D].

2. P. Kozma et al., “Integrated planar optical waveguide interferometer biosensors: A comparative review,” Biosens. Bioelectron. **58**, 287–307 (2014) [doi:10.1016/j.bios.2014.02.049].

3. F. Prieto et al., “Integrated Mach–Zehnder interferometer based on ARROW structures for biosensor applications,” Sensors Actuators B Chem. **92**(1), 151–158 (2003) [doi:10.1016/S0925-4005(03)00257-0].

4. B. Sepúlveda et al., “Optical biosensor microsystems based on the integration of highly sensitive Mach–Zehnder interferometer devices,” J. Opt. A Pure Appl. Opt. **8**(7), S561–S566, IOP Publishing (2006) [doi:10.1088/1464-4258/8/7/S41].

5. A. Ymeti et al., “Integration of microfluidics with a four-channel integrated optical Young interferometer immunosensor,” Biosens. Bioelectron. **20**(7), 1417–1421 (2005) [doi:10.1016/j.bios.2004.04.015].

6. X. Fan et al., “Sensitive optical biosensors for unlabeled targets: A review,” Anal. Chim. Acta **620**(1), 8–26 (2008) [doi:10.1016/j.aca.2008.05.022].

7. M. Chistiakova, C. Shi, and A. Armani, “Label-Free, Single Molecule Resonant Cavity Detection: A Double-Blind Experimental Study,” Sensors **15**(3), 6324–6341, Multidisciplinary Digital Publishing Institute (2015) [doi:10.3390/s150306324].

8. F. Vollmer et al., “Protein detection by optical shift of a resonant microcavity,” Appl. Phys. Lett. **80**(21), 4057–4059, American Institute of Physics (2002) [doi:10.1063/1.1482797].

9. R. Mendis et al., “Terahertz microfluidic sensor based on a parallel-plate waveguide resonant cavity,” Appl. Phys. Lett. **95**(17), 171113, American Institute of Physics (2009) [doi:10.1063/1.3251079].

10. C. Fenzl, T. Hirsch, and O. S. Wolfbeis, “Photonic Crystals for Chemical Sensing and Biosensing,” Angew. Chemie Int. Ed. **53**(13), 3318–3335, WILEY-VCH Verlag (2014) [doi:10.1002/anie.201307828].

11. E. Chow et al., “Ultracompact biochemical sensor built with two-dimensional photonic crystal microcavity,” Opt. Lett. **29**(10), 1093, Optical Society of America (2004) [doi:10.1364/OL.29.001093].

12. D. Yang, H. Tian, and Y. Ji, “Nanoscale photonic crystal sensor arrays on monolithic substrates using side-coupled resonant cavity arrays,” Opt. Express **19**(21), 20023, Optical Society of America (2011) [doi:10.1364/OE.19.020023].

13. H. Nguyen et al., “Surface Plasmon Resonance: A Versatile Technique for Biosensor Applications,” Sensors **15**(5), 10481–10510, Multidisciplinary Digital Publishing Institute (2015) [doi:10.3390/s150510481].

14. S. G. Patching, “Surface plasmon resonance spectroscopy for characterisation of membrane protein–ligand interactions and its potential for drug discovery,” Biochim. Biophys. Acta - Biomembr. **1838**(1), 43–55 (2014) [doi:10.1016/j.bbamem.2013.04.028].

15. C. L. Wong and M. Olivo, “Surface Plasmon Resonance Imaging Sensors: A Review,” Plasmonics **9**(4), 809–824, Springer US (2014) [doi:10.1007/s11468-013-9662-3].

16. N. J. Halas and M. Moskovits, “Surface-enhanced Raman spectroscopy: Substrates and materials for research and applications,” MRS Bull. **38**, 607–611 (2013).

17. L. Ming, S. K. Cushing, and N. Wu, “Plasmon-enhanced optical sensors: a review,” Analyst **140**(2), 386–406, The Royal Society of Chemistry (2015) [doi:10.1039/C4AN01079E].

18. K. Bantz, A. Meyer, and N. Wittenberg, “Recent progress in SERS biosensing,” Phys. Chem. Chem. Phys. **13**, 11551–11567 (2011) [doi:10.1039/C0CP01841D].

19. M. Fan and A. G. Brolo, “Silver nanoparticles self assembly as SERS substrates with near single molecule detection limit,” Phys. Chem. Chem. Phys. **11**(34), 7381, The Royal Society of Chemistry (2009) [doi:10.1039/b904744a].

20. S. Nie and S. R. Emory, “Probing Single Molecules and Single Nanoparticles by Surface-Enhanced Raman Scattering,” Science **275**(5303), 1102–1106, American Association for the Advancement of Science (1997) [doi:10.1126/science.275.5303.1102].

21. A. M. Michaels, M. Nirmal, and L. E. Brus, “Surface Enhanced Raman Spectroscopy of Individual Rhodamine 6G Molecules on Large Ag Nanocrystals,” J. Am. Chem. Soc. **121**(43), 9932–9939, American Chemical Society (1999) [doi:10.1021/ja992128q].

22. Eric Le Ru and P. Etchegoin, *Principles of Surface-Enhanced Raman Spectroscopy: and Related Plasmonic Effects*, Elsevier (2008).

23. M. J. Banholzer et al., “Rationally designed nanostructures for surface-enhanced Raman spectroscopy,” Chem. Soc. Rev. **37**(5), 885, Royal Society of Chemistry (2008) [doi:10.1039/b710915f].

24. J. F. Betz, Y. Cheng, and G. W. Rubloff, “Direct SERS detection of contaminants in a complex mixture: rapid, single step screening for melamine in liquid infant formula,” Analyst **137**(4), 826, The Royal Society of Chemistry (2012) [doi:10.1039/c2an15846a].

25. J. Chen et al., “Fabrication of Large-Area, High-Enhancement SERS Substrates with Tunable Interparticle Spacing and Application in Identifying Microorganisms at the Single Cell Level,” J. Phys. Chem. C **116**(5), 3320–3328, American Chemical Society (2012) [doi:10.1021/jp210147c].

26. A. J. Chung, Y. S. Huh, and D. Erickson, “Large area flexible SERS active substrates using engineered nanostructures.,” Nanoscale **3**(7), 2903–2908, Royal Society of Chemistry (2011) [doi:10.1039/c1nr10265f].

27. J.-J. Feng et al., “Novel Au-Ag hybrid device for electrochemical SE(R)R spectroscopy in a wide potential and spectral range.,” Nano Lett. **9**(1), 298–303, American Chemical Society (2009) [doi:10.1021/nl802934u].

28. R. Freeman et al., “Self-assembled metal colloid monolayers: an approach to SERS substrates,” Science (80-.). **267**(5204), 1629 (1995).

29. B. C. Galarreta, P. R. Norton, and F. Lagugné-Labarthet, “SERS Detection of Streptavidin/Biotin Monolayer Assemblies,” Langmuir **27**(4), 1494–1498, American Chemical Society (2011) [doi:10.1021/la1047497].

30. U. Huebner et al., “Microfabricated polymer-substrates for SERS,” Microelectron. Eng. **98**, 444–447 (2012) [doi:10.1016/j.mee.2012.05.036].

31. Y. Jiao et al., “Patterned nanoporous gold as an effective SERS template,” Nanotechnology **22**(29), 295–302, IOP Publishing (2011) [doi:10.1088/0957-4484/22/29/295302].

32. R. Alvarez-Puebla et al., “Nanoimprinted SERS-Active Substrates with Tunable Surface Plasmon Resonances,” J. Phys. Chem. C **111**(18), 6720–6723, American Chemical Society (2007) [doi:10.1021/JP070906S].

33. C. A. Smyth et al., “Surface-enhanced Raman spectroscopy (SERS) using Ag nanoparticle films produced by pulsed laser deposition,” Appl. Surf. Sci. **264**, 31–35 (2013) [doi:10.1016/j.apsusc.2012.09.078].

34. M. Suzuki et al., “Surface-Enhanced Nonresonance Raman Scattering of Rhodamine 6G Molecules Adsorbed on Gold Nanorod Films,” Jpn. J. Appl. Phys. **43**(No. 4B), L554–L556, IOP Publishing (2004) [doi:10.1143/JJAP.43.L554].

35. Xin Sun and Hao Li, “A Review: Nanofabrication of Surface-Enhanced Raman Spectroscopy (SERS) substrates,” Curr. Nanosci. **12**, 175–183 (2016).

36. S. Z. Oo et al., “Disposable plasmonic plastic SERS sensor.,” Opt. Express **21**(15), 18484–18491, Optical Society of America (2013) [doi:10.1364/OE.21.018484].

37. J. R. Ferraro, *Introductory raman spectroscopy*, Academic Press (2003).

38. S. Friedrich and P. Hildebrandt, *Vibrational spectroscopy in life science*, John Wiley & Sons, Ltd. (2008).

39. E. Smith and G. Dent, “Modern Raman spectroscopy: a practical approach” (2013).

40. A. Fadini and F. Schnepel, *Vibrational Spectroscopy, Methods and Applications*, D. Haaland, Ed., Ellis Horwood Ltd (1989).

41. D. L. Jeanmaire and R. P. Van Duyne, “Surface raman spectroelectrochemistry,” J. Electroanal. Chem. Interfacial Electrochem. **84**(1), 1–20 (1977) [doi:10.1016/S0022-0728(77)80224-6].

42. M. G. Albrecht and J. A. Creighton, “Anomalously intense Raman spectra of pyridine at a silver electrode,” J. Am. Chem. Soc. **99**(15), 5215–5217, American Chemical Society (1977) [doi:10.1021/ja00457a071].

43. M. J. Banholzer et al., “Rationally designed nanostructures for surface-enhanced Raman spectroscopy,” Chem. Soc. Rev. **37**(5), 885, Royal Society of Chemistry (2008) [doi:10.1039/b710915f].

44. Y. S. Yamamoto and Y. Ozaki, “Recent progress and frontiers in the electromagnetic mechanism of surface-enhanced Raman scattering,” J. Photochem. Photobiol. C Photochem. Rev. **21**, 81–104 (2014) [doi:10.1016/j.jphotochemrev.2014.10.001].

45. L. Tong, T. Zhu, and Z. Liu, “Approaching the electromagnetic mechanism of surface-enhanced Raman scattering: from self-assembled arrays to individual gold nanoparticles,” Chem. Soc. Rev. **40**(3), 1296–1304, Royal Society of Chemistry (2011) [doi:10.1039/C001054P].

46. G. C. Schatz, M. A. Young, and R. P. Duyne, “Electromagnetic Mechanism of SERS,” in Surface-Enhanced Raman Scattering, pp. 19–45, Springer Berlin Heidelberg (2006) [doi:10.1007/3-540-33567-6_2].

47. P. G. Etchegoin and E. C. Le Ru, “Basic Electromagnetic Theory of SERS,” in Surface Enhanced Raman Spectroscopy: Analytical, Biophysical and Life Science Applications, S. Schlücker, Ed., iley-VCH Verlag GmbH & Co. KGaA (2010) [doi:10.1002/9783527632756.ch1].

48. G. Ozin, A. Arsenault, and L. Cademartiri, “Nanochemistry: a chemical approach to nanomaterials” (2009).

49. B. Sharma et al., “SERS: Materials, applications, and the future,” Mater. Today **15**(1–2), 16–25 (2012).

50. L. G. Quagliano, “Observation of Molecules Adsorbed on III-V Semiconductor Quantum Dots by Surface-Enhanced Raman Scattering,” J. Am. Chem. Soc. **126**(23), 7393–7398, American Chemical Society (2004) [doi:10.1021/JA031640F].

51. R. Livingstone et al., “Surface Enhanced Raman Spectroscopy of Pyridine on CdSe/ZnBeSe Quantum Dots Grown by Molecular Beam Epitaxy,” J. Phys. Chem. C **114**(41), 17460–17464, American Chemical Society (2010) [doi:10.1021/jp105619m].

52. A. Musumeci et al., “SERS of Semiconducting Nanoparticles (TiO2 Hybrid Composites),” J. Am. Chem. Soc. **131**(17), 6040–6041, American Chemical Society (2009) [doi:10.1021/ja808277u].

53. C. Qiu et al., “Investigation of *n* -Layer Graphenes as Substrates for Raman Enhancement of Crystal Violet,” J. Phys. Chem. C **115**(20), 10019–10025, American Chemical Society (2011) [doi:10.1021/jp111617c].

54. X. Ling et al., “Can Graphene be used as a Substrate for Raman Enhancement?,” Nano Lett. **10**(2), 553–561, American Chemical Society

(2010) [doi:10.1021/nl903414x].

55. C. N. Roy et al., “Reductant Control on Particle Size, Size Distribution and Morphology in the Process of Surface Enhanced Raman Spectroscopy Active Silver Colloid Synthesis,” J. Nanosci. Nanotechnol. **15**(2), 1771–1779 (2015) [doi:10.1166/jnn.2015.9511].

56. J. Neddersen, G. Chumanov, and T. M. Cotton, “Laser Ablation of Metals: A New Method for Preparing SERS Active Colloids,” Appl. Spectrosc. Vol. 47, Issue 12, pp. 1959-1964 **47**(12), 1959–1964, Society for Applied Spectroscopy (1993).

57. M. Kerker, D.-S. Wang, and H. Chew, “Surface enhanced Raman scattering (SERS) by molecules adsorbed at spherical particles,” Appl. Opt. **19**(19), 3373, Optical Society of America (1980) [doi:10.1364/AO.19.003373].

58. K. D. Alexander et al., “A high-throughput method for controlled hot-spot fabrication in SERS-active gold nanoparticle dimer arrays,” J. Raman Spectrosc. **40**(12), 2171–2175, John Wiley & Sons, Ltd. (2009) [doi:10.1002/jrs.2392].

59. P. Lee and D. Meisel, “Adsorption and surface-enhanced Raman of dyes on silver and gold sols,” J. Phys. Chem. **86**(17), 3391–3395 (1982).

60. K. Kneipp et al., “Detection and identification of a single DNA base molecule using surface-enhanced Raman scattering (SERS),” Phys. Rev. E **57**(6), R6281–R6284, American Physical Society (1998) [doi:10.1103/PhysRevE.57.R6281].

61. K. Kneipp et al., “Single Molecule Detection Using Surface-Enhanced Raman Scattering (SERS),” Phys. Rev. Lett. **78**(9), 1667–1670, American Physical Society (1997) [doi:10.1103/PhysRevLett.78.1667].

62. V. S. Tiwarib et al., “Non-resonance SERS effects of silver colloids with different shapes,” Chem. Phys. Lett. **446**(1–3), 77–82 (2007).

63. L. Tanga et al., “SERS-active Au@Ag nanorod dimers for ultrasensitive dopamine detection,” Biosens. Bioelectron. **71**, 7–12 (2015).

64. J. L. Yao et al., “A complementary study of surface-enhanced Raman scattering and metal nanorod arrays,” Pure Appl. Chem. **72**, 221–228 (2000).

65. Seung Joon Lee, A. Andrew R. Morrill, and M. Moskovits*, “Hot Spots in Silver Nanowire Bundles for Surface-Enhanced Raman Spectroscopy,” J.

Am. Chem. Soc. **128**(7), 2200–2201, American Chemical Society (2006) [doi:10.1021/JA0578350].

66. Jiatao Zhang et al., “Surface Enhanced Raman Scattering Effects of Silver Colloids with Different Shapes,” J. Phys. Chem. B **109**(25), 12544–12548, American Chemical Society (2005) [doi:10.1021/JP050471D].

67. D. S. dos Santos, Jr. et al., “Controlling the size and shape of gold nanoparticles in fulvic acid colloidal solutions and their optical characterization using SERS,” J. Mater. Chem. **15**(29), 3045, The Royal Society of Chemistry (2005) [doi:10.1039/b506218g].

68. P. H. C. Camargo et al., “Measuring the SERS enhancement factors of dimers with different structures constructed from silver nanocubes,” Chem. Phys. Lett. **484**(4–6), 304–308 (2010).

69. Y. Yang et al., “Galvanic Replacement-Free Deposition of Au on Ag for Core–Shell Nanocubes with Enhanced Chemical Stability and SERS Activity,” J. Am. Chem. Soc. **136**(23), 8153–8156, American Chemical Society (2014) [doi:10.1021/ja502472x].

70. Q. Su et al., “A Reproducible SERS Substrate Based on Electrostatically Assisted APTES-Functionalized Surface-Assembly of Gold Nanostars,” ACS Appl. Mater. Interfaces **3**(6), 1873–1879, American Chemical Society (2011) [doi:10.1021/am200057f].

71. A. M. Fales, H. Yuan, and T. Vo-Dinh, “Silica-Coated Gold Nanostars for Combined Surface-Enhanced Raman Scattering (SERS) Detection and Singlet-Oxygen Generation: A Potential Nanoplatform for Theranostics,” Langmuir **27**(19), 12186–12190, American Chemical Society (2011) [doi:10.1021/la202602q].

72. M. Schütz et al., “Hydrophilically stabilized gold nanostars as SERS labels for tissue imaging of the tumor suppressor p63 by immuno-SERS microscopy,” Chem. Commun. **47**(14), 4216, Royal Society of Chemistry (2011) [doi:10.1039/c0cc05229a].

73. W. Shen et al., “Reliable Quantitative SERS Analysis Facilitated by Core-Shell Nanoparticles with Embedded Internal Standards,” Angew. Chemie Int. Ed. **54**(25), 7308–7312, WILEY-VCH Verlag (2015) [doi:10.1002/anie.201502171].

74. G. L. Liu et al., “Magnetic Nanocrescents as Controllable Surface-Enhanced Raman Scattering Nanoprobes for Biomolecular Imaging,” Adv. Mater. **17**(22), 2683–2688, WILEY-VCH Verlag (2005) [doi:10.1002/adma.200501064].

75. Dustin J. Maxwell, and Steven R. Emory, and S. Nie*, “Nanostructured Thin-Film Materials with Surface-Enhanced Optical Properties,” American Chemical Society (2001) [doi:10.1021/CM0009120].

76. Z. Wang et al., “The structural basis for giant enhancement enabling single-molecule Raman scattering.,” Proc. Natl. Acad. Sci. U. S. A. **100**(15), 8638–8643, National Academy of Sciences (2003) [doi:10.1073/pnas.1133217100].

77. R. Freeman et al., “Self-assembled metal colloid monolayers: an approach to SERS substrates,” Science (80-.). **267**(5204), 1629–1632 (1995).

78. S. Lal et al., “Tailoring plasmonic substrates for surface enhanced spectroscopies.,” Chem. Soc. Rev. **37**(5), 898–911, Royal Society of Chemistry (2008) [doi:10.1039/b705969h].

79. Hui Wang, A. Carly S. Levin, and N. J. Halas, “Nanosphere Arrays with Controlled Sub-10-nm Gaps as Surface-Enhanced Raman Spectroscopy Substrates,” J. Am. Chem. Soc. **127**(43), 14992–14993, American Chemical Society (2005) [doi:10.1021/JA055633Y].

80. Y. V. Ryabchikov et al., “Structural properties of gold-silicon nanohybrids formed by femtosecond laser ablation in water at different fluences,” 9 March 2016, 97370F, International Society for Optics and Photonics [doi:10.1117/12.2217777].

81. H. Zhang et al., “Determination of Pesticides by Surface-Enhanced Raman Spectroscopy on Gold Nanoparticle Modified Polymethacrylate,” Anal. Lett. **49**(14), 2268–2278, Taylor & Francis (2016).

82. A. M. Schwartzberg et al., “Unique Gold Nanoparticle Aggregates as a Highly Active Surface-Enhanced Raman Scattering Substrate,” J. Phys. Chem. B **108**(50), 19191–19197, American Chemical Society (2004) [doi:https://doi.org/10.1021/jp048430p].

83. S. Farquharson et al., “Rapid detection and identification of overdose drugs in saliva by surface-enhanced Raman scattering using fused gold colloids.,” Pharmaceutics **3**(3), 425–439, Molecular Diversity Preservation International (2011) [doi:10.3390/pharmaceutics3030425].

84. E. P. Hoppmann, W. W. Yu, and I. M. White, “Inkjet-Printed Fluidic Paper Devices for Chemical and Biological Analytics Using Surface Enhanced Raman spectroscopy,” IEEE J. Sel. Top. Quantum Electron. **20**(3), 195–204 (2014) [doi:10.1109/JSTQE.2013.2286076].

85. K. C. Vernon et al., “Physical mechanisms behind the SERS enhancement

of pyramidal pit substrates," J. Raman Spectrosc. **41**(10), 1106–1111, John Wiley & Sons, Ltd. (2010) [doi:10.1002/jrs.2557].

86. M. Lin et al., "Detection of Melamine in Gluten, Chicken Feed, and Processed Foods Using Surface Enhanced Raman Spectroscopy and HPLC," J. Food Sci. **73**(8), T129–T134, Blackwell Publishing Inc (2008) [doi:10.1111/j.1750-3841.2008.00901.x].

87. L. He et al., "A new approach to measure melamine, cyanuric acid, and melamine cyanurate using surface enhanced Raman spectroscopy coupled with gold nanosubstrates," Sens. Instrum. Food Qual. Saf. **2**(1), 66–71, Springer-Verlag (2008) [doi:10.1007/s11694-008-9038-0].

88. Y. Sawai et al., "Observation of a Small Number of Molecules at a Metal Nanogap Arrayed on a Solid Surface Using Surface-Enhanced Raman Scattering," J. Am. Chem **129**(6), 1658–1662, American Chemical Society (2007) [doi:10.1021/JA067034C].

89. M. Fleischmann, P. J. Hendra, and A. J. McQuillan, "Raman spectra of pyridine adsorbed at a silver electrode," Chem. Phys. Lett. **26**(2), 163–166 (1974) [doi:10.1016/0009-2614(74)85388-1].

90. J. Law et al., "Rapid methods for the detection of foodborne bacterial pathogens: principles, applications, advantages and limitations.," Front. Microbiol. **5**(770) (2014).

91. V. Velusamy et al., "An overview of foodborne pathogen detection: in the perspective of biosensors.," Biotechnol. Adv. **28**(2), 232–254 (2010) [doi:10.1016/j.biotechadv.2009.12.004].

92. N. A. Mungroo, G. Oliveira, and S. Neethirajan, "SERS based point-of-care detection of food-borne pathogens," Microchim. Acta **183**(2), 697–707 (2015) [doi:10.1007/s00604-015-1698-y].

93. S. Efrima and B. V Bronk, "Silver colloids impregnating or coating bacteria," J. Phys. Chem. B **102**(31), 5947–5950, American Chemical Society (1998) [doi:10.1021/jp9813903].

94. K. Hering et al., "SERS: a versatile tool in chemical and biochemical diagnostics," Anal. Bioanal. Chem. **390**(1), 113–124, Springer-Verlag (2008) [doi:10.1007/s00216-007-1667-3].

95. Y.-S. Lia and J. S. Church, "Raman spectroscopy in the analysis of food and pharmaceutical nanomaterials," J. Food Drug Anal. **22**(1), 29–48 (2014).

96. X. X. Han, Y. Ozaki, and B. Zhao, “Label-free detection in biological applications of surface-enhanced Raman scattering,” TrAC Trends Anal. Chem. **38**, 67–78 (2012).

97. M. Harz, P. Rösch, and J. Popp, “Vibrational spectroscopy—A powerful tool for the rapid identification of microbial cells at the single-cell level,” Cytometry. A **75**(2), 104–113 (2009) [doi:10.1002/cyto.a.20682].

98. L. Zeiri and S. Efrima, “Surface-enhanced Raman spectroscopy of bacteria: the effect of excitation wavelength and chemical modification of the colloidal milieu,” J. Raman Spectrosc. **36**(6–7), 667–675, John Wiley & Sons, Ltd. (2005) [doi:10.1002/jrs.1349].

99. L. Zeiri et al., “Surface-Enhanced Raman Spectroscopy as a Tool for Probing Specific Biochemical Components in Bacteria,” Appl. Spectrosc. **58**(1), 33–40, SAGE PublicationsSage UK: London, England (2004) [doi:10.1366/000370204322729441].

100. R. M. Jarvis, A. Brooker, and Royston Goodacre, “Surface-Enhanced Raman Spectroscopy for Bacterial Discrimination Utilizing a Scanning Electron Microscope with a Raman Spectroscopy Interface,” Anal. Chem. **76**(17), 5198–5202, American Chemical Society (2004) [doi:10.1021/AC049663F].

101. A. Sengupta, M. Mujacic, and E. J. Davis, “Detection of bacteria by surface-enhanced Raman spectroscopy,” Anal. Bioanal. Chem. **386**(5), 1379–1386, Springer-Verlag (2006) [doi:10.1007/s00216-006-0711-z].

102. H. Zhou et al., “SERS detection of bacteria in water by in situ coating with Ag nanoparticles.,” Anal. Chem. **86**(3), 1525–1533, American Chemical Society (2014) [doi:10.1021/ac402935p].

103. S. P. Ravindranath, Y. Wang, and J. Irudayaraj, “SERS driven cross-platform based multiplex pathogen detection,” Sensors Actuators B Chem. **152**(2), 183–190 (2011) [doi:10.1016/j.snb.2010.12.005].

104. T. A. Alexander, P. M. Pellegrino, and J. B. Gillespie, “Near-Infrared Surface-Enhanced-Raman-Scattering-Mediated Detection of Single Optically Trapped Bacterial Spores,” Appl. Spectrosc. **57**(11), 1340–1345, SAGE PublicationsSage UK: London, England (2003) [doi:10.1366/000370203322554482].

105. V. Biju et al., “Combined Spectroscopic and Topographic Characterization of Nanoscale Domains and Their Distributions of a Redox Protein on Bacterial Cell Surfaces,” American Chemical Society (2006) [doi:10.1021/LA061343Z].

106. E. Temur et al., “A highly sensitive detection platform based on surface-enhanced Raman scattering for Escherichia coli enumeration.,” Anal. Bioanal. Chem. **397**(4), 1595–1604 (2010) [doi:10.1007/s00216-010-3676-x].

107. C. Fan et al., “Rapid detection of food- and waterborne bacteria using surface-enhanced Raman spectroscopy coupled with silver nanosubstrates.,” Appl. Microbiol. Biotechnol. **92**(5), 1053–1061 (2011) [doi:10.1007/s00253-011-3634-3].

108. W. R. Premasiri et al., “Characterization of the surface enhanced raman scattering (SERS) of bacteria.,” J. Phys. Chem. B **109**(1), 312–320, American Chemical Society (2005) [doi:10.1021/jp040442n].

109. A. Szeghalmi et al., “Time Fluctuations and Imaging in the SERS Spectra of Fungal Hypha Grown on Nanostructured Substrates,” J. Phys. Chem. B **111**(44), 12916–12924, American Chemical Society (2007) [doi:10.1021/JP075422A].

110. Ö. Aydin et al., “Surface-Enhanced Raman Scattering of Rat Tissues,” Appl. Spectrosc. **63**(6), 662–668, SAGE PublicationsSage UK: London, England (2009) [doi:10.1366/000370209788559647].

111. K. Kneipp et al., “Surface-Enhanced Raman Spectroscopy in Single Living Cells Using Gold Nanoparticles,” Appl. Spectrosc. **56**(2), 150–154, SAGE PublicationsSage UK: London, England (2002) [doi:10.1366/0003702021954557].

112. M. Culha et al., “Rapid identification of bacteria and yeast using surface-enhanced Raman scattering,” Surf. Interface Anal. **42**(6–7), 462–465, John Wiley & Sons, Ltd. (2010) [doi:10.1002/sia.3256].

113. P. Rösch et al., “The identification of microorganisms by micro-Raman spectroscopy,” J. Mol. Struct. **661**, 363–369 (2003) [doi:10.1016/j.molstruc.2003.06.004].

114. S. B. Rodriguez, M. A. Thornton, and R. J. Thornton, “Raman Spectroscopy and Chemometrics for Identification and Strain Discrimination of the Wine Spoilage Yeasts Saccharomyces cerevisiae, Zygosaccharomyces bailii, and Brettanomyces bruxellensis,” Appl. Environ. Microbiol. **79**(20), 6264–6270, American Society for Microbiology (2013) [doi:10.1128/AEM.01886-13].

115. M. Stratford, *Food and beverage spoilage yeasts*, in Yeasts in food and beverages, Springer Berlin Heidelberg (2006).

116. C. Greulich et al., “The toxic effect of silver ions and silver nanoparticles towards bacteria and human cells occurs in the same concentration range,” RSC Adv. **2**(17), 6981, Royal Society of Chemistry (2012) [doi:10.1039/c2ra20684f].

117. R. Shukla et al., “Biocompatibility of Gold Nanoparticles and Their Endocytotic Fate Inside the Cellular Compartment: A Microscopic Overview,” Langmuir **21**(23), 10644–10654, American Chemical Society (2005) [doi:https://doi.org/10.1021/la0513712].

118. A. M. Alkilany and C. J. Murphy, “Toxicity and cellular uptake of gold nanoparticles: what we have learned so far?,” J. Nanoparticle Res. **12**(7), 2313–2333, Springer Netherlands (2010) [doi:10.1007/s11051-010-9911-8].

119. I. R. Lewis and H. G. M. Edwards, *Handbook of Raman spectroscopy from the research laboratory to the process line*, Marcel Dekker (2001).

120. G. S. Bumbrah and R. M. Sharma, “Raman spectroscopy – Basic principle, instrumentation and selected applications for the characterization of drugs of abuse,” Egypt. J. Forensic Sci. **6**(3), 209–215 (2016) [doi:10.1016/j.ejfs.2015.06.001].

121. W. Song, D. Psaltis, and K. B. Crozier, “Superhydrophobic bull’s-eye for surface-enhanced Raman scattering,” Lab Chip **14**(20), 3907–3911, Royal Society of Chemistry (2014) [doi:10.1039/C4LC00477A].

122. F. Xu et al., “Silver Nanoparticles Coated Zinc Oxide Nanorods Array as Superhydrophobic Substrate for the Amplified SERS Effect,” J. Phys. Chem. C **115**(20), 9977–9983, American Chemical Society (2011) [doi:10.1021/jp201897j].

123. F. De Angelis et al., “Breaking the diffusion limit with super-hydrophobic delivery of molecules to plasmonic nanofocusing SERS structures,” Nat. Photonics **5**(11), 682–687, Nature Research (2011) [doi:10.1038/nphoton.2011.222].

124. L. Chen et al., “Label-free NIR-SERS discrimination and detection of foodborne bacteria by in situ synthesis of Ag colloids,” J. Nanobiotechnology **13**(45) (2015) [doi:10.1186/s12951-015-0106-4].

125. X. Zhao et al., “Advances in rapid detection methods for foodborne pathogens,” J. Microbiol. Biotechnol **24**(3), 297–312 (2014).

126. A. E. Grow et al., “New biochip technology for label-free detection of pathogens and their toxins,” J. Microbiol. Methods **53**(2), 221–233 (2003)

[doi:10.1016/S0167-7012(03)00026-5].

127. Z. Tian et al., “Expanding generality of surface-enhanced Raman spectroscopy with borrowing SERS activity strategy,” Chem. Commun.(34) (2007).

128. K. Weidemaier et al., “Real-time pathogen monitoring during enrichment: a novel nanotechnology-based approach to food safety testing.,” Int. J. Food Microbiol. **198**, 19–27 (2015) [doi:10.1016/j.ijfoodmicro.2014.12.018].

129. U. Tamer et al., “Fabrication of magnetic gold nanorod particles for immunomagnetic separation and SERS application,” J. Nanoparticle Res. **13**(8), 3167–3176 (2011) [doi:10.1007/s11051-010-0213-y].

130. A. Bogner et al., “A history of scanning electron microscopy developments: Towards ‘wet-STEM’ imaging,” Micron **38**(4), 390–401 (2007).

131. K. D. Vernon-Parry, “Scanning electron microscopy: an introduction,” III-Vs Rev. **13**(4), 40–44 (2000) [doi:10.1016/S0961-1290(00)80006-X].

132. R. F. Egerton, *Physical principles of electron microscopy : an introduction to TEM, SEM, and AEM*, Springer Science+Business Media (2005).

133. C. Y. Tang and Z. Yang, “Transmission Electron Microscopy (TEM),” in Membrane Characterization, pp. 145–159, Elsevier (2017) [doi:10.1016/B978-0-444-63776-5.00008-5].

134. J. Workman and A. W. Springsteen, *Applied spectroscopy : a compact reference for practitioners*, Academic Press (1998).

135. B. S. Luo and M. Lin, “A portable Raman system for the identification of foodborne pathogenic bacteria,” J. Rapid Methods Autom. Microbiol. **16**(3), 238–255 (2008) [doi:10.1111/j.1745-4581.2008.00131.x].

136. M. Zimmermann et al., “Modeling and Optimization of High-Sensitivity, Low-Volume Microfluidic-Based Surface Immunoassays,” Biomed. Microdevices **7**(2), 99–110, Kluwer Academic Publishers (2005) [doi:10.1007/s10544-005-1587-y].

137. W. Hüttner et al., “Implementation of substrates for surface-enhanced Raman spectroscopy for continuous analysis in an optofluidic device,” Microfluid. Nanofluidics **12**(1–4), 521–527, Springer-Verlag (2012) [doi:10.1007/s10404-011-0893-3].

138. A. Troy A. and L. Dianna, “Characterization of a commercialized SERS-active substrate and its application to the identification of intact Bacillus

endospores," Appl. Opt. **46**(18), 3878 (2007).

139. C. Fan et al., "Detecting Food- and Waterborne Viruses by Surface-Enhanced Raman Spectroscopy," J. Food Sci. **75**(5), Blackwell Publishing Inc (2010) [doi:10.1111/j.1750-3841.2010.01619.x].

140. M. Çulha and M. Kahraman, "Surface-Enhanced Raman Scattering of Bacteria in Microwells Constructed from Silver Nanoparticles," J. Nanotechnol. (2012) [doi:http://dx.doi.org/10.1155/2012/297560].

141. S. Vohník et al., "Conformation, stability, and active-site cysteine titrations of Escherichia coli D26A thioredoxin probed by Raman spectroscopy.," Protein Sci. **7**(1), 193–200 (1998) [doi:10.1002/pro.5560070120].

142. C. Fan et al., "Rapid detection of food-and waterborne bacteria using surface-enhanced Raman spectroscopy coupled with silver nanosubstrates," Appl. Microbiol. Biotechnol. **92**(5), 1053–1061 (2011).

143. H. Al-Qadiri and M. Lin, "Detection of Sublethal Thermal Injury in Salmonella enterica Serotype Typhimurium and Listeria monocytogenes Using Fourier Transform Infrared (FT-IR)," J. Food Sci. **73**(2) (2008).

144. K. Maquelin et al., "Identification of medically relevant microorganisms by vibrational spectroscopy," J. Microbiol. Methods **51**(3), 255–271 (2002) [doi:10.1016/S0167-7012(02)00127-6].

145. L. Cui et al., "Interrogating chemical variation via layer-by-layer SERS during biofouling and cleaning of nanofiltration membranes with further investigations into cleaning efficiency," Water Res. **87**(15), 282–291 (2015).

146. Y. Liu et al., "Potential of Surface-Enhanced Raman Spectroscopy for the Rapid Identification of *Escherichia Coli* and *Listeria Monocytogenes* Cultures on Silver Colloidal Nanoparticles," Appl. Spectrosc. **61**(8), 824–831, Society for Applied Spectroscopy (2007).

147. X. Lu et al., "Application of Mid-infrared and Raman Spectroscopy to the Study of Bacteria," Food Bioprocess Technol. **4**(6), 919–935 (2011) [doi:10.1007/s11947-011-0516-8].

148. K. Maquelin and L. Choo-Smith, "Raman spectroscopic method for identification of clinically relevant microorganisms growing on solid culture medium," Anal. Chem. **72**(1), 12–19 (2000).

149. K. Kairyte, Z. Luksiene, and V. Sablinskas, "Identification of different Listeria monocytogenes strains by surface enhanced FT Raman

spectroscopy," Chem. Technol. **61**(3), 46–49 (2012) [doi:10.5755/j01.ct.61.3.2712].

150. G. Long and J. Winefordner, "Limit of detection. A closer look at the IUPAC definition," Anal. Chem. (1983).

151. N. Gnanou Besse et al., "Evolution of Listeria populations in food samples undergoing enrichment culturing.," Int. J. Food Microbiol. **104**(2), 123–134 (2005) [doi:10.1016/j.ijfoodmicro.2005.01.012].

152. M. Li et al., "Stamping surface-enhanced Raman spectroscopy for label-free, multiplexed, molecular sensing and imaging.," J. Biomed. Opt. **19**(5), 50501, International Society for Optics and Photonics (2014) [doi:10.1117/1.JBO.19.5.050501].

153. V. Loureiro and M. Malfeito-Ferreira, "Spoilage yeasts in the wine industry," Int. J. Food Microbiol. **86**(1), 23–50 (2003) [doi:10.1016/S0168-1605(03)00246-0].

154. V. Loureiro and A. Querol, "The prevalence and control of spoilage yeasts in foods and beverages," Trends Food Sci. Technol. **10**(11), 356–365 (1999) [doi:10.1016/S0924-2244(00)00021-2].

155. V. Loureiro, "Spoilage yeasts in foods and beverages: characterisation and ecology for improved diagnosis and control," Food Res. Int. **33**(3), 247–256 (2000) [doi:10.1016/S0963-9969(00)00044-2].

156. M. Amorim et al., "Nutritional ingredients from spent brewer's yeast obtained by hydrolysis and selective membrane filtration integrated in a pilot process," J. Food Eng. **185**, 42–47 (2016) [doi:10.1016/j.jfoodeng.2016.03.032].

157. J. I. Pitt and A. D. Hocking, "Methods for Isolation, Enumeration and Identification," in Fungi and Food Spoilage, pp. 19–52, Springer US, Boston, MA (2009) [doi:10.1007/978-0-387-92207-2_4].

158. A. F. Chrimes et al., "In situ SERS probing of nano-silver coated individual yeast cells," Biosens. Bioelectron. **49**, 536–541 (2013) [doi:10.1016/j.bios.2013.05.053].

159. A. Sujith et al., "Imaging the cell wall of living single yeast cells using surface-enhanced Raman spectroscopy," Anal. Bioanal. Chem. **394**(7), 1803–1809, Springer-Verlag (2009) [doi:10.1007/s00216-009-2883-9].

160. R. Gessner et al., "Raman spectroscopy investigation of biological materials by use of etched and silver coated glass fiber tips," Biopolymers

67(4–5), 327–330, Wiley Subscription Services, Inc., A Wiley Company (2002) [doi:10.1002/bip.10090].

161. K. M. Syamala et al., “Inhibition Assay of Yeast Cell Walls by Plasmon Resonance Rayleigh Scattering and Surface-Enhanced Raman Scattering Imaging,” Langmuir **28**(24), 8952–8958, American Chemical Society (2012) [doi:https://doi.org/10.1021/la3004245].

162. I. Sayin et al., “Characterization of Yeast Species Using Surface-Enhanced Raman Scattering,” Appl. Spectrosc. **63**(11), 1276–1282, Society for Applied Spectroscopy (2009).

163. A. Sujith et al., “Surface enhanced Raman scattering analyses of individual silver nanoaggregates on living single yeast cell wall,” Appl. Phys. Lett. **92**(10), 103901, AIP Publishing (2008) [doi:10.1063/1.2891086].

164. E. Martin et al., “Isolation of a Wickerhamomyces anomalus yeast strain from the sandfly Phlebotomus perniciosus , displaying the killer phenotype,” Med. Vet. Entomol. **30**(1), 101–106, Blackwell Publishing Ltd (2016) [doi:10.1111/mve.12149].

165. N. Hayashi et al., “Detection and identification of Brettanomyces/Dekkera sp. yeasts with a loop-mediated isothermal amplification method,” Food Microbiol. **24**(7), 778–785 (2007) [doi:10.1016/j.fm.2007.01.007].

166. Z. Aksu and A. T. Eren, “Carotenoids production by the yeast Rhodotorula mucilaginosa: Use of agricultural wastes as a carbon source,” Process Biochem. **40**(9), 2985–2991 (2005) [doi:10.1016/j.procbio.2005.01.011].

167. A. Laitila et al., “Yeasts in malting, with special emphasis on Wickerhamomyces anomalus (synonym Pichia anomala).,” Antonie Van Leeuwenhoek **99**(1), 75–84 (2011) [doi:10.1007/s10482-010-9511-8].

168. Marek Prochazka, *Surface-Enhanced Raman Spectroscopy Bioanalytical, Biomolecular and Medical Applications*, Springer International Publishing (2016) [doi:https://doi.org/10.1007/978-3-319-23992-7].

169. M. Çulha et al., “Surface-Enhanced Raman Scattering on Aggregates of Silver Nanoparticles with Definite Size,” J. Phys. Chem. C **112**(28), 10338–10343, American Chemical Society (2008) [doi:10.1021/jp711177z].

170. M. Z. Pacia et al., “Interplay between carotenoids, hemoproteins and the ‘life band’ origin studied in live Rhodotorula mucilaginosa cells by means of Raman microimaging,” Analyst **140**(6), 1809–1813, The Royal Society

of Chemistry (2015) [doi:10.1039/C4AN01787K].

171. S. Meisel et al., “Identification of meat-associated pathogens via Raman microspectroscopy,” Food Microbiol. **38**, 36–43 (2014) [doi:http://dx.doi.org/10.1016/j.fm.2013.08.007].

172. J. Guicheteau et al., “Bacterial mixture identification using Raman and surface-enhanced Raman chemical imaging,” J. Raman Spectrosc. **41**(12), 1632–1637, John Wiley & Sons, Ltd. (2010) [doi:10.1002/jrs.2601].

173. S. M. Lemma et al., “Removal of bacteria and yeast in water and beer by nylon nanofibrous membranes,” J. Food Eng. **157**, 1–6 (2015) [doi:10.1016/j.jfoodeng.2015.02.005].

174. Hamamatsu Photonics, “SERS detection module C13560,” <http://www.hamamatsu.com/eu/en/C13560.html>.

PAPER I

Performance and flow dynamics studies of polymeric optofluidic SERS sensors

Journal of the European Optical Society
– Rapid publications, 10,
DOI information: 10.2971/jeos.2015.15043.

Performance and flow dynamics studies of polymeric optofluidic SERS sensors

S. Uusitalo Sanna.uusitalo@vtt.fi — VTT Technical Research Centre of Finland, Kaitoväylä 1, 90590 Oulu, Finland; University of Oulu, Pentti Kaiteran katu 1, 90014 Oulu, Finland
J. Hiltunen — VTT Technical Research Centre of Finland, Kaitoväylä 1, 90590 Oulu, Finland
P. Karioja — VTT Technical Research Centre of Finland, Kaitoväylä 1, 90590 Oulu, Finland
S. Siitonen — Nanocomp Oy Ltd, Ensolantie 6, 80710 Lehmo, Finland
V. Kontturi — Nanocomp Oy Ltd, Ensolantie 6, 80710 Lehmo, Finland
R. Myllylä — University of Oulu, Pentti Kaiteran katu 1, 90014 Oulu, Finland
M. Kinnunen — University of Oulu, Pentti Kaiteran katu 1, 90014 Oulu, Finland
I. Meglinski — University of Oulu, Pentti Kaiteran katu 1, 90014 Oulu, Finland

We present a polymer-based optofluidic surface enhanced Raman scattering chip for biomolecule detection, serving as a disposable sensor choice with cost-effective production. The SERS substrate is fabricated by using industrial roll-to-roll UV-nanoimprinting equipment and integrated with adhesive-based polymeric microfluidics. The functioning of the SERS detection on-chip is confirmed and the effect of the polymer lid on the obtainable Raman spectra is analysed. Rhodamine 6G is used as a model analyte to demonstrate continuous flow measurements on a planar SERS substrate in a microchannel. The relation between the temporal response of the sensors and sample flow dynamics is studied with varied flow velocities, using SERS and fluorescence detection. The response time of the surface-dependent SERS signal is longer than the response time of the fluorescence signal of the bulk flow. This observation revealed the effect of convection on the temporal SERS responses at 25 µl/min to 1000 µl/min flow velocities. The diffusion of analyte molecules from the bulk concentration into the sensing surface induces about a 40-second lag time in the SERS detection. This lag time, and its rising trend with slower flow velocities, has to be taken into account in future trials of the optofluidic SERS sensor, with active analyte binding on the sensing surface.
[DOI: http://dx.doi.org/10.2971/jeos.2015.15043]

Keywords: SERS optofluidic polymer biosensor continuous flow

1 INTRODUCTION

Optical biosensing is a diverse and evolving research field aiming for simplified and high-sensitivity diagnostic tools for the detection of biologicals/chemicals in environmental monitoring, medical analysis, food safety, and security. In particular, label-free approaches are interesting since they do not require label molecules to be added, which could disturb the binding event, non-specifically adsorb to the surface and complicate the process with extra cleaning steps. This has motivated the development of label-free optical sensor technologies, including interferometric, resonant-cavity, photonic crystal, surface plasmon resonance (SPR), and surface-enhanced Raman scattering (SERS) sensors [1]–[3].

Polymer materials are particularly attractive in optical sensing because of their ability to be processed rapidly and cost-effectively with high yields. Polymers attain a large number of good optical properties, including high optical transmittance, versatile processability at relatively low temperatures, and the potential for low-cost mass-production. UV lithography has been widely used in the fabrication of conventional optical devices. The resolution obtained with this technique is limited by the effects of wave diffraction and scattering. Compared with conventional techniques, UV-imprint lithography is easy to perform, requires low-cost equipment, and can provide high-resolution nano-scale features down to sub-10 nm. UV-imprint lithography is performed by pressing a mould onto a UV-sensitive precursor resin coating on a substrate, and by curing under UV light, a replica of the mould is formed. The process takes place at room temperature and does not require high pressure during the imprinting process. Quite recently, new fabrication methods have been developed for the UV-imprinting of optical nanophotonic sensor structures with industrial roll-to-roll devices [4].

Received June 30, 2015; revised ms. received August 17, 2015; published September 15, 2015 ISSN 1990-2573

The integration of polymeric optical sensor structures with microfluidic sample-handling circuits enables the fabrication of fully polymer-based optofluidic biosensors. In optofluidic sensors with planar sensing surfaces [5], the detection of analytes from the bulk sample relies on the transport of the analytes to the detection area and to the detection surface. Since the concentration of the analytes in the sample solution is typically low and the diffusion of the molecules is slow, the used detection method has to be sensitive in order to detect and quantify the molecules. SERS is an attractive method for the detection to meet these requirements. It does not only have high detection sensitivity, in some cases even in the range of a few molecules [6]–[9], but it also has an ability to identify the analytes through specific Raman spectra. The Raman spectra consist of the inelastically scattered light of the medium under inspection. The detected spectral lines act as individual features of the sample and can distinguish the sample contents. The sensitivity of the SERS detection is a result of interaction between metal substrates or colloids and the incident light. Surface plasmons of metal enhance the Raman scattering mainly through electromagnetic enhancement mechanism, but in some cases chemical enhancement due to chemical bonds between molecules and metal can also play a part in the phenomenon [10]. The enhancement factor has been proved to be even as high as 10^{10} for a bunch of aggregated metal colloids and commonly around 10^6 -10^7 for metal substrates. Although the enhancement induced by the colloid aggregates can be stronger than the signal strength acquired with metal substrates, the repeatability of the signal response is worse. A similar problem exists with randomly ragged metal substrates [11]. During the last decade the repeatability issue has been tackled by fabrication of more consistent planar SERS surfaces [12]–[16]. These surfaces have plasmonic elements with a defined shape, leading to a more uniform enhancement effect. Consistent solid SERS surfaces have inspired the idea of an optofluidic SERS chip, and this has raised wide research interest in the last 10 years [17].

The current aim of a disposable optofluidic sensor requires new fabrication methods and parting from the conventional fabrication of silicon-based sensors. There are a couple of recent studies focusing on low-cost approaches such as soft lithography. In the study by Liu et al., polydimethylsiloxane (PDMS) patterning was utilised in the fabrication of SERS structures with an integrated glass microfluidic circuit [18]. Lamberti et al introduced an all-PDMS-based system in which the SERS structures were fabricated by sputtering nanoparticles on PDMS [19]. However, the industrial-scale production of consistently and accurately patterned PDMS is still quite difficult.

In this work, we introduce an optofluidic sensor, which combines polymeric roll-to-roll nano-imprinted (NIL) SERS surfaces with adhesive-based microfluidic parts. According to the previous study with a benzyl mercaptan ($C_6H_5CH_2SH$) test molecule on top of the R2R fabricated SERS structure without fluidics integration, the used SERS surface can provide up to 10^7 a enhancement factor with good reproducibility (5%) [4]. A SEM image of the R2R patterned SERS surface and a close-up picture of one pyramid-shaped well are shown in Figure 1.

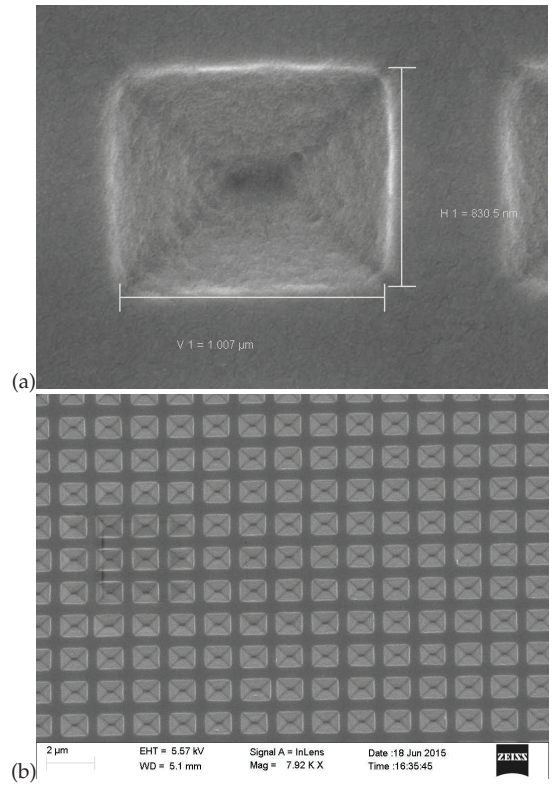

FIG. 1 a) Close-up picture of the pyramid-shaped well of the R2R fabricated SERS surface; b) A top picture of multiple SERS patterns.

The combination of a UV-imprinted SERS surface on plastic and polymer microfluidics makes the whole sensor polymer-based, with an evaporated thin gold layer as the only exception to the rule. This disposable sensor is suitable for industrial-scale fabrication with low material costs and easy fabrication methods. It enables constant monitoring of chemical and biological reactions on-chip, due to the high sensitivity of the SERS and the miniaturised sample volumes offered by the microfluidic liquid handling. Continuous flow on-chip enables consecutive sampling and washing steps, and reveals the dynamic abilities of the sensor. We studied the optical capabilities of the sensor with Rhodamine 6G (R6G) model analyte.

2 BASIC THEORY OF FLUIDICS AND MOLECULE TRANSPORT

To understand the effect of flow dynamics on the detected optical signal, the phenomena behind the transport of the sample molecules from the bulk flow into the detection surface must be considered. With optical detection surfaces, such as in SPR and planar SERS, the flow in a microchannel has a strong influence on the recorded signal. The bulk flow in the microfluidic channels is often produced by pump-inflicted pressure. The pressure-driven flow carries the sample molecules into the detection area, where the induced signal can be observed. In SERS, the sample molecules arriving on top of the detec-

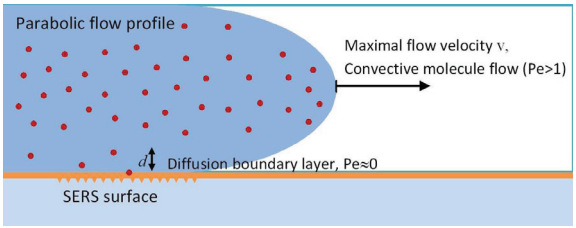

FIG. 2 A schematic of the relation between convective and diffusive flow in a microchannel. The effect of diffusion and convection can be theoretically considered through diffusion boundary layer thickness d and the Peclet number. The dimensionless Peclet number is a ratio between the conductive and the diffusive transport rate of the analyte molecules. In the middle of the channel Pe $\ll$ 1, near the walls Pe≈0 [26].

tion area need to be in the near vicinity of the plasmonic surface to be detected. Typically, the induced signal originates from the sample molecules adsorbed onto the detection surface. The nature of the flow in a microchannel can be theoretically assessed using Reynold's number. Reynold's number is a dimensionless value defining the ratio between inertial and viscous forces encountered by the fluid in the channel:

$$Re = \rho_m u_m D_h / \mu_m \ , \tag{1}$$

where u_m, ρ_m and μ_m are the mean flow velocity, the mean density, and the mean dynamic viscosity of the fluid, respectively. D_h is the hydraulic diameter of the detection chamber. For a rectangular chamber, the diameter can be computed from the equation

$$D_h = \frac{2WH}{W+H} \ , \tag{2}$$

where W is the width of the microchannel and H is the height of the channel [20]. The flow is surely laminar when the Reynold's number is 2100 or less [21]. For a microchannel with smooth channel walls, the number is typically well under this limit. In our case the Reynolds number is 10 or less for the flow velocities used in this study, and the flow is thus laminar. The molecule transport inside a microchannel can be divided into three regions: the middle region far from channel walls, where convection (drift) is the dominant driving force of the molecules; the hybrid region, where convection is fainter and diffusion plays a role in the net effect; and the region very near the channel walls, where diffusion is the only transport mechanism. The flow profile of the pressure-driven aqueous fluid in a microfluidic channel is characteristically parabolic due to the friction between the fluid and the channel walls [21, 22]. Thus the fluid has the highest velocity in the middle of the channel, and the velocity reduces as the observation point moves nearer to the walls. Typically the fluid velocity vanishes completely at a distance of one molecule layer from the wall. This is called the non-slip condition, in which the molecules adjacent to the channel wall do not move with the flow due to the friction between the wall and the molecules [23]–[25]. Since the flow velocity diminishes near the walls, the transport of the sample molecules inside this region by convection is negligible. Figure 2 depicts a situation where the flow velocity of the fluid is at maximum in the middle of the channel, and the convective flow vanishes near the walls.

The zone near the wall, where diffusion is the dominant transport mechanism, is called the diffusion boundary layer. There are several studies on the effect of the diffusion boundary layer on the detection mechanism of the biosensor analysed using empirical and computational methods [21, 22], [27]–[31]. The phenomena affecting the results include the binding reaction of the analytes to the sensor surface (association and dissociation rate constants) and the relation of convection and diffusion in the diffusion boundary layer [26], [32]–[35]. Studies on SPR have shown that the measured kinetic reaction rates deviate from the values acquired using other verified methods if all the phenomena related to the signal construction with planar sensing are not carefully considered. The finite element method (FEM) has been used to study the relationship between molecule transport and the adsorption process at the surface [21, 30, 31]. The optical signal response depends on the flow dynamics through the limitations of mass transport of molecules and kinetic binding reactions. In mass transport limited flow, the transport of analytes to the sensor surface is so slow that the signal rise times are growing by the lack of analyte molecules in the vicinity of the surface. This phenomenon includes the effects of insufficient molecule transport to the diffusion boundary layer by convective flow and the effect of the diffusion boundary layer. While insufficient molecule transport can cause analyte depletion near the sensor surface, the effect of the diffusion boundary layer in non-slip conditions makes the signal rise times longer due to slow molecule diffusion. As the bulk flow velocity increases, the effect of transport limitation decreases. This is due to the disappearance of the depletion effect caused by the slow convective flow. For example, kinetic reaction studies using commercial SPR sensors strive to stay outside the region where the optical response is heavily influenced by the mass transport limitation [26], [36]–[38]. By using high enough flow rates ($\geq$ 50 µl/min), the concentration of the analyte at the surface can be the same as that in the bulk, and the measured signal reflects binding kinetics [38]. However, with too high flow rates, the signal response can encounter a new limitation due to the reaction kinetics of the analyte binding. This kinetic limitation occurs when the binding rates are slow and bulk flow velocity is high. The analytes are transported over the detection zone so rapidly that very few of them have enough time to bind to the surface. When maximal surface coverage of analytes is desired, the used flow rate is often a compromise between the efficient transport of analyte molecules to the surface and the suitable flow velocity for adsorption [21]. Adsorption can occur with physical or chemical bonding to the surface or to the receptors/ligands on top of the surface. In this study, we can ignore the factor of analyte-ligand binding, since no ligands are at the detection surface and the bonding happens through Van der Walls forces by physisorption [39, 40]. Arrival of the analytes at the surface and the binding through physisorption can be described as a two-phase process:

$$A_{Bulk} \overset{\text{Diffusion}}{\Longleftrightarrow} A_{Surface} \tag{3}$$

$$A_{Surface} \overset{\text{Adsorption}}{\Longleftrightarrow} A_{Bound} \ , \tag{4}$$

where A_{Bulk} is the free analyte in bulk flow of liquid medium [1/cm^3], $A_{Surface}$ is the free analyte in liquid medium in the

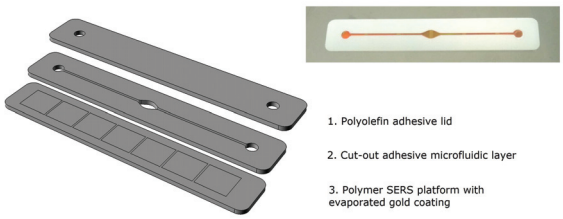

FIG. 3 Schematic of the optofluidic SERS chip with an oval detection chamber: Lid layer optically clear 3M 9795R polyolefin adhesive patterned with a cutting plotter, middle layer 220 µm 3M adhesive patterned with the cutting plotter, and bottom layer with UV-imprinted SERS patterns and metal coating.

immediate vicinity of the surface [$1/cm^3$], and A_{Bound} is the adsorbed analyte on the surface [$1/cm^2$].

3 DEVICE FABRICATION

The SERS substrates used in this study were produced by replicating the SERS pattern on top of a polymer sheet with a roll-to-roll (R2R) process. A UV-curable lacquer coating was applied on top of a PMMA carrier web using a reverse gravure technique. The SERS structure was imprinted onto the lacquer by the embossing reel, and the lacquer was cured by UV light exposure through the PMMA carrier film. The procedure is explained in detail by Oo et al. in [4]. After die-cutting separate SERS sheets from the roll, the SERS active plasmonic layer was added by evaporating a 240 nm gold layer on top of the polymer SERS surface. The microfluidic circuits were cut from 3M adhesive by cutting plotter CraftRobo Pro S. The detection chamber of the fluidic circuit had an oval shape for optimal liquid filling with a steady fluid front, and the chamber sample volume was 2 µl. The chamber dimensions were 220 µm height and 2.67 mm maximal width. The channels leading into the chamber were 400 µm wide. The SERS substrate and the microfluidic circuit were integrated by Yosan roll laminator at room temperature. To minimise the effect of the chamber lid on the Raman signal, the microfluidic circuit was lidded with a polyolefin diagnostic adhesive (3M 9795R), which declares high optical clarity and minimal auto-fluorescence. The picture of the SERS chip and the schematic of the layers can be seen in Figure 3.

4 MEASUREMENT SET-UP

Rhodamine 6G (dye content ~95%, SigmaAldrich) solution diluted in deionized water was used as a model analyte to analyse the functioning of the polymer-based SERS chip. The optical properties of the chip were studied by filling the chip with the R6G samples and DI H_2O serving as a reference medium for the R6G in water solutions. Water is the preferred medium to be used in Raman spectroscopy as a basis for the sample solutions and as a reference, because it does not produce Raman peaks itself. In flow trials, the chip was filled with under-pressure suction produced by a syringe pump (Nexus 3000). The sample was injected into a 2 ml Eppendorf tube, from where it was transferred through the chip and Dolomite

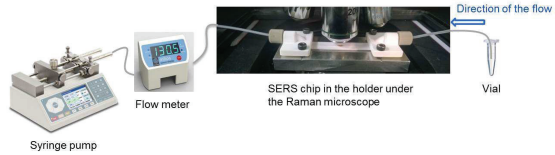

FIG. 4 The set-up for the flow studies with sample vial, chip holder, chip, Raman microscope, flow meter, and syringe pump.

flow meter into a syringe. A schematic of the flow system is presented in Figure 4.

The surface-enhanced Raman spectra were recorded using a BaySpec Nomadic Raman microscope with a 785 nm excitation wavelength. The power of the laser was set at 40 mW and a 20X magnifying objective was used in the experiments. Integration times were varied between 15 s and 30 s depending on the used R6G concentration. The BaySpec camera was used to focus the system by adjusting a sharp edge between the patterned SERS area and the smooth gold area through the polyolefin lid of the chamber before each Raman spectrum acquisition.

In a continuous flow study, the fluid flow velocity was varied from 25 µl/min to 1000 µl/min. To separate the effect of the convective flow of molecules and the mass transport of molecules on the detection surface, we measured the flow of the bulk liquid using fluorescence microscopy and the arrival of the molecules to the detection surface with SERS. To our knowledge, this is a novel method for analysing the dynamic behaviour of an optofluidic chip. 0.5 mM R6G was used as the model analyte. R6G fluoresces around the 570 nm wavelength. Water was first flowed by a syringe pump induced under pressure into the detection chamber before filling the system with dilute 0.5 mM R6G in DI H_2O. The actual flow velocities were observed during the trials with a Dolomite Mitos flow sensor. The flow was recorded as avi-files using a Zeiss fluorescence microscope camera time lapse mode with a 10 ms exposure time and 1 s interval. The same flow trial was executed for SERS detection under the BaySpec Nomadic Raman microscope and the surface-enhanced Raman spectra were recorded with a 15 s integration time and 1 s interval. The results were analysed using Matlab and Origin Pro.

5 MEASUREMENTS, RESULTS, AND DISCUSSION

With a novel polymer-based SERS sensor, we have to first validate the function of the sensor. To see if the recorded signal is surface enhanced, we began the validation by comparing the SERS signals of the R6G sample on top of the patterned SERS structure and the smooth gold coating. The used integration time for the SERS signal recording was 15 seconds. The chip was filled with DI water to gain the reference Raman spectrum caused by the polyolefin lid. Water was replaced by a 1 mM R6G sample and the Raman spectra were detected with 2*3 point image mapping on top of the patterned SERS detection area and the smooth gold area without patterning.

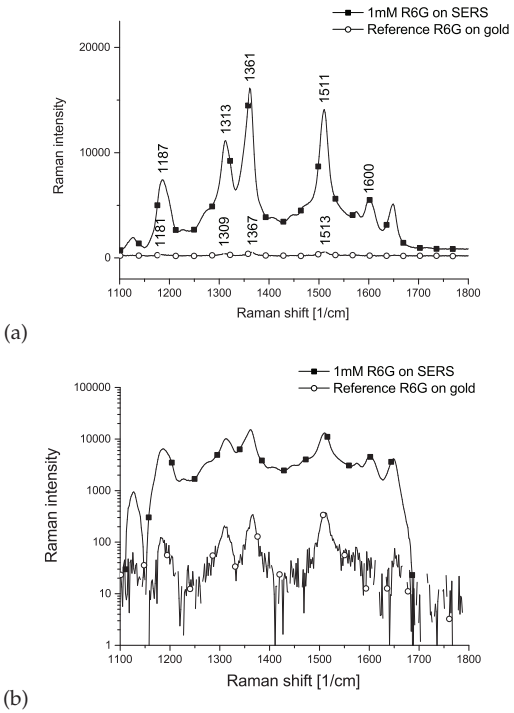

FIG. 5 a) The Raman spectra for a 1 mM R6G solution on top of the SERS patterned area and the smooth gold area; b) The difference in the intensity can be estimated on a logarithmic scale.

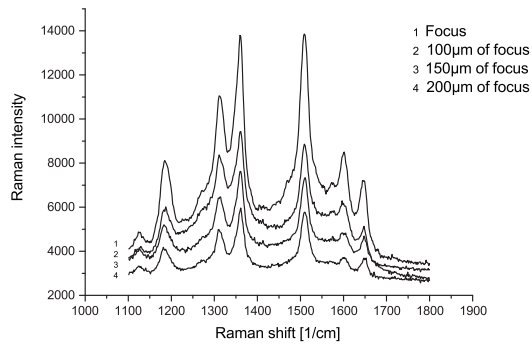

FIG. 6 Misalignment of the focus of the Raman microscope from SERS surface.

The Raman spectra with subtracted background spectrum can be seen in Figure 5(a) and 5(b) with a linear and logarithmic y-axis scale. Since the distinctive peaks for R6G are found in the Raman shift area of 1100 1/cm to 1800 1/cm, this range has been used in the spectrum analysis. The results showed high R6G peaks for the patterned SERS area in comparison to the smooth gold. The peak height difference is more than 30 folds. The result can be compared to the result of Liu et al. [18], with low intensity R6G peaks for smooth a Ag/PDMS structure. As Liu states, the metal coating alone can enhance the Raman signal, although with less intensity. The results in Figure 5 and the background knowledge we have from the study of Oo et al. [4] suggests that the detected signal could be SERS originated.

To confirm the prior analysis of the SERS, and to see the effect of the optical focus on the detected signals, we conducted a trial in which we changed the focus depth of the detection. The focus was misaligned by lowering the chip to see if the R6G signal remains constant as the signal is collected from the bulk sample above the SERS surface. If the signal is generated by the non-enhanced Raman from bulk R6G in DI water solutions, the signal intensity should remain constant without varying along the change of focus depth. As we can see from the results in Figure 6, the signal intensity drops as the chip is lowered (focus level raised from the SERS surface), and thus we can, together with the observations shown in Figure 5, confirm that we are detecting surface-enhanced Raman instead of conventional Raman.

To investigate the effect of the polyolefin lid on the SERS response, we measured the R6G spectra with 10 µM and 100 µM concentrations. The used integration time for the SERS signal recording was 30 seconds. The chip was filled with DI water to gain the reference polyolefin spectrum. Water was replaced by R6G samples and the Raman spectra were detected. Figure 7(a) shows the Raman spectra of the R6G samples and the polyolefin reference, and Figure 7(b) shows the 10 µM and 100 µM R6G spectra with subtracted polyolefin reference. The results show that although the polyolefin lid induces low Raman peaks, it has a minor effect on the R6G spectra. The effect of the lid can be further minimised by subtracting the reference spectrum from the R6G spectra.

The effect of flow dynamics on the optical SERS signal was studied with a continuous flow with 0.5 mM R6G solution in DI H_2O. A similar study has been conducted previously by Hüttner et al. with a glass slide-based optofluidic SERS chip using R6G molecules in ethanol with preceding and following pure ethanol cycles [41]. In our experiment, we focused more on the dynamics of the optical signal response to the used flow velocity than on the relation of sample concentration to the signal intensity, as Hüttner et al. have done.

In the study, the fluid flow velocity was varied from 25 µl/min to 1000 µl/min. The rise of the R6G signal was measured with a Raman microscope and a fluorescence microscope, as described in the Measurement set-up, to obtain the effect of the molecule diffusion and the partial mass transport limitation, and the effect of the convective flow. An image of the R6G Raman signal growth with a 50 µl/min flow velocity can be seen in Figure 8. The baseline tilt of the Raman spectrum was removed from the results for the analysed Raman shift area: 1100 1/cm to 1800 1/cm. Peak intensity for the main R6G peaks (1188 1/cm, 1310 1/cm, 1360 1/cm, 1510 1/cm and 1600 1/cm) was counted and averaged from 5 pixels. The change in the peak intensity as a function of time was calculated. Results of the measured signals were normalised and the average signal of 5 repeated measurements was calculated.

We recorded the signal rise without the dissociation phase, because the R6G molecules did not detach from the surface by washing with the H_2O flow. The binding strength of the R6G

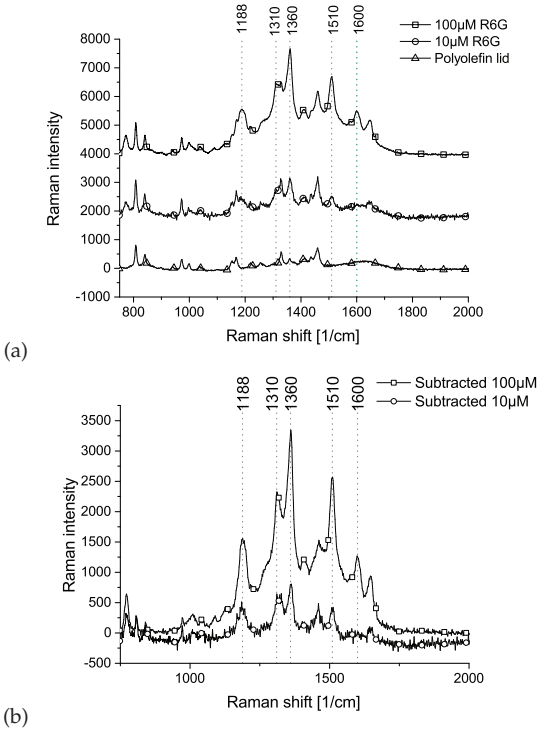

FIG. 7 a) The Raman spectra for 10 µM and 100 µM R6G solutions are compared to the polyolefin reference (785 nm laser, 40 mW power, 20 X objective and 30 s integration time); b) The reference spectrum has been reduced from the 10 µM and 100 µM R6G spectra.

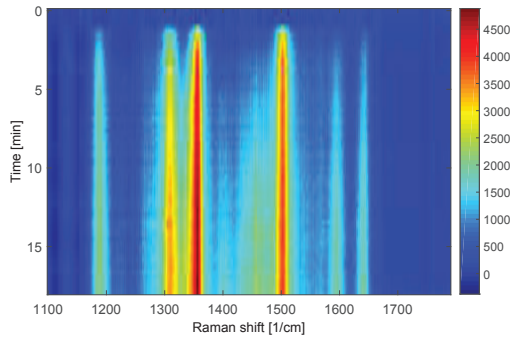

FIG. 8 Image of the signal growth during the flow trial of 0.5 mM R6G with 50 µl/min flow velocity.

molecules to the gold surface was too strong, and the signal did not return to zero intensity. A cleaning step was carried out by oxygen plasma etching (5 min 300 W) between the flow runs. Each flow velocity was recorded 5 times and each chip was reused 3 times. The detected average fluorescence and SERS signals for the measured flow velocities are depicted in Figure 9(a) and 9(b) as a function of time.

To analyse the results, linear functions were fitted on the rising edge of the fluorescence and SERS signals. In Figure 9(a), the fitted functions are depicted for the fluorescence, and in

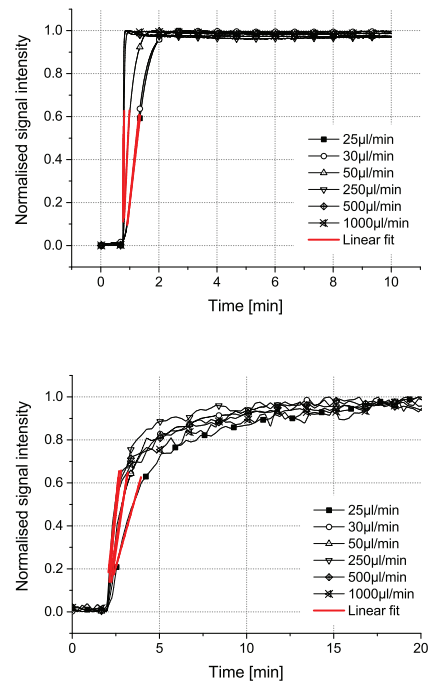

FIG. 9 a) Fluorescence signals as a function of time; b) SERS signals as a function of time. Linear function has been fitted for the rising edge of signals.

Figure 9(b) for the SERS signals. Linear functions are fitted for the range of 10% to 60% of the maximum intensity. The slope values attained are used to calculate the rise time of the signals for the aforementioned range. Figure 10(a) presents the comparative results of the SERS signal rise times and the fluorescence signal rise times. When comparing the results, it can be seen that the detected SERS signal rise is slower than the fluorescence signal rise of the R6G with all velocities in the study. The median of the lag time between the arrival of R6G molecules in the detection chamber by convective flow and the arrival and binding of R6G molecules on the SERS surface is 40.7 seconds, as depicted in Figure 10(b).

From the results, we can see that the lag time is larger for slower flow velocities. This could be due to insufficient molecule transport to the diffusion boundary layer. The lag time settles for the higher velocities and the dynamics of the diffusion and surface binding turn constant. In the future, these results will help us to plan studies with bioanalyte samples and active ligands on the surface, through the knowledge of the influence of an increasing mass transport limitation with flow velocities of 50 µl/min and less.

6 CONCLUSIONS

A novel method for fabricating a polymer-based optofluidic sensor with roll-to-roll imprinted SERS patterning and integrated adhesive microfluidic circuit was presented. The SERS substrates showed 30 folds higher enhancement than

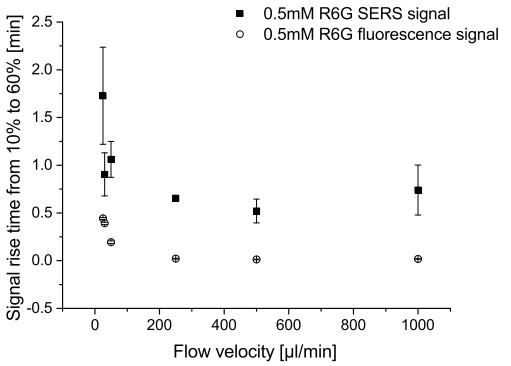

(a)

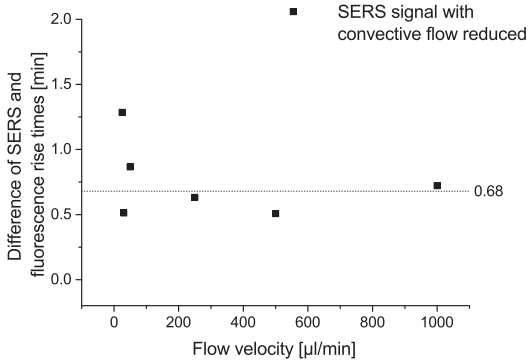

(b)

FIG. 10 a) Signal rise times for the 0.5 mM R6G SERS signal and the fluorescence signal; b) Difference in the signal rise times between the SERS and the fluorescence signal.

the smooth evaporated gold with the 1 mM Rhodamine 6G sample. Substrates were easily integrated into adhesive-based microfluidic devices, and the effect of the polyolefin lid could be removed from the R6G spectra. The SERS measurements of R6G fluid in the microfluidic circuit under constant flow conditions were successfully performed with a standard deviation even as low as 5% for a 250 µl/min flow velocity. The comparison of the signal rise of excited fluorescence with a 0.5 mM R6G sample and the recorded SERS signal showed that there is a median lag time of 40.7 seconds between the arrival of the sample molecules with the bulk flow into the detection chamber and the arrival and adsorption of the molecules on the detection surface. For flow values of 50 µl/min and less, the concentration of R6G molecules near the sensor surface rises slowly, and the transport is insufficient due to the depletion of analytes near the sensor surface. The high throughput fabrication can be developed in future by transferring the fabrication of the microfluidics from table top cutter to roll-to-roll process [42]. By further applying automated assembly of fluidic and optical layers instead on manual lamination, it is possible to achieve a truly disposable sensor chips offering a low cost solution for analytical applications.

7 ACKNOWLEDGEMENTS

This work was supported by University of Oulu Graduate School, Infotech Oulu Doctoral Programme and Tekes (Finnish Funding Agency for Innovation) under the FMA project.

References

[1] A. Liu, H. Huang, L. Chin, Y. Yu, and X. Li, "Label-free detection with micro optical fluidic systems (MOFS): a review," Anal. Bioanal. Chem. **391**, 2443–2452 (2008).

[2] H. K. Hunt, and A. M. Armani, "Label-free biological and chemical sensors," Nanoscale **2**, 1544–1559 (2010).

[3] M. Nirschl, F. Reuter, and J. Vörös, "Review of transducer principles for label-free biomolecular interaction analysis," Biosensors **1**, 70–92 (2011).

[4] S. Z. Oo, R. Chen, S. Siitonen, V. Kontturi, D. Eustace, J. Tuominen, S. Aikio, and M. Charlton, "Disposable plasmonic plastic SERS sensor," Opt. Express **21**, 18484–18491 (2013).

[5] X. Fan, and I. M. White, "Optofluidic microsystems for chemical and biological analysis," Nat. Photonics **5**, 591–597 (2011).

[6] K. Kneipp, Y. Wang, H. Kneipp, L. T. Perelman, I. Itzkan, R. R. Dasari, and M. S. Feld, "Single molecule detection using surface-enhanced Raman scattering (SERS)," Phys. Rev. Lett. **78**, 1667 (1997).

[7] A. M. Michaels, M. Nirmal, and L. Brus, "Surface enhanced Raman spectroscopy of individual rhodamine 6G molecules on large Ag nanocrystals," J. Am. Chem. Soc. **121**, 9932–9939 (1999).

[8] S. Nie, and S. R. Emory, "Probing Single Molecules and Single Nanoparticles by Surface-Enhanced Raman Scattering," Science **275**, 1102–1106 (1997).

[9] A. Virga, P. Rivolo, F. Frascella, A. Angelini, E. Descrovi, F. Geobaldo, and F. Giorgis, "Silver nanoparticles on porous silicon: approaching single molecule detection in resonant SERS regime," J. Phys. Chem. C **117**, 20139–20145 (2013).

[10] G. C. Schatz, M. A. Young, and R. P. Van Duyne, "Electromagnetic mechanism of SERS," Top. Appl. Phys. **103**, 19–45 (2006).

[11] K. C. Bantz, A. F. Meyer, N. J. Wittenberg, H. Im, Ö. Kurtulus, S. H. Lee, N. C. Lindquist, S. Oh, et al., "Recent progress in SERS biosensing," Phys. Chem. Chem. Phys. **13**, 11551–11567 (2011).

[12] C. L. Haynes, and R. P. Van Duyne, "Plasmon-Sampled Surface-Enhanced Raman Excitation Spectroscopy," J. Phys. Chem. B **107**, 7426–7433 (2003).

[13] T. R. Jensen, R. P. V. Duyne, S. A. Johnson, and V. A. Maroni, "Surface-Enhanced Infrared Spectroscopy: A Comparison of Metal Island Films with Discrete and Nondiscrete Surface Plasmons," Appl. Spectrosc. **54**, 371–377 (2009).

[14] L. A. Dick, A. J. Haes, and R. P. Van Duyne, "Distance and orientation dependence of heterogeneous electron transfer: a surface-enhanced resonance Raman scattering study of cytochrome c bound to carboxylic acid terminated alkanethiols adsorbed on silver electrodes," J. Phys. Chem. B **104**, 11752–11762 (2000).

[15] M. Litorja, C. L. Haynes, A. J. Haes, T. R. Jensen, and R. P. Van Duyne, "Surface-enhanced Raman scattering detected temperature programmed desorption: optical properties, nanostructure, and stability of silver film over Si02 nanosphere surfaces," J. Phys. Chem. B **105**, 6907–6915 (2001).

[16] L. A. Dick, A. D. McFarland, C. L. Haynes, and R. P. Van Duyne, "Metal film over nanosphere (MFON) electrodes for surface-enhanced Raman spectroscopy (SERS): Improvements in surface nanostructure stability and suppression of irreversible loss," J. Phys. Chem. B **106**, 853–860 (2002).

[17] I. M. White, S. H. Yazdi, and W. Y. Wei, "Optofluidic SERS: synergizing photonics and microfluidics for chemical and biological analysis," Microfluid. Nanofluid. **13**, 205–216 (2012).

[18] G. L. Liu, and L. P. Lee, "Nanowell surface enhanced Raman scattering arrays fabricated by soft-lithography for label-free biomolecular detections in integrated microfluidics," Appl. Phys. Lett. **87**, 074101 (2005).

[19] A. Lamberti, A. Virga, A. Angelini, A. Ricci, E. Descrovi, M. Cocuzza, and F. Giorgis, "Metal-elastomer nanostructures for tunable SERS and easy microfluidic integration," RSC Advances **5**, 4404–4410 (2015).

[20] J. Teng, J. Chu, C. Liu, T. Xu, Y. Lien, J. Cheng, S. Huang, et al., "Fluid Dynamics in Microchannels," in *Fluid Dynamics, Computational Modeling and Applications* L.H. Juarez, ed., 403–436 (InTech, Rijeka, 2012).

[21] M. Zimmermann, E. Delamarche, M. Wolf, and P. Hunziker, "Modeling and optimization of high-sensitivity, low-volume microfluidic-based surface immunoassays," Biomed. Microdevices **7**, 99–110 (2005).

[22] N. Orgovan, D. Patko, C. Hos, S. Kurunczi, B. Szabo, J. J. Ramsden, and R. Horvath, "Sample handling in surface sensitive chemical and biological sensing: A practical review of basic fluidics and analyte transport," Adv. Colloid Interfac. **211**, 1–16 (2014).

[23] J. Koplik, J. R. Banavar, and J. F. Willemsen, "Molecular dynamics of fluid flow at solid surfaces," Phys. Fluids A - Fluid. **1**, 781–794 (1989).

[24] J. Lauri, M. Wang, M. Kinnunen, and R. Myllylä, "Measurement of microfluidic flow velocity profile with two Doppler optical coherence tomography systems," in Biomed. Optics **2008** 68630F–68630F-8 (2008).

[25] J. Lauri, J. Czajkowski, R. Myllylä, and T. Fabritius, "Measuring flow dynamics in a microfluidic chip using optical coherence tomography with 1 μm axial resolution," Flow Meas. Instrum. **43**, 1–5 (2015).

[26] M. L. Yarmush, D. B. Patankar, and D. M. Yarmush, "An analysis of transport resistances in the operation of BIAcoreâĎć; implications for kinetic studies of biospecific interactions," Mol. Immunol. **33**, 1203–1214 (1996).

[27] M. Stenberg, and H. Nygren, "Kinetics of antigen-antibody reactions at solid-liquid interfaces," J. Immunol. Methods **113**, 3–15 (1988).

[28] T. E. Starr, and N. L. Thompson, "Total internal reflection with fluorescence correlation spectroscopy: combined surface reaction and solution diffusion," Biophys. J. **80**, 1575–1584 (2001).

[29] T. Gervais, and K. F. Jensen, "Mass transport and surface reactions in microfluidic systems," Chem. Eng. Sci., **61**, 1102–1121 (2006).

[30] A. Lionello, J. Josserand, H. Jensen, and H. H. Girault, "Dynamic protein adsorption in microchannels by "stop-flow" and continuous flow," Lab Chip **5**, 1096–1103 (2005).

[31] G. Hu, Y. Gao, and D. Li, "Modeling micropatterned antigen-antibody binding kinetics in a microfluidic chip," Biosens. Bioelectron. **22**, 1403–1409 (2007).

[32] D. G. Myszka, T. A. Morton, M. L. Doyle, and I. M. Chaiken, "Kinetic analysis of a protein antigen-antibody interaction limited by mass transport on an optical biosensor," Biophys. Chem. **64**, 127–137 (1997).

[33] K. Lebedev, S. Mafe, and P. Stroeve, "Convection, diffusion and reaction in a surface-based biosensor: modeling of cooperativity and binding site competition on the surface and in the hydrogel," J. Colloid Interface Sci. **296**, 527–537 (2006).

[34] R. Karlsson, A. Michaelsson, and L. Mattsson, "Kinetic analysis of monoclonal antibody-antigen interactions with a new biosensor based analytical system," J. Immunol. Methods **145**, 229–240 (1991).

[35] R. W. Glaser, "Antigen-antibody binding and mass transport by convection and diffusion to a surface: a two-dimensional computer model of binding and dissociation kinetics," Anal. Biochem. **213**, 152–161 (1993).

[36] L. L. Christensen, "Theoretical analysis of protein concentration determination using biosensor technology under conditions of partial mass transport limitation," Anal. Biochem. **249**, 153–164 (1997).

[37] R. W. Glaser, "Antigen-antibody binding and mass transport by convection and diffusion to a surface: a two-dimensional computer model of binding and dissociation kinetics," Anal. Biochem. **213**, 152–161 (1993).

[38] P. M. Richalet-Secordel, N. Rauffer-Bruyere, L. L. Christensen, B. Ofenloch-Haehnle, C. Seidel, and M. H. Van Regenmortel, "Concentration measurement of unpurified proteins using biosensor technology under conditions of partial mass transport limitation," Anal. Biochem. **249**, 165–173 (1997).

[39] L. Lee, "Adsorption: the solid-fluid interface," in *Molecular Thermodynamics of Nonideal Fluids* H. Brenner, ed., 424–462 (Butterworth-Heinemann, Boston, 1988).

[40] D. Murzin, "Physisorption and chemisorption," in *Engineering Catalysis*, 16 (De Gruyter, Berlin, 2013).

[41] W. Hüttner, K. Christou, A. Göhmann, V. Beushausen, and H. Wackerbarth, "Implementation of substrates for surface-enhanced Raman spectroscopy for continuous analysis in an optofluidic device," Microfluid. Nanofluid. **12**, 521–527 (2012).

[42] R. Liedert, L. K. Amundsen, A. Hokkanen, M. Mäki, A. Aittakorpi, M. Pakanen, J. R. Scherer, et al., "Disposable roll-to-roll hot embossed electrophoresis chip for detection of antibiotic resistance gene mecA in bacteria," Lab Chip **12**, 333–339 (2012).

PAPER II

Detection of *Listeria innocua* on roll-to-roll produced SERS substrates with gold nanoparticles

RSC Advances, 6(67), 62981–62989,
DOI information: 10.1039/C6RA08313G.

RSC Advances

PAPER

View Article Online
View Journal | View Issue

Cite this: *RSC Adv.*, 2016, **6**, 62981

Detection of *Listeria innocua* on roll-to-roll produced SERS substrates with gold nanoparticles

S. Uusitalo,†[a] M. Kögler,†[bg] A.-L. Välimaa,[c] A. Popov,[d] Yu. Ryabchikov,[ei] V. Kontturi,[f] S. Siitonen,[f] J. Petäjä,[a] T. Virtanen,[h] R. Laitinen,[c] M. Kinnunen,[d] I. Meglinski,[d] A. Kabashin,[e] A. Bunker,[b] T. Viitala[b] and J. Hiltunen*[a]

Received 31st March 2016
Accepted 21st June 2016

DOI: 10.1039/c6ra08313g

www.rsc.org/advances

The rapid and accurate detection of food pathogens plays a critical role in the early prevention of foodborne epidemics. Current bacteria identification practices, including colony counting, polymerase chain reaction (PCR) and immunological methods, are time consuming and labour intensive; they are not ideal for achieving the required immediate diagnosis. Different SERS substrates have been studied for the detection of foodborne microbes. The majority of the approaches are either based on costly patterning techniques on silicon or glass wafers or on methods which have not been tested in large scale fabrication. We demonstrate the feasibility of analyte specific sensing using mass-produced, polymer-based low-cost SERS substrate in analysing the chosen model microbe with biological recognition. The use of this novel roll-to-roll fabricated SERS substrate was combined with optimised gold nanoparticles to increase the detection sensitivity. Distinctive SERS spectral bands were recorded for *Listeria innocua* ATCC 33090 using an in-house build (785 nm) near infra red (NIR) Raman system. Results were compared to both those found in the literature and the results obtained from a commercial time-gated Raman system with a 532 nm wavelength laser excitation. The effect of the SERS enhancer metal and the excitation wavelength on the detected spectra was found to be negligible. The hypothesis that disagreements within the literature regarding bacterial spectra results from conditions present during the detection process has not been supported. The sensitivity of our SERS detection was improved through optimization of the concentration of the sample inside the hydrophobic polydimethylsiloxane (PDMS) wells. Immunomagnetic separation (IMS) beads were used to assist the accumulation of bacteria into the path of the beam of the excitation laser. With this combination we have detected *Listeria* with gold enhanced SERS in a label free manner from such low sample concentrations as 10^4 CFU ml^{-1}.

Introduction

Foodborne diseases represent a serious public health issue. The incidence of epidemics related to food pathogens has increased significantly due to the greatly accelerated range and speed of distribution that has resulted from the increasingly global trade network for food products.[1] For this reason, food safety authorities around the world have realized the need for a strict regulatory framework, including an exhaustive food testing regime.[2,3] Traditional methods for the detection of bacteria, include direct culture and colony counting, polymerase chain reaction (PCR) and immunological methods. These are all extremely labour intensive and time consuming;[1,4–6] the extent to which a rapid and efficient food testing regime can be achieved using the currently available methodologies is limited.

Raman spectroscopy is a promising new methodology for bacteria detection, with many advantages including identification of the specific species of the bacteria, rapid detection, multiple simultaneous analyses and being label free.[7–11] The identification of the species of bacteria through Raman

[a]*VTT Technical Research Centre of Finland, Kaitoväylä 1, 90590 Oulu, Finland. E-mail: Jussi.hiltunen@vtt.fi*

[b]*Centre for Drug Research, Division of Pharmaceutical Biosciences, Faculty of Pharmacy of the University of Helsinki, Finland*

[c]*National Resources Institute Finland (LUKE), Bio-based Business and Industry, University of Oulu, P. O. Box 413 (Paavo Havaksen Tie 3), FI-90014, Finland*

[d]*Optoelectronics and Measurement Techniques, Faculty of Information Technology and Electrical Engineering, University of Oulu, Finland*

[e]*Laboratoire Lasers, Plasmas Procédés Photoniques, Aix-Marseille University (AMU), 163 Avenue de Luminy, Case 917, 13288 Marseille Cedex 09, France*

[f]*Nanocomp Oy Ltd, Ensolantie 6, 80710 Lehmo, Finland*

[g]*Laboratory of Bioprocess Engineering, Institute of Biotechnology, Technische Universität Berlin, Ackerstr. 71-76, D-13355 Berlin, Germany*

[h]*Lappeenranta University of Technology, School of Engineering Science, Research Group of Membrane Technology, P. O. Box 20, FI-53851 Lappeenranta, Finland*

[i]*P. N. Lebedev Physical Institute of Russian Academy of Sciences, 53 Leninskii Prospekt, 119 991, Moscow, Russia*

† S. Uusitalo and M. Kögler contributed equally to this work.

spectroscopy is achieved through the detection of organic molecules on the surface of the bacterial membrane and wall. Their chemical structure provides a specific fingerprint of the bacterium that shows up in the Raman spectrum.[7] The detection of a small concentration of bacteria with conventional Raman spectroscopy can demand a level of sensitivity greater than what it is capable of. The usual lowest detected bacterial concentration being around 10^8 CFU ml^{-1}.[9,10,12] Regulatory agencies demand finding a single cell in 25 g of food and such low concentrations require a brief pre-enrichment step to reach a more detectable level of 10^4 to 10^5 CFU ml^{-1}.[3] The conventional Raman spectroscopy cannot reach this level and the signal thus needs to be amplified. This can be achieved through the use of noble metallic materials, for example gold or silver, to trigger localised surface plasmons.[13] Surface Enhanced Raman Scattering (SERS) is a special type of Raman spectroscopy, where irregular or patterned metal substrates or metal nanocolloids of different shape and size can be used for the signal enhancement.[13–16]

Typically the best enhancement effect is achieved with silver induced SERS.[17] However, the use of silver has some drawbacks. As a substance it is antimicrobial and thus affects the sample under inspection. It is chemically quite reactive and the stability and reproducibility of the silver substrates and colloids (AgNP) can also be an issue.[13,15] Gold is preferred in microbe detection as it is stable, non-toxic and has the optimal excitation wavelength in the near-infra red region, reducing auto-fluorescence issues generated by the microbes.

Among the foodborne pathogens *Listeria monocytogenes* is the most common culprit in causing death due to food poisoning. The fatality rate for *L. monocytogenes* infection is relatively high, ranging from 20 to 30%.[4] *L. monocytogenes* is an especially difficult pathogen to control, as a result of its tolerance to a wide range of temperatures and pH conditions. The detection of *Listeria* spp. with SERS has been studied previously with different SERS enhancers including different SERS substrate[4,18] approaches and SERS colloid[17,19–23] research. The SERS substrates have several advantages over the colloids; these include more consistent patterns without unforeseen aggregation and the ability to act as a base for the entire analysis chip. On the other hand, colloids can reach better sensitivity and be preferable when there is a need to detect features in the region of a larger organism like bacteria.

The direct detection of bacteria in food is difficult due to background signals and requires the disintegration of the solid food containing the bacteria, *e.g.* by mechanical methods, followed by culturing of the bacteria at elevated temperatures in the food matrix to accelerate the bacteria growth to a detectable level. Weidemaier *et al.*,[24] has studied the detection of *L. monocytogenes* inside the food matrix with the help of immunomagnetic beads and nanoparticle SERS tags with antibodies, as they point out, the method is sensitive to the extent to which the magnetic particles can be concentrated within the area of the laser beam and care must be taken to succeed with reproducible pelleting of the magnetic particles. A more common method for bacteria detection is to remove the bacteria from the food matrix, often with immunocapture and subsequently pre-enrich the concentration before detection.[6] Although the pre-enrichment technique requires culturing this can be used as a normalising factor for the state of the pathogen. The growth of *Listeria* at different temperatures, for example 4, 25 or 37 °C, produces bacteria with different amount of flagella and a different level of virulence. This affects the spectral fingerprint of the bacteria; in order to obtain reproducible spectra for bacteria, the same growing conditions in addition to detection processes are required.[18,25]

In previous research, it has been shown that it is possible to differentiate bacteria through SERS analysis.[25–28] Preliminary results also indicate that SERS can be used for identifying bacteria and spores even at a strain level.[18,25] Usually this requires a high concentration of bacteria. With low concentration the assistance of immunocapture may be needed for the separation of different bacteria. The genus *Listeria* consists of fifteen species from which only *Listeria monocytogenes* is pathogenic to humans.[29] Immunocapture by current commercially available antibodies can seldom distinguish between the *Listeria* species. There are studies focussing on the production of high quality antibodies only for *L. monocytogenes*.[30] The presence of non-pathogenic *Listeria* such as *Listeria innocua* may, however, indicate also contamination with *L. monocytogenes*.[30] Furthermore, as the morphologic structure of *L. innocua* is similar to *L. monocytogenes* and their Raman/SERS-spectra are quite similar, *L. innocua* can be used as a model for *Listeria* detection.[20]

The detection of *Listeria* with SERS has been previously studied by several research groups. The majority of studies have focussed on the detection of *Listeria* at high concentration, 10^8 to 10^{10} CFU ml^{-1},[4,17–19,22,23,30,31] and many have used chemometric analysis for the separation of *Listeria* spectra from the spectra of other pathogenic bacteria.[4,17,19,31] Fewer studies have focussed on lowering the detection limit of the SERS procedure for *Listeria* detection than on the acquisition of representative spectra. Chen *et al.* have developed a method for detection of *L. monocytogenes* and *L. innocua* by *in situ* synthesis of silver nanoparticles.[21] The limit of detection for the model sample *L. innocua* was found to be 10^3 CFU ml^{-1}. The assay for bacteria detection was, however, performed for bacteria in pure water and required an extra incubation step with the silver colloids and two washing steps after the incubation.

The objective of this study was to develop a simplified and affordable method for label-free detection of *Listeria* with high sensitivity that is possible to perform on a structured SERS substrate. The conventional way for fabricating structured SERS substrates is to use methods such as spin-coating, dip coating, chemical vapour deposition, electrochemical synthesis, electron beam lithography and etching.[32–35] However, they are not optimised for manufacturing single use chips in terms of through-put volume or cost. There are also many methods such as liquid–liquid interface formation, pulsed laser deposition on microscope slides and reduction of gold chloride III in natural rubber membranes which have been only tested in lab scale as batch fabrication.[36–39] The fabricated sensor areas are often small and the fabrication methods are difficult to transfer into high volume production required of truly disposable sensor

chips. Our approach is to fabricate the structured SERS substrates on polymer webs in large scale with UV imprint lithography. This enables the fabrication of large sensor surface areas which can be easily cut into smaller SERS substrates.[40,41] The fabricated SERS substrates are coated with a thin layer of gold by evaporation before integration of hydrophobic sample wells. This SERS platform is suitable for low cost high volume production and is practical for one-time use, which diminishes the contamination issues often encountered in microbe detection. Gold colloids were added to gain additional plasmonic enhancement. The method uses immunomagnetic separation (IMS) beads as bacteria cell concentrators and the only washing steps occur during the pre-enrichment phase. SERS enhancement of different types of gold nanoparticles with *Listeria* was studied and the colloids with the best enhancement effect were used in combination of R2R nanostructured gold SERS substrates.

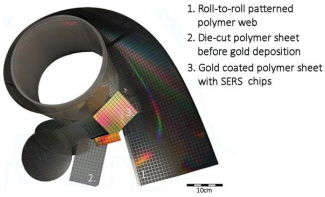

Fig. 1 Photograph of roll-to-roll patterned polymer webs and die-cut sheets before and after gold deposition.

Experimental

Gold nanoparticle synthesis

Ultrapure nanoparticle fabrication. Hurricane Spectra Physics Ti/sapphire laser operated at 800 nm with pulse duration 110 fs and repetition rate 1000 Hz was used for formation of gold nanoparticles (AuNPs) with a two-step approach.[42,43] In the first step, a gold target was immersed in 5 ml of deionized water at 10 mm below the water surface. Colloidal solution of AuNPs was produced by ablating the target at 150 μJ per pulse fluence for 30 minutes. The target was moved during the ablation step when material was collected from larger area. In the second step, additional laser fragmentation was performed to narrow the size distribution of AuNPs and to improve their stability. The fragmentation was performed by focussing a laser beam with 85 μJ per pulse fluence in the centre of the liquid volume that was stirred with a permanent magnet for 60 minutes.[43]

AuNP fabrication for medium and large size particles. Colloidal AuNPs were synthesized by following the Frens-method.[44] 100 ml of 0.01% (wt/vol) $HAuCl_4$ aqueous solution was heated to boil under vigorous and continuous stirring, followed by dropwise addition of 0.6 ml of 1% (wt/vol) trisodium citrate solution. The solution was kept boiling for approximately 1 h until the color changed to light red. The final AuNP-solution was prepared by centrifugation at 3500 rpm for 5 minutes (Eppendorf model 5430R) and subsequently followed by the removal of the supernatant. The final dark red AuNP-solution with a concentration of about 5500 mg l^{-1} was used and partially diluted in ratio 1 : 5 in H_2O.

AgNPs with the average size of 40 nm were purchased from Sigma-Aldrich for reference measurements with the commercial time-gated Raman spectrometer.[45]

SERS substrate fabrication

The SERS patterns were imprinted on top of a poly(methyl methacrylate) (PMMA) polymer sheet with roll-to-roll UV-nanoimprint lithography.[41] The produced polymer webs and die-cut sheets before and after gold deposition are presented in Fig. 1. Reverse gravure technique was used to apply UV-curable lacquer on top of the PMMA web. Embossing reel was used to imprint the SERS patterns and the lacquer was cured through the PMMA web with UV light exposure. After die-cutting SERS substrates from the roll, a 240 nm gold layer was added by evaporating on top of the polymer SERS surface.[41]

PDMS well integration

Sample wells were created into 1 mm thick PDMS sheets (Wacker, Elastosil) by biopsy punches of a diameter of 1–2 mm. These PDMS wells were bonded onto the polymer SERS substrates by physical adsorption. The hydrophobicity of the wells forces the sample to retreat inside the PDMS well and have contact with the gold layered patterned SERS surface.

Cultivation of *L. innocua* and IMS bead separation

L. innocua ATCC 33090 was cultivated in LEE Broth (Labema, Lab M Limited, pH 7.2 ± 0.2) at 35 °C for 20 h without shaking. The concentration was analysed spectrophotometrically (Dynamica HALO DB-20S) and diluted into concentration series (10^3 CFU ml^{-1} to 10^9 CFU ml^{-1}) in LEE broth. IMS was performed using Dynabeads® anti-*Listeria* (Life Technologies (Invitrogen) 71006), and a Dynal Magnetic Particle Concentrator DynaMag™-2 (Invitrogen Dynal) as follows: 1 ml volumes of bacterial culture was added to each of the microcentrifuge tubes containing a 20 μl volume of Dynabeads® anti-*Listeria* (Dynal) followed by incubation at room temperature for 10 min with continuous mixing by Mix-Mate (Eppendorf). The beads were concentrated by magnetic field (in the Dynal MPC-M) onto the side of the tube for 3 min, supernatants were carefully aspirated and the samples were washed with the washing buffer (0.15 M NaCl, 0.01 M sodium phosphate buffer, pH 7.4 with 0.05% Tween 20). After that the beads were concentrated and the supernatant removed. Finally, the bead–bacteria complexes were resuspended into 100 ml of washing buffer for the SERS detection. For reference a concentration analysis was performed with 50 μl volumes of bead–bacteria complexes streaked onto differential selective agar *Listeria* acc. to Ottaviani and Agosti (ALOA) chromogenic agar (Labema) and incubated at 35 ± 0.5 °C for 24–48 h.

SERS spectral acquisition of *Listeria innocua* and post-processing of data

Surface-enhanced Raman spectroscopy (SERS) spectra of *L. innocua* with AuNPs was detected from samples pipetted into PDMS wells integrated on top of SERS-active substrates. Sample amounts varied from 5 to 10 μl and well diameter varied from 1 to 2 mm. Bacteria samples were pipetted into the wells and the chosen AuNPs were pipetted sequentially. SERS spectra were recorded with an in-house built Raman system coupled into an Olympus microscope with a 785 nm continuous wave (cw) laser. The minimum laser power irradiation used was 10 mW with 40× magnification to excite the samples. A maximum of 40 mW was used in combination with low magnification (20×). The signal collection time was 5 seconds without averaging.

Reference spectra for *L. innocua* were recorded with 40 nm sized AgNPs by a commercial 532 nm picosecond pulsed laser time-gated Raman spectrometer (TimeGate Instruments Oy, Finland) with an average power of 10 mW, as well coupled into Olympus microscope.[45] The signal integration time was set to cover the SERS-signal and the fluorescence decay-time from 0.9–1.6 ns. The bacteria sample was pipetted on top of a glass slide prior to the detection. TimeGate measurements where analysed with TimeGate spectral processing tool and the acquired data was baseline corrected with a simple linear algorithm in Matlab (release 2015a, Mathworks Inc., USA) after opening the data with the PLS toolbox, version 2.0 (Eigenvector Research Inc., Manson, WA, USA). Further data handling and figure plotting was executed with Origin Pro (version 9.4, OriginLab corp., USA).

Results and discussion

Methods for the detection of *Listeria innocua*

Typically *Listeria* spp. has been identified by the SERS method from highly concentrated samples, mostly in the range of 10^7 CFU ml^{-1} to 10^{10} CFU ml^{-1}. When the detected concentrations are more realistic and the bacterial cells available for the detection are fewer, then the intensity of the detected Raman peaks diminishes and many of the peaks disappear from the spectrum. Thus it is more difficult to identify the bacteria from other bacterial species and the background with incomplete spectra. In these cases the identification of the bacteria can be handled by pathogen-capture proteins while SERS is used for the detection.[29] Grow *et al.* have detected *Listeria* on planar SERS substrates by capturing and accumulating bacterial cells near the surface with an antibody layer.[18] Although they concluded that the use of antibodies was possible and identification of bacteria was successful, the use of antibodies on the surface weakened the signal. This was assumed to be due to the increased separation distance between the surface and the bacterial cells.[46] Thus, this approach with planar SERS substrates was not optimal. Another possibility for capturing bacteria is the use of immunomagnetic separation beads which have been used in several *Escherichia coli* studies[34,35] and at least in one *Listeria* growth study.[24] Usually, the IMS beads are either removed before detection or used as a part of a customised sandwich assay with SERS labels. In order to simplify the detection process we have developed a method to detect *L. innocua* in a label-free manner with IMS beads present during the SERS detection. The bacterial cells were captured by using a commercially available IMS separation kit. The sample was placed into the hydrophobic PDMS well on top of the polymer SERS substrate as is shown in Fig. 2 with the gold nanoparticles. Without IMS beads and PDMS well the bacterial cells in the liquid droplets spread wide apart and typically due to evaporation accumulated randomly to the droplet edges. We found that by using immunomagnetic separation beads during the detection we obtained a more stable SERS signal due to the more constant settling of the heavy IMS beads on to the sensor surface. A close-up transmission electron microscopy (TEM) picture of the IMS beads and a scanning electron microscopy (SEM) picture of IMS beads on top of the patterned SERS substrate can be seen in Fig. 3a and b respectively. In order to further enhance the SERS signal and to detect the features of the bacterial cells, gold nanoparticles were added around the bacteria bound to IMS beads.

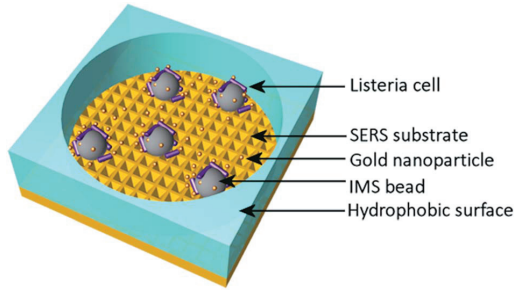

Fig. 2 Schematic of a PDMS well on top of a patterned SERS substrate with IMS bound *L. innocua* and AuNPs. The integrated hydrophobic PDMS well concentrates the sample inside the well on top of the SERS substrate in a more consistent manner than a free droplet on top of the substrate would. AuNPs are located around the bacteria giving a stronger SERS enhancement. IMS beads bind the bacteria around them and concentrate them inside the excitation laser beam strengthening the SERS signal.

AuNP characterisation

In search for the optimal gold nanoparticles (AuNPs) for bacteria detection with SERS, 3 candidates were selected.

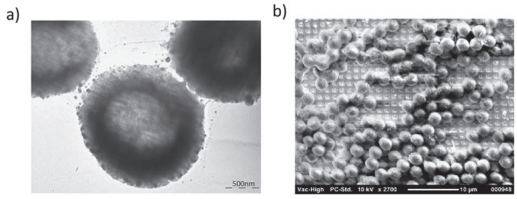

Fig. 3 (a) TEM image of IMS beads with gold nanoparticles. The scale in the picture is 500 nm. (b) SEM image of the IMS beads (Invitrogen dynabeads) on top of patterned SERS substrate.

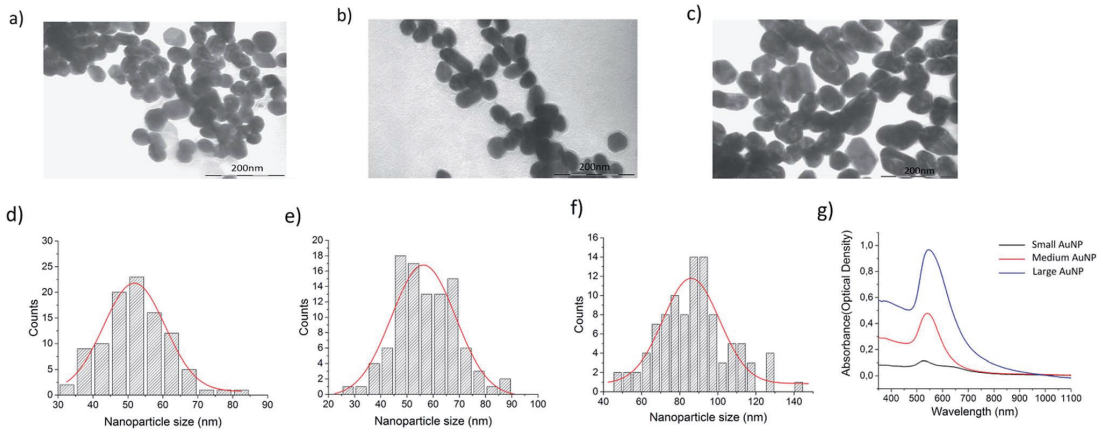

Fig. 4 (a–c) TEM images of the different sized AuNPs: small, medium and large size AuNPs respectively. (d–f) The corresponding size distribution histograms calculated from TEM images of the AuNPs with Gaussian fit: small, medium and large size AuNPs respectively. Each histogram has been calculated from 100 particle sizes with ImageJ software. (g) UV-Vis spectrum for the small, medium and large size AuNPs.

Ultrapure small AuNPs fabricated by femtosecond laser fragmentation were chosen as they could show better biocompatibility with bacteria cells than the synthesized AuNPs.[42,47] The physically fabricated AuNPs lack the traces of non-reacted starting reagents, by-products, ions and surfactants, and have an additional advantage of lower background signal. Chemically synthesized medium size AuNPs and larger AuNPs were chosen to compare the signal intensity using differently shaped and sized particles. The NP size has been previously shown to matter in micro-organism detection and a rod like shape has seemed beneficial for SERS enhancement.[48] The size and morphology of the fabricated AuNPs were retrieved by transmission electron microscopy (TEM) by using a LEO 912 OMEGA (Zeiss, Germany). One droplet of the 10 μl of aqueous nanostructure suspension was deposited onto a carbon-coated copper grid for TEM characterization. Fig. 4 shows the TEM images, the corresponding size distributions of the AuNP with Gaussian fit and the UV-Vis spectra of the AuNP. The maximum size for the different AuNP was estimated with the help of Gaussian fit shown in Fig. 4d–f. For the ultra-pure AuNPs the maximum size was found to be around 50 nm. The medium sized AuNPs showed a maximum of 60 nm with occasional large 90 nm sized particles. The large AuNPs had a maximum of 85 nm and a more rod like shape. From the UV-Vis spectra in Fig. 4g it can be seen how the maximum absorption peak of AuNPs shifts closer to 600 nm wavelength as the maximum size of the particles grows from 50 nm to 85 nm.

The SERS effectiveness of the different sized AuNPs was studied by pipetting 5 μl of bacteria sample and 2 μl of concentrated NP solution into 2 PDMS wells positioned on top of the patterned SERS substrate. The acquired SERS spectra are presented in Fig. 5a. According to the bar plot of the intensity of 737 cm^{-1} peak presented in Fig. 5b, the medium size and the large size particles gave similar intensities for a bacteria concentration of 5×10^5 CFU ml^{-1}. However, the large

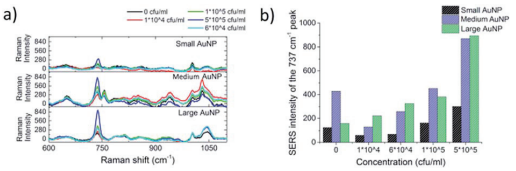

Fig. 5 (a) A concentration series of the IMS bound *L. innocua* ATCC 33090 with the AuNPs inside a PDMS well on top of a patterned SERS surface shows how the large AuNPs have the best separation ability between the smallest concentrations and the 0 reference. The results are an average of 18 spectrums. (b) A bar plot of the SERS intensity for the dominant *L. innocua* peak at 737 cm^{-1} for different concentrations with the AuNPs inside a PDMS well on top of patterned SERS surface clarifies the choice of large AuNP as the one to use for further studies for best sensitivity.

nanoparticles were chosen for further studies because the maximum of their UV-Vis spectra was closest to 785 nm and they provided more consistent spectra compared to the other AuNPs, which originated from the lower amount of background peaks thus giving a better resolution. These results strengthen the hypothesis that larger nanoparticles enhances the signal more than small round ones for microbe detection.[49] The way the AuNPs were fabricated played a minor role in enhancing the signal. Physical ablation could not benefit the detection in such a manner which would have counterweighted the advantage of the size and the shape of the particles.

The development of the detection process

Commercial Dynabeads were used to capture the *L. innocua* cells for the SERS detection. The SERS signal recorded with IMS beads, possibly due to accumulation of more bacterial cells inside the excitation laser spot, was found to be 20 times stronger than the signal recorded without the beads. Fig. 6a

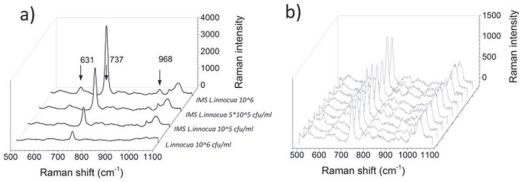

Fig. 6 (a) The effect of IMS concentration to the *L. innocua* ATCC 33090 SERS intensity with the AuNPs inside a PDMS well on top of patterned SERS surface. The cumulative effect of the IMS beads to the bacteria strengthens the SERS signal considerably. The intensity of 1×10^5 CFU ml^{-1} sample with IMS has 2 times stronger 737 cm^{-1} peak than the 1×10^6 CFU ml^{-1} sample without IMS. (b) The variation in SERS spectra of 1×10^5 CFU ml^{-1} *L. innocua* with IMS between 9 measured points.

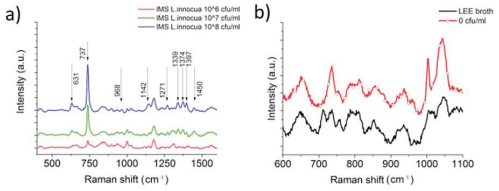

Fig. 8 (a) Baseline corrected SERS spectra from *L. innocua* ATCC 33090 with large AuNPs inside a PDMS well on top of patterned SERS surface with IMS beads. Detected with 20× magnification with a detection limit between 1×10^7 CFU ml^{-1} and 1×10^6 CFU ml^{-1}. The peaks maintaining their height with lower concentrations are caused by cultivation media residuals, AuNPs, IMS beads and other disturbances coming from the sample matrix. (b) Comparison of baseline corrected Raman intensities for the culturing media, *i.e.* LEE broth, and the 0 CFU ml^{-1} sample. The reason behind the peaks remaining in the *L. innocua* spectrum as the sample concentration is lowered are the peaks originating from the culture broth and the buffer solutions used for IMS bead washing steps.

shows the results for the comparison of studies with and without IMS beads and Fig. 6b shows the variation between 9 measurements points measured with IMS beads. The detection of *L. innocua* with the IMS beads was further studied on top of the patterned SERS substrate without AuNPs, as well as on top of silicon wafer with AuNPs and on top of patterned SERS substrate with AuNPs to see if there was an advantage in combining the SERS substrate with the AuNPs for bacteria detection. Fig. 7 represents the intensity differences between the measurements and it can be seen that the best intensities for the main dominant peak of 737 cm^{-1} were reached with the combination of the SERS substrate and AuNPs.

The detected SERS lines for *L. innocua* ATCC 33090 and the effect of the traces of culture media and buffers on the SERS spectra

The captured *L. innocua* was first detected inside a PDMS well in a liquid state with a 40 mW laser power and a 20× magnification. Fig. 8a shows the mean spectra for the *L. innocua* specific Raman bands. It can be noted that when the bacterial amount diminishes some lines stay constant showing the lines created by the traces of culture medium and buffer liquids. Thus, it can be concluded that 9 Raman bands initiating from the bacterial cells were detected. Fig. 8b shows the Raman bands created by the sample matrix and by the original cultivation media of the bacterial cells, *i.e.* the LEE broth. Most of the background bands seem to originate from traces of the LEE broth.

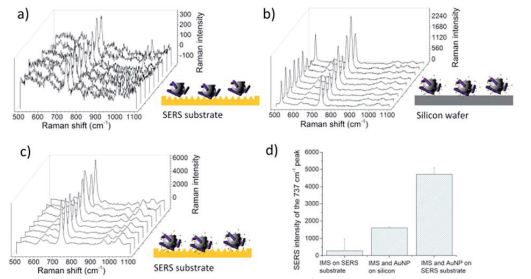

Fig. 7 (a) IMS bound 1×10^7 CFU ml^{-1} *L. innocua* ATCC 33090 inside a PDMS well on top of patterned SERS surface. (b) IMS bound 1×10^7 CFU ml^{-1} *L. innocua* ATCC 33090 with large AuNPs inside a PDMS well on top of a silicon wafer. (c) IMS bound 1×10^7 CFU ml^{-1} *L. innocua* ATCC 33090 with large AuNPs inside a PDMS well on top of a patterned SERS surface. (d) A bar plot of the SERS intensity for the dominant *L. innocua* peak 737 cm^{-1} for the cases presented in (a)–(c).

The nine Raman lines detected for *L. innocua* are listed in Table 1 with tentative assignments found in literature references. The dominant peak at 737 cm^{-1} has been previously suggested to originate from a glycosidic ring, adenine or CH_2 rocking.[50] Since the presence of adenine on the surface of the bacterial cell is unlikely and since the outer wall structure of Gram-positive bacteria such as *Listeria* spp. consists of a thick peptidoglycan structure rich in *N*-acetyl D-glucosamine (NAG), the origin of the peak is more likely caused by a glycosidic ring mode of NAG than adenine.[23,51]

The three closely aligned lines in the range of 1300–1400 cm^{-1} are interesting since three of them together have not been detected with *L. innocua* or *L. monocytogenes* in previous studies. The line 1339 cm^{-1} has been previously detected with *Listeria* by Luo *et al.*[52] as a shifted line 1331 cm^{-1} which was suggested to originate from CH_2 deformation. However, there are closer assignments to the detected 1339 cm^{-1} listed in *E. coli* studies. Vohník *et al.*[53] have suggested that the exact line 1339 cm^{-1} could be originating from amide III and Harz *et al.* suggest that the line is due to the signature of adenosine monophosphate and guanosine monophosphate, aromatic amino acids tyrosine and tryptophan. Harz *et al.*[7] also have a listing very near to the second line 1374 cm^{-1} assigned to DNA. The last line of the group 1397 cm^{-1} is most likely due to the symmetric deformation of CH_3 group which has also been detected for the case of *E. coli*.[54,55]

When comparing the Raman bands detected for *L. innocua* with the previous research, it is interesting to note that the SERS spectrum in different studies varies. Liu *et al.* among others has stated that this could be due to the differences in the measurement conditions such as the culture broth and temperature that have been used, excitation wavelength of the

Table 1 Raman bands detected for *L. innocua* ATCC 33090

Detected lines	Raman shift (cm^{-1})	Tentative assignments	Reference
631	627/620	Phenylalanine (skeletal)	Luo, Lin 2008,[23] Maquelin *et al.* 2002 (ref. 56)
737	732	Glycosidic ring mode of D-glucosamine (NAG), adenine or CH_2 rocking	Luo, Lin 2008,[52] Cui *et al.* 2015 (ref. 57)
968	955	N–C stretching	Vohník *et al.* 1998 (ref. 53)
1142	1134/1130	C–N and C–C stretch (carbohydrates)	Fan, Hu 2011,[54] Chen *et al.* 2015 (ref. 58)
1271	1230–1295	Amide III	Liu, Chen 2007,[59] Lu, Al-Qadiri 2011,[60] Maquelin *et al.* 2002 (ref. 56)
1339	1334/1339/1338	Deformation CH/amide III/signature of adenosine monophosphate and guanosine monophosphate, aromatic amino acids tyrosine and tryptophan	Maquelin *et al.* 2000,[61] Vohník *et al.* 1998,[53] Harz, Rösch, Popp 2008 (ref. 62)
1374	1371	DNA	Harz, Rösch, Popp 2008 (ref. 62)
1397	1392/1398	Symmetric deformation of CH_3 groups	Fan, Hu 2011,[54] Al-Qadiri, Lin 2008 (ref. 55)
1450	1453	CH_2 deformation (lipids)	Fan, Hu 2011,[54] Cui *et al.* 2015 (ref. 57)

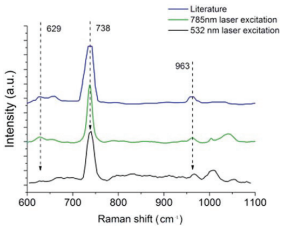

Fig. 9 Three SERS spectra of *L. innocua* were compared to confirm that the measured spectrum originates from the assumed bacteria. The literature reference has been borrowed from a publication by Luo, B. Steven *et al.* (2008) with a concentration of 10^8 CFU ml^{-1} *L. innocua* measured with cw 785 nm laser excitation with AgNPs. The 785 nm cw laser excitation with the in-house built device has been recorded from 10^6 CFU ml^{-1} IMS bound *L. innocua* ATCC 33090 with large AuNPs inside a PDMS well on top of a patterned SERS surface with IMS beads, detected with 40× magnification. The 532 nm pulsed laser excitation is a AgNP-enhanced SERS spectra of 10^6 CFU ml^{-1} IMS bound *L. innocua* ATCC 33090 placed on top of a glass slide and 40× magnification.

laser or the SERS enhancer.[19,51] To test this hypothesis we recorded the SERS spectra of the same *L. innocua* sample with changed SERS conditions. Fig. 9 shows the peaks detected around the dominant peak 737 cm^{-1} for 3 different SERS conditions. In the first case the combination of AuNPs on top of the patterned SERS substrate with 785 nm cw excitation was used, while in the second case a SERS spectrum was detected from the same sample on top of a glass slide with AgNPs and pulsed laser excitation at a different wavelength of 532 nm. The results are consistent. They are also similar to the third case published by Luo *et al.* who used AgNPs with 785 nm cw excitation wavelength. Another research group of Kairyte *et al.*[22] used silver NPs with 1064 nm excitation with a similar outcome. Clearly when comparing the results, there is no connection between the variations in spectra and the enhancer used (silver/gold). Additionally the excitation wavelength does not seem to affect the detected spectrum.

The detection process was developed further by manually lowering the minimum laser power of the Raman system to 10 mW. This enabled the use of larger magnification with the microscope without burning of the dried specimen during the measurement procedure. The sample density on the SERS substrate was also reduced to prevent the blocking of signal by the media traces of the sample liquids. It was noted that the

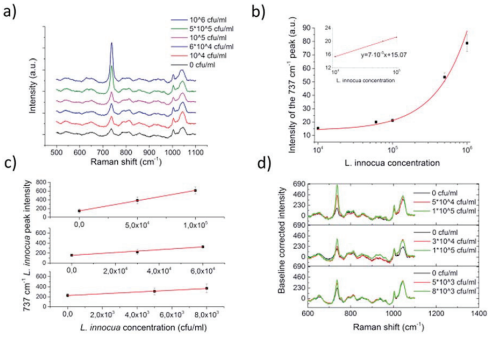

Fig. 10 (a) A normalised concentration series for LOD estimation. (b) An exponential fit for the normalised concentration series in logarithmic scale for the entire series and a linear fit for the small concentrations. (c) Comparison of the 737 cm^{-1} peak intensity for different concentration series with 5–10 μl dried IMS bound *L. innocua* ATCC 33090 samples placed with AuNPs into a 1–1.5 mm PDMS well on top of SERS substrate. (d) Comparison of baseline corrected Raman intensities for three of the concentration series. All figures are a mean of 9 measurement points with mean absolute deviations.

media was disturbing the SERS signal if an excessive amount of traces had dried on top of the SERS substrate. Limit of detection and repeatability of the detection process could have been enhanced further with extra washing steps for the IMS beads, but this was avoided in order to not complicate the sample handling. Fig. 10 shows the mean intensity changes of the dominant peak of 737 cm^{-1} as a function of *L. innocua* concentration with 40× magnification and 10 mW laser excitation power for several concentration series. For the concentration series in Fig. 10a and b the Raman intensity was normalised by the background peak at 787 cm^{-1}. The intensity of the dominant 737 cm^{-1} peak is displayed in Fig. 10b as a function of logarithmic *L. innocua* concentration that follows an exponential curve. For the concentration range below 10^5 CFU ml^{-1} the relation was found linear. Since the blank 0 CFU ml^{-1} sample exhibits a signal at 737 cm^{-1}, the lowest limit of detection was considered through the deviation of the background signal generated by the sample matrix. According to the international union of pure and applied chemistry, IUPAC, the limit of detection (LOD) can be defined as the smallest concentration detected with reasonable certainty, and derived from

$$\mathrm{LOD} = k s_{\mathrm{bi}} S \quad (1)$$

where s_{bi} is the standard deviation of the blank measures, $k = 3$ is a numerical factor of confidence level approved by IUPAC and S is the slope of the calibration curve. S is defined as

$$S = \Delta c/\Delta I,^{63} \quad (2)$$

where Δc is the change in concentration and ΔI is the change in Raman intensity. By using eqn (1) and determining S from the linear fit shown in Fig. 10b, the LOD was calculated to be 1.4×10^4 CFU ml^{-1}. The concentration series shown in Fig. 10c and d confirm the LOD, since the deviation of the concentrations below 10^4 CFU ml^{-1} coincide with the deviations of the mean blank samples. This means that samples with lower concentrations cannot reliably be detected. In case of model *L. innocua* sample, the estimated detection time including pre-culture[64] (6 hours) for 10^4 CFU ml^{-1} sample concentration, IMS preparation (15 minutes), sample deposition on SERS chip (15 minutes), SERS detection (10 minutes) and data handling (5 minutes), the total microbe analysis is estimated to be 7 hours. The time-saving of the developed method compared to the conventional official ISO 11290-1:1996/amd.1:2004 method in case of the model sample is approximately 41 hours with pre-cultivation.

As a summary, we demonstrated in this study the use of disposable polymer SERS platforms and AuNPs with integrated sample wells for fast and simple detection of *L. innocua*. We have shown how the capture and deposit of the IMS bound bacteria cells onto the SERS substrate benefits the detection. In the future, the detection process could be further developed by utilizing the magnetic nature of the IMS beads on the SERS substrate for the removal of matrix traces *e.g.* by removing the matrix with wicking.

Conclusions

This study analyses the use of different types of AuNPs in addition to a structured polymer SERS substrate for *Listeria* detection. The polymer based SERS substrate has been produced with roll-to-roll fabrication and thus it is suitable for one time use due to the high volume production and the low cost per substrate. The results of this study provide new insights into *Listeria* diagnostics. We also demonstrate the benefit of using immunomagnetic separation beads as an accumulation assistant of the bacteria for enhanced signal intensity. The use of novel hydrophobic PDMS wells for sample preparation on SERS chips enables controlled sample appliance and reduces mean absolute deviation of SERS signals. The limit of detection in this methodology was determined to be in the range of $\sim 10^4$ CFU ml^{-1} shown for the first time with label-free gold enhanced SERS using optimized AuNPs combined with an Au based SERS substrate.

Acknowledgements

This project was funded by TEKES (the Finnish Funding Agency for Technology and Innovation) through FMA project and University of Oulu Graduate School through Infotech Oulu Doctoral Program and by Academy of Finland through FOULSENS (Grant No. 292253), M-SPEC (Grant No. 284907) and multi Diagnostics (Grant No. 290596). The financial support of the aforementioned institutes is gratefully acknowledged. We also thank Tiina Väyrynen (National Resources Institute Finland (LUKE)) for helping with the bacterial sample preparation. Yury Ryabchikov acknowledges a support from COST project (ECOST-STSM-BM1205-120416-072252) for performing experiments.

Notes and references

1 J. Law, N. A. Mutalib, K. Chan and L. Lee, *Front Microbiol*, 2013, **5**, 770.
2 M. Gandhi and M. L. Chikindas, *Int. J. Food Microbiol.*, 2007, **113**, 1–15.
3 U. Gasanov, *FEMS Microbiol. Rev.*, 2005, **29**, 851–875.
4 N. A. Mungroo, G. Oliveira and S. Neethirajan, *Microchim. Acta*, 2015, **183**, 697–707.
5 V. Velusamy, K. Arshak, O. Korostynska, K. Oliwa and C. Adley, *Biotechnol. Adv.*, 2010, **28**, 232–254.
6 X. Zhao, C. Lin, J. Wang and D. Oh, *J. Microbiol. Biotechnol.*, 2014, **24**, 297–312.
7 M. Harz, P. Rösch and J. Popp, *Cytometry, Part A*, 2009, **75**, 104–113.
8 X. Lu, H. M. Al-Qadiri, M. Lin and B. A. Rasco, *Food Bioprocess Technol.*, 2011, **4**, 919–935.
9 X. Lu, B. A. Rasco, D. H. Kang, J. M. F. Jabal, D. E. Aston and M. E. Konkel, *Anal. Chem.*, 2011, **83**, 4137–4146.
10 J. Wang, X. Xie, J. Feng, J. C. Chen, X. Du, J. Luo, X. Lu and S. Wang, *Int. J. Food Microbiol.*, 2015, **204**, 66–74.
11 I. Boyaci, H. Temiz and H. Geniş, *RSC Adv.*, 2015, **5**, 56606–56624.

12 E. Smith and G. Dent, *Modern Raman spectroscopy: a practical approach*, 2013.
13 J. Anker, W. Hall, O. Lyandres and N. Shah, *Nat. Mater.*, 2008, **7**, 442–453.
14 S. Nie, *Science*, 1997, **275**, 1102–1106.
15 K. Bantz, A. Meyer and N. Wittenberg, *Phys. Chem. Chem. Phys.*, 2011, **13**, 11551–11567.
16 O. Bibikova, A. Popov, A. Bykov, A. Prilepskii, M. Kinnunen, K. Kordas, V. Bogatyrev, N. Khlebtsov, S. Vainio and V. Tuchin, *J. Biomed. Opt.*, 2015, **20**, 076017.
17 C. Fan, Z. Hu, A. Mustapha and M. Lin, *Appl. Microbiol. Biotechnol.*, 2011, **92**, 1053–1061.
18 A. E. Grow, L. L. Wood, J. L. Claycomb and P. A. Thompson, *J. Microbiol. Methods*, 2003, **53**, 221–233.
19 Y. Liu, Y.-R. Chen, X. Nou and K. Chao, *Appl. Spectrosc.*, 2007, **61**, 824–831.
20 G. Green and A. Chan, *Instrumentation and Measurement Technology Conference Proceedings (IMTC '08)*, 2008, pp. 513–517.
21 L. Chen, N. Mungroo, L. Daikuara and S. Neethirajan, *J. Nanobiotechnol.*, 2015, **13**, 45.
22 K. Kairyte, Z. Luksiene and V. Sablinskas, *Chem. Technol.*, 2012, **61**, 46–49.
23 B. S. Luo and M. Lin, *J. Rapid Methods Autom. Microbiol.*, 2008, **16**, 238–255.
24 K. Weidemaier, E. Carruthers, A. Curry, M. Kuroda, E. Fallows, J. Thomas, D. Sherman and M. Muldoon, *Int. J. Food Microbiol.*, 2015, **198**, 19–27.
25 S. Efrima and L. Zeiri, *J. Raman Spectrosc.*, 2009, **40**, 277–288.
26 M. Knauer, N. Ivleva, R. Niessner and C. Haisch, *Anal. Sci.*, 2010, **26**, 761–766.
27 H. Zhou, D. Yang, N. P. Ivleva, N. E. Mircescu, R. Niessner and C. Haisch, *Anal. Chem.*, 2014, **86**, 1525–1533.
28 W. R. Premasiri, D. T. Moir, M. S. Klempner, N. Krieger, G. Jones and L. D. Ziegler, *J. Phys. Chem. B*, 2005, **109**, 312–320.
29 D. Weller, A. Andrus, M. Wiedmann and H. C. den Bakker, *Int. J. Syst. Evol. Microbiol.*, 2015, **65**, 286–292.
30 M. Mendonça, N. L. Conrad, F. R. Conceição, A. N. Moreira, W. P. da Silva, J. A. Aleixo and A. K. Bhunia, *BMC Microbiol.*, 2012, **12**, 275.
31 Y. Liu, K. Chao, X. Nou and Y.-R. Chen, *Sens. Instrum. Food Qual. Saf.*, 2008, **3**, 100–107.
32 J. Chen, B. Shen, G. Qin, X. Hu, L. Qian, Z. Wang, S. Li, Y. Ren and L. Zuo, *J. Phys. Chem. C*, 2012, **116**, 3320–3328.
33 A. J. Chung, Y. S. Huh and D. Erickson, *Nanoscale*, 2011, **3**, 2903–2908.
34 U. Huebner, K. Weber, D. Cialla, R. Haehle, H. Schneidewind, M. Zeisberger, R. Mattheis, H.-G. Meyer and J. Popp, *Microelectron. Eng.*, 2012, **98**, 444–447.
35 B. C. Galarreta, P. R. Norton and F. Lagugné-Labarthet, *Langmuir*, 2011, **27**, 1494–1498.
36 C. A. Smyth, I. Mirza, J. G. Lunney and E. M. McCabe, *Appl. Surf. Sci.*, 2013, **264**, 31–35.
37 M. Suzuki, Y. Niidome, N. Terasaki, K. Inoue, Y. Kuwahara and S. Yamada, *Jpn. J. Appl. Phys.*, 2004, **43**, L554–L556.
38 F. C. Cabrera, P. H. B. Aoki, R. F. Aroca, C. J. L. Constantino, D. S. dos Santos and A. E. Job, *J. Raman Spectrosc.*, 2012, **43**, 474–477.
39 E. P. Hoppmann, W. W. Yu and I. M. White, *IEEE J. Sel. Top. Quantum Electron.*, 2014, **20**, 195–204.
40 S. Uusitalo, J. Hiltunen, P. Karioja, S. Siitonen, V. Kontturi, R. Myllyla, M. Kinnunen and I. Meglinski, *J. Eur. Opt. Soc, Rapid Publ.*, 2015, **10**, 15043.
41 S. Z. Oo, R. Y. Chen, S. Siitonen, V. Kontturi, D. A. Eustace, J. Tuominen, S. Aikio and M. D. B. Charlton, *Opt. Express*, 2013, **21**, 18484–18491.
42 K. Maximova, A. Aristov, M. Sentis and A. Kabashin, *Nanotechnology*, 2015, **26**, 065601.
43 S. Besner, A. Kabashin and M. Meunier, *Appl. Phys. A*, 2007, **88**, 269–272.
44 M. Kögler, B. Zhang, L. Cui, Y. Shi, M. Yliperttula, T. Laaksonen, T. Viitala and K. Zhang, *Sens. Actuators, B*, 2016, **230**, 411–421.
45 T. Rojalin, L. Kurki and T. Laaksonen, *Anal. Bioanal. Chem.*, 2016, **408**, 761–774.
46 Z. Tian, B. Ren, J. Li and Z. Yang, *Chem. Commun.*, 2007, **34**, 3514–3534.
47 P. Blandin and K. Maximova, *J. Mater. Chem. B*, 2013, **1**, 2489–2495.
48 U. Tamer, İ. H. Boyacı, E. Temur, A. Zengin, İ. Dincer and Y. Elerman, *J. Nanopart. Res.*, 2011, **13**, 3167–3176.
49 H. Butler, S. Fogarty and J. Kerns, *Analyst*, 2015, **140**, 3090–3097.
50 T. Szymborski, E. Witkowska and W. Adamkiewicz, *Analyst*, 2014, **139**, 5061–5064.
51 M. Çulha, M. M. Yazıcı, M. Kahraman, F. Şahin and S. Kocagöz, *J. Nanotechnol.*, 2012, 297560.
52 B. Luo and M. Lin, *J. Rapid Methods Autom. Microbiol.*, 2008, **16**, 238–255.
53 S. Vohník, C. Hanson, R. Tuma, J. A. Fuchs, C. Woodward and G. J. Thomas, *Protein Sci.*, 1998, **7**, 193–200.
54 C. Fan, Z. Hu, A. Mustapha and M. Lin, *Appl. Microbiol. Biotechnol.*, 2011, **92**, 1053–1061.
55 H. Al-Qadiri and M. Lin, *J. Food Sci.*, 2008, **73**, M54–M61.
56 K. Maquelin, C. Kirschner, L.-P. Choo-Smith, N. van den Braak, H. P. Endtz, D. Naumann and G. Puppels, *J. Microbiol. Methods*, 2002, **51**, 255–271.
57 L. Cui, P. Chen, B. Zhang, D. Zhang and J. Li, *Water Res.*, 2015, **87**, 282–291.
58 L. Chen and N. Mungroo, *J. Nanobiotechnol.*, 2015, **13**, 45.
59 Y. Liu, Y. Chen, X. Nou and K. Chao, *Appl. Spectrosc.*, 2007, **61**, 824–831.
60 X. Lu, H. Al-Qadiri, M. Lin and B. Rasco, *Food Bioprocess Technol.*, 2011, **4**, 919–935.
61 K. Maquelin and L. Choo-Smith, *Anal. Chem.*, 2000, **72**, 12–19.
62 M. Harz, P. Rösch and J. Popp, *Cytometry, Part A*, 2009, **75**, 104–113.
63 G. Long and J. Winefordner, *Anal. Chem.*, 1983, **55**, 712A–724A.
64 N. Gnanou Besse, N. Audinet, A. Kérouanton, P. Colin and M. Kalmokoff, *Int. J. Food Microbiol.*, 2005, **104**, 123–134.

PAPER III

Stability optimization of microbial surface-enhanced Raman spectroscopy detection with immunomagnetic separation beads

Optical Engineering, 56(3), 037102,
DOI information: 10.1117/1.OE.56.3.037102.

Optical Engineering 56(3), 037102 (March 2017)

Stability optimization of microbial surface-enhanced Raman spectroscopy detection with immunomagnetic separation beads

Sanna Uusitalo,[a,*] Martin Kögler,[b,c] Anna-Liisa Välimaa,[d] Jarno Petäjä,[a] Ville Kontturi,[e] Samuli Siitonen,[e] Riitta Laitinen,[d] Matti Kinnunen,[f] Tapani Viitala,[b] and Jussi Hiltunen[a,*]
[a]VTT Technical Research Centre of Finland, Oulu, Finland
[b]University of Helsinki, Centre for Drug Research, Division of Pharmaceutical Biosciences, Faculty of Pharmacy, Helsinki, Finland
[c]Technische Universität Berlin, Chair of Bioprocess Engineering, Institute of Biotechnology, Berlin, Germany
[d]National Resources Institute Finland (LUKE), Bio-based Business and Industry, Oulu, Finland
[e]Nanocomp Oy Ltd., Lehmo, Finland
[f]University of Oulu, Faculty of Information Technology and Electrical Engineering, Optoelectronics and Measurement Techniques Research Unit, Oulu, Finland

Abstract. Immunomagnetic separation (IMS) beads with antibody coating are an interesting option for biosensing applications for the identification of biomolecules and biological cells, such as bacteria. The paramagnetic properties of the beads can be utilized with optical sensing by migrating and accumulating the beads and the bound analytes toward the focus depth of the detection system by an external magnetic field. The stability of microbial detection with IMS beads was studied by combining a flexible, inexpensive, and mass producible surface-enhanced Raman spectroscopy (SERS) platform with gold nanoparticle detection and antibody recognition by the IMS beads. *Listeria innocua* ATCC 33090 was used as a model sample and the effect of the IMS beads on the detected Raman signal was studied. The IMS beads were deposited into a hydrophobic sample well and accumulated toward the detection plane by a neodymium magnet. For the first time, it was shown that the spatial stability of the detection could be improved up to 35% by using IMS bead capture and sample well placing. The effect of a neodymium magnet under the SERS chip improved the temporal detection and significantly reduced the necessary time for sample stabilization for advanced laboratory testing. [DOI: 10.1117/1.OE.56.3.037102]

Keywords: surface-enhanced Raman spectroscopy; immunomagnetic separation beads; optical detection; biological cells.

Paper 161981 received Dec. 22, 2016; accepted for publication Feb. 17, 2017; published online Mar. 7, 2017.

1 Introduction

Optical sensing has a long history in biological and molecular analysis.[1,2] Typically, the photonics-based detection methods are either label-free or utilize a conjugated label, such as a fluorophore. Although the fluorophores can often enhance detection sensitivity, they can also complicate the analysis procedure. Surface-enhanced Raman spectroscopy (SERS) is a recent optical detection method, which can offer both identification of the analyte and enhanced sensitivity without the use of labels.[3] Additionally, SERS can offer a multiplexed analysis and quick discrimination of analytes, such as biological cells through their specific Raman spectra at the current state. Immunomagnetic separation (IMS) beads are an interesting alternative for the trapping and separation of biological cells before cell analysis.[4–13] IMS beads combine the ability of cell separation with an antibody-assisted identification of the captured cells. In comparison to the more conventionally used membrane filtration and centrifugation, the IMS beads can show higher specificity and separation efficiency.[6] During the past two decades, IMS beads have been used efficiently for biological cell trapping in food pathogen analysis and in environmental monitoring.[4–9,11–13] SERS is a vibrational spectroscopy technique, which can be used for the detection and recognition of captured biological cells.[14–30] In SERS, the Raman scattering of excitation light forms a spectrum containing information about the chemical structure and bonds of the biomolecules on the surface of the cells. Nobel metals, such as gold and silver, enhance the detected signal through localized surface plasmon resonance and enable sensitive detection for near-infrared Raman.[3,31,32] As reported by Li et al.,[33] by combining SERS nanoparticle detection with a structured SERS substrates, it is possible to increase the total plasmonic electromagnetic field, and consequently, SERS enhancement, through a weak coupling of local fields if the substrate and the nanoparticles are gathered in the near vicinity of each other. The use of IMS beads in combination with detection is usually conducted by removing the beads before the detection[34,35] or by using custom-made sandwich assays with Raman labels for signal enhancement.[36,37] There are, to our knowledge, hardly any studies focusing on the effect of IMS beads on the signal construction during SERS detection. Although SERS has been receiving a lot of attention in the last decade because it is label free and it can ultimately be used even for single-cell detection,[32,38,39] the practical use of SERS has encountered challenges in the repeatability and stability of the measurements. Detection of biological cells in liquid samples is highly dependent on the fact that the cells have to be in close proximity of SERS-active colloids or

*Address all correspondence to: Sanna Uusitalo, E-mail: sanna.uusitalo@vtt.fi

0091-3286/2017/$25.00 © 2017 SPIE

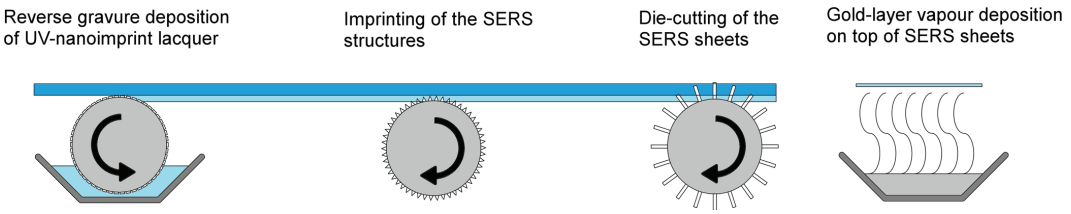

Fig. 1 A schematic illustration of the roll-to-roll UV-nanoimprint method for structured SERS substrate fabrication. The SERS pattern is imprinted onto a PMMA web with UV sensitive lacquer. The lacquer is set with UV light exposure through a transparent polymer web.

surfaces, and that both the cells and the SERS active agents have to be within the focus depth of the detection system.[40] Detecting a sample droplet on a surface can show low SERS signal reproducibility and stability due to microcurrents generated by the evaporation of the liquid and shrinkage of the droplet.[29] During the evaporation, enhanced with the focussed laser beam, the microcurrents move the cells toward the edges of the droplet, where the signal can be significantly higher than in the middle of the droplet. This phenomenon is referred to as the coffee ring effect.[41] The flow of cells to the edges of the droplet can be suppressed by the use of IMS beads, which are heavier objects and do not flow as easily along the microcurrents, thus showing higher stability in respect to their location. Herein, we have studied the positive effect of IMS beads on the spatial and temporal stability of cell detection with SERS. The use of a magnetic field to accumulate paramagnetic IMS beads with gold nanoparticles near the surface of the SERS substrate was analyzed. *Listeria innocua* ATCC 33090 was used as a model sample for biological cell capture.

2 Experimental Methods

2.1 *Gold Nanoparticle Synthesis*

The Frens method[42] was used for the synthesis of gold nanocolloids (AuNPs) with a median size of 85 nm as determined from transmission electron microscopy images. In brief, a 0.01% (wt/vol) $HAuCl_4$ aqueous solution was heated up to boiling point while continuously stirring the solution. 1% (wt/vol) trisodium citrate solution was dropwise added to the $HAuCl_4$ aqueous solution. This low viscous solution boiled for ~45 min until the color of the solution changed to dark-red. The resulting AuNP solution was centrifuged at 3500 rpm for 5 min to remove the supernatant sequentially. The concentration of the final AuNP solution was ~5500 mg/L, which was diluted in a 1:5 ratio in deionized water before experiments.

2.2 *Surface-Enhanced Raman Spectroscopy Substrate Fabrication*

The structured SERS substrates were fabricated with a high throughput method by using UV-nanoimprint lithography with roll-to-roll equipment, as shown in Fig. 1.[17,43] A poly(methyl methacrylate) (PMMA) polymer sheet was coated with a UV-curable lacquer by reverse gravure technique. The lacquer was patterned with embossing reel and UV light was used to cure the structures through the PMMA web. The rolls were die-cut into smaller sensor strips, which were coated with a 240-nm gold layer by evaporation.

2.3 *PDMS Well Integration*

Hydrophobic sample wells with a diameter of 1 mm were cut into 1-mm thick polydimethylsiloxane (PDMS) foil. The wells were bonded to the gold layer by physical adsorption. The hydrophobicity of the PDMS around the wells allowed for the sample amount to be larger than the well volume. A neodymium magnet was placed underneath the wells and the SERS substrate to force the IMS beads near the sensing surface and accumulate the bacteria cells. Figure 2 depicts a

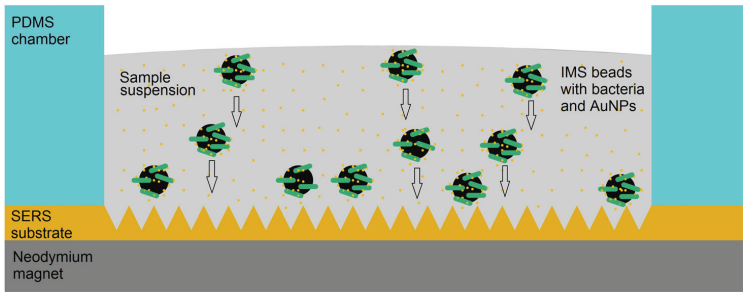

Fig. 2 SERS substrate with an integrated hydrophobic sample well, IMS beads with *L. innocua* ATCC 33090 cells and gold nanoparticles for signal enhancement around the microbe cells. A neodymium magnet placed below the chip for optimal signal collection through the rapid descending of the IMS beads onto the SERS substrate. The arrows show the direction of the IMS bead motion.

situation where the *L. innocua* ATCC 33090 cells are bound by the IMS beads and the sample is placed into a sample well on a SERS substrate. The SERS chip with the well is positioned on top of a neodymium magnet for the studies of rapid IMS bead migration.

2.4 *Cultivation of L. innocua and Capture of Cells with Immunomagnetic Separation Beads*

The bacteria, *L. innocua* ATCC 33090, was grown in Listeria Express Enrichment (LEE) Broth (Labema, Lab M Limited, pH 7.2 ± 0.2) at 35°C for 20 h. Spectrophotometry (Dynamica HALO DB-20S) was used to determine the concentration of the bacteria, which was then diluted into the used concentrations (10^6 to 10^9 CFU/ml) in LEE Broth. Dynabeads® anti-Listeria [Life Technologies (Invitrogen) 71006] with the standard IMS protocol was used for IMS capture of bacteria with a Dynal Magnetic Particle Concentrator DynaMag™-2 (Invitrogen Dynal). Briefly, 1 ml of bacterial culture was incubated at room temperature in a microcentrifuge tube containing 20 μl of Dynabeads® anti-Listeria (Dynal) for 10 min with continuous mixing. Dynal MPC-M magnetic field was used to concentrate the IMS beads. After the supernatant was removed, a washing buffer (0.15 M NaCl, 0.01 M sodium phosphate buffer, pH 7.4 with 0.05% Tween 20) was used for sample washing. The beads were again concentrated to remove the supernatant and the IMS beads with the bacteria were resuspended into 100 ml of washing buffer for SERS detection.

2.5 *Surface-Enhanced Raman Spectroscopy Experiments and Postprocessing of Data*

An in-house built Raman system, coupled with an optical microscope (Olympus BX-51) and a 785-nm excitation laser wavelength, was used for spectral recording. For signal collection, a laser power of 40 mW was used with 20× objective magnification. The sample volume in the experiments for spatial stability without a PDMS well was 6 μl. The signal integration time was 5 s without averaging for the 10^9 CFU/ml samples and 10 s for the 10^8 CFU/ml samples. A sample volume of 5 μl was used with the IMS bound microbe samples mixed with gold nanoparticles (AuNPs) in hydrophobic (PDMS) sample wells. The mixing ratio for microbe samples and AuNPs before dispensing was 2.5 parts AuNP solution (AuNP concentration 1000 mg/l in H_2O) to 10 parts microbe sample solution. The AuNPs are mixed with gold colloids before the stability testing for 30 s. For consistency, the amount of gold nanoparticles in a sample droplet with each concentration was kept constant at 3.6×10^7 particles in a 5-μl droplet volume. The relation between AuNP amount and the bacteria cell amount in one droplet ranges from 10 particles/cell with a higher cell concentration of 10^9 cfu/ml to 10^3 particles/cell with a lower cell concentration of 10^6 cfu/ml. Therefore, the amount of nanoparticles adsorbing to one bacteria cell can differ with different concentrations, although the particle density in the droplet volume is constant. MATLAB (release 2015a, Mathworks Inc.) and PLS toolbox (version 2.0, Eigenvector Research Inc., Manson, Washington) were used for a simple baseline correction (linear fitting) and transfer of the data into Origin Pro (version 9.4, OriginLab Corp.). Origin Pro was used for data postprocessing and plotting.

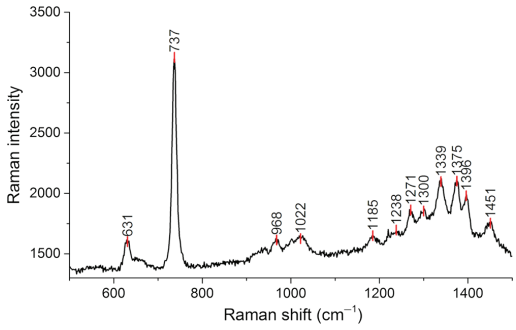

Fig. 3 SERS spectrum of IMS bound *L. innocua* with a concentration of 10^8 CFU/ml, 5-s integration time and 40-mW excitation laser power. Savitsky–Golay function was used for spectrum smoothing.

3 Results and Discussion

The SERS spectrum of the model bacteria *L. innocua* ATCC 33090, measured with the combination of AuNP and a roll-to-roll produced SERS substrate, is presented in Fig. 3. The *L. innocua* ATCC 33090 cells exhibit a strong Raman peak at a Raman shift of 737 cm^{-1}. This main peak, related to a glycosidic ring mode, will be utilized when analyzing the effect of the IMS beads on the signal construction and stability. The measured spectrum is in good agreement with similar spectra previously presented by Luo et al. and Kairyte et al.[16,29]

The difference in the stability of the SERS signal as a deposited SERS droplet on a surface without and with IMS bead capture is presented in Figs. 4(a) and 4(b), respectively. The 44% average deviation of the signal intensity of the main Raman peak at 737 cm^{-1} in the case of Fig. 4(a) is too large even for semiquantitative detection. By using IMS beads, as shown in Fig. 4(b), the average deviation of the signal intensity of the main Raman peak at 737 cm^{-1} diminishes to 13%, thus yielding a better signal stability and repeatability. However, detecting a SERS signal from a droplet can be affected by many factors. Repetitively pipetting a droplet with a constant shape and a similar footprint is difficult. The lens like shape of the droplet can cause challenges with correct focus depth and the efficient capture of the scattered Raman signal. By placing the sample droplet into a hydrophobic PDMS well, the repeatability of the detection can be enhanced. As can be seen from Fig. 4(c), the use of the PDMS well also lowers the average deviation of the signal intensity of the main Raman peak at 737 cm^{-1}.

Although the spatial stability of the signal can be increased with the combination of IMS bead capture and an integrated sample well, the temporal stability is still low. Figures 5(a)–5(c) show the temporal growth of the SERS signal of the main Raman peak at 737 cm^{-1} as a function of time. The signal growth requires at least a 10- to 20-min waiting time for the signal to reach the maximal peak height. This is the time from the appliance of the sample into the well, until the majority of the IMS beads slowly descend to the SERS substrate and to the focus depth of the Raman system. The waiting time adds variance into the detected signal height and delays the signal recording. However, it does increase the intensity of the Raman bands originating from the analyte. Figure 5(d) shows the intensity relation of 10^6 to 10^8 CFU/ml sample concentrations of IMS captured

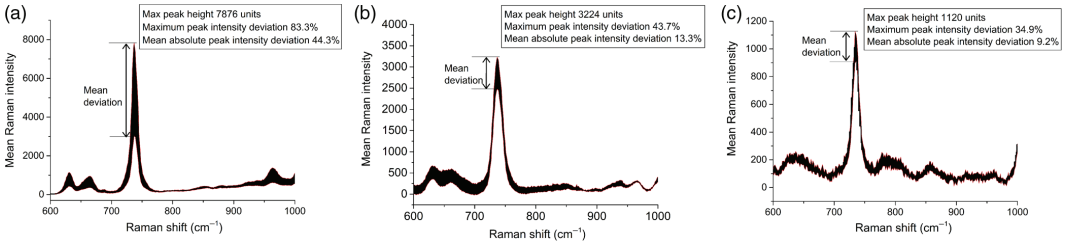

Fig. 4 (a) Deviation of *L. innocua* spectrum measured from a 10^9 CFU/ml droplet. Result of eight spectra measured from 1 mm^2 area. (b) *L. innocua* spectrum with microbes bound to IMS beads from a 10^8 CFU/ml droplet. Result of 10 spectra measured 1 mm^2. (c) *L. innocua* spectrum with microbes bound to IMS beads from a 10^6 CFU/ml sample in a PDMS well. Result of nine spectra measured 1 mm^2.

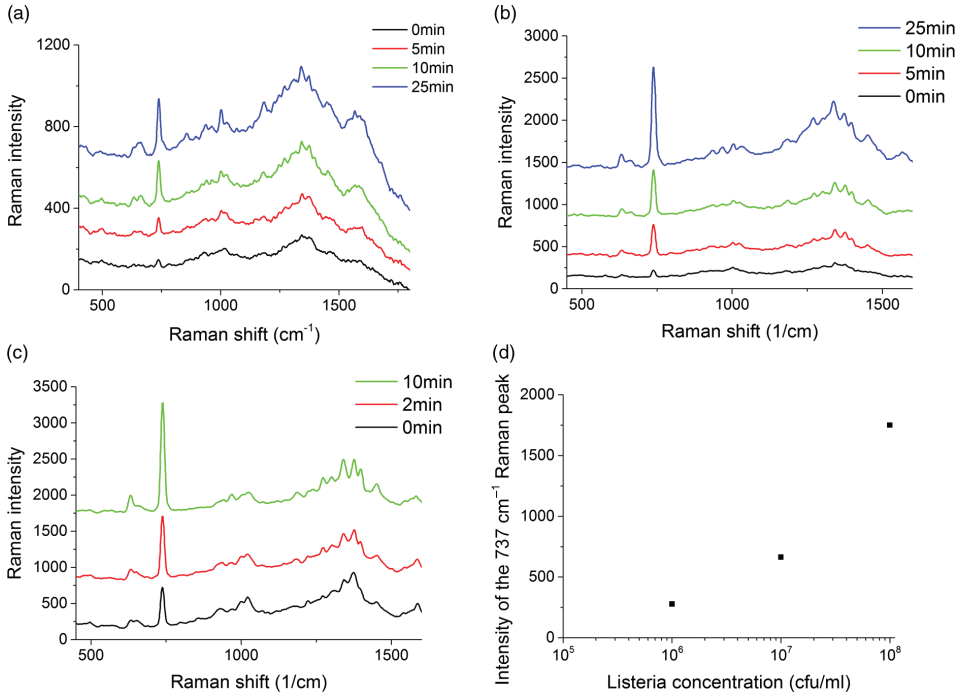

Fig. 5 SERS signal growth of IMS bound *L. innocua* samples with different concentrations in a hydrophobic sample well as a function of time. As the heavy IMS beads slowly descent to the surface of the structured SERS substrate, the signal intensity grows. (a) 10^6 CFU/ml *L. innocua* sample, (b) 10^7 CFU/ml *L. innocua* sample, and (c) 10^8 CFU/ml *L. innocua* sample. (d) Relation of the intensity of the main Raman peak at 737 cm^{-1} as a function of sample concentration after allowing the beads to descend for 10 min. Savitsky–Golay function was used for spectrum smoothing.

L. innocua ATCC 33090 cells detected after allowing the beads to slowly migrate toward the SERS substrate for 10 min. The limit of detection (LoD) with the method is clearly smaller than the lowest detected concentration 10^6 cfu/ml, possibly near 10^5 cfu/ml or lower. According to our previous study without magnet stabilization, an LoD of 1.4×10^4 cfu/ml can be achieved.[17]

By employing the paramagnetic property of the IMS beads, the beads rapidly accumulate onto the SERS substrate. From Figs. 6(a) and 6(b), it can be seen how a neodymium magnet located underneath the SERS substrate functions as an IMS bead attractor. The overall quality of the SERS peaks is increased with the magnetically stabilized samples. Minor peaks of the spectrum can be identified more clearly.

The saturation in the rise of signal intensity is reached within 2 min or less after depositing the sample. The changes in SERS signal intensity with and without the magnet as

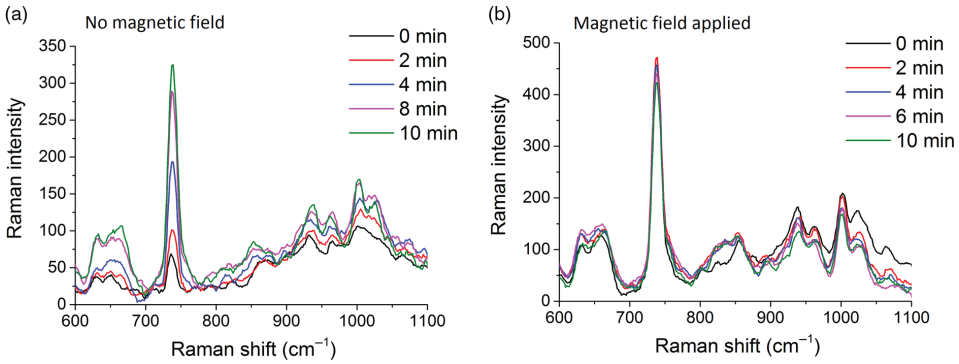

Fig. 6 SERS signal of IMS bound *L. innocua* samples (a) without and (b) with a neodymium magnet placed underneath the SERS chip. The neodymium magnet placed underneath the SERS chip clearly forces the beads to descend faster to the bottom of the hydrophobic sample well. Sample concentration: 10^6 CFU/ml. Savitsky–Golay function was used for spectrum smoothing.

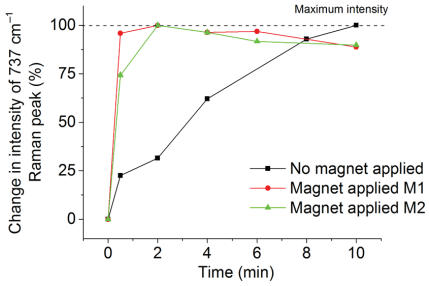

Fig. 7 The change in relative SERS signal intensity of IMS bound *L. innocua* samples as a function of time detected without and with a neodymium magnet placed underneath the SERS chip. Sample concentration: 10^6 CFU/ml.

a function of time are presented in Fig. 7. When the magnetic field is applied, the signal intensity changes only 4.9% after 2 min. The slope of the signal after 2 min is attributed to the local heating of the measurement spot and the degrading effect of the heating to the bacteria cells and IMS beads. Whereas, without the magnetic field, the signal intensity is growing at a constant rate of 2.5%/min up to 10 min and continues to rise further as time progresses even up to 20 min.

In the present study, the effect of IMS beads on the SERS signal stability of bacteria cells was analyzed. The IMS beads stabilized both the temporal and the spatial variance, and accumulated the bacteria cells evenly into the focus depth and to the focal point of the laser beam. The results show the superiority of bacteria cell detection employing IMS capture in comparison to biological cell detection with free cells.

4 Conclusions

The spatial and temporal stability of SERS detection of bacteria cells in solution phase was studied with IMS bead capture and hydrophobic PDMS sample wells. We demonstrate significant improvements of the spatial signal stability by 35% when the bacteria cells were captured by the heavier IMS beads, which were placed into the restricted area of the sample well. The temporal stability was affected by the descending time of the IMS bead inside the sample well. A sample stabilization time of 10 to 20 min was required to achieve saturated SERS signal intensity when no magnetic field was present. However, by using a neodymium magnet as an IMS bead attractor underneath the SERS substrate, the lag time for sample stabilization could be reduced to below 2 min. Besides producing reproducible and more reliable SERS results, this method enables quicker and straightforward laboratory testing.

Acknowledgments

The funding for this project was provided, in part, by TEKES (the Finnish Funding Agency for Technology and Innovation) and University of Oulu Graduate School through Infotech Oulu Doctoral Program. Academy of Finland joined in funding the work through research projects (Foulsens Grant No. 292253 and M-SPEC Grant No. 284907). We thank Tiina Väyrynen (National Resources Institute Finland) for the work with the bacterial sample preparation.

References

1. G. Keiser, *Optical Probes and Biosensors*, pp. 197–232, Springer, Singapore (2016).
2. X. Fan and I. M. White, "Optofluidic microsystems for chemical and biological analysis," *Nat. Photonics* **5**(10), 591–597 (2011).
3. M. Li et al., "Plasmon-enhanced optical sensors: a review," *Analyst* **140**(2), 386–406 (2015).
4. Q. Xiong et al., "Development of an immunomagnetic separation method for efficient enrichment of Escherichia coli O157:H7," *Food control* **37**, 41–45 (2014).
5. I.-H. Cho, L. Mauer, and J. Irudayaraj, "In-situ fluorescent immunomagnetic multiplex detection of foodborne pathogens in very low numbers," *Biosens. Bioelectron.* **57**, 143–148 (2014).
6. H. Wang et al., "Rapid, sensitive, and simultaneous detection of three foodborne pathogens using magnetic nanobead-based immunoseparation and quantum dot-based multiplex immunoassay," *J. Food Prot.* **12**, 2000–2228 (2011).
7. K. Ma et al., "Rapid and simultaneous detection of Salmonella, Shigella, and Staphylococcus Aureus in fresh pork using a multiplex real-time

PCR assay based on immunomagnetic separation," *Food Control* **42**, 87–93 (2014).
8. H. Jayamohan et al., "Highly sensitive bacteria quantification using immunomagnetic separation and electrochemical detection of guanine-labeled secondary beads," *Sensors* **15**(5), 12034–12052 (2015).
9. X.-L. Su and Y. Li, "Quantum dot biolabeling coupled with immunomagnetic separation for detection of Escherichia coli O157:H7," *Anal. Chem.* **76**(16), 4806–4810 (2004).
10. D. W. Inglis et al., "Continuous microfluidic immunomagnetic cell separation," *Appl. Phys. Lett.* **85**(21), 5093–5095 (2004).
11. M. Uyttendaele, I. Van Hoorde, and J. Debevere, "The use of immunomagnetic separation (IMS) as a tool in a sample preparation method for direct detection of L. monocytogenes in cheese," *Int. J. Food Microbiol.* **54**(3), 205–212 (2000).
12. M. A. M. Gijs, "Magnetic bead handling on-chip: new opportunities for analytical applications," *Microfluid. Nanofluid.* **1**(1), 22–40 (2004).
13. O. Olsvik et al., "Magnetic separation techniques in diagnostic microbiology," *Clin. Microbiol. Rev.* **7**(1), 43–54 (1994).
14. A. Sujith et al., "Imaging the cell wall of living single yeast cells using surface-enhanced Raman spectroscopy," *Anal. Bioanal. Chem.* **394**(7), 1803–1809 (2009).
15. L. Chen et al., "Label-free NIR-SERS discrimination and detection of foodborne bacteria by in situ synthesis of Ag colloids," *J. Nanobiotechnol.* **13**(1), 45 (2015).
16. K. Kairyte, Z. Luksiene, and V. Sablinskas, "Identification of different Listeria monocytogenes strains by surface enhanced FT Raman spectroscopy," *Chem. Technol.* **61**(3), 46–49 (2012).
17. S. Uusitalo et al., "Detection of Listeria innocua on roll-to-roll produced SERS substrates with gold nanoparticles," *RSC Adv.* **6**(67), 62981–62989 (2016).
18. C. Fan et al., "Rapid detection of food-and waterborne bacteria using surface-enhanced Raman spectroscopy coupled with silver nanosubstrates," *Appl. Microbiol. Biotechnol.* **92**(5), 1053–1061 (2011).
19. K. M. Syamala et al., "Inhibition assay of yeast cell walls by plasmon resonance Rayleigh scattering and surface-enhanced Raman scattering imaging," *Langmuir* **28**(24), 8952–8958 (2012).
20. .M. Culha et al., "Rapid identification of bacteria and yeast using surface-enhanced Raman scattering," *Surf. Interface Anal.* **42**(6–7), 462–465 (2010).
21. W. R. Premasiri et al., "Characterization of the surface enhanced Raman scattering (SERS) of bacteria," *J. Phys. Chem. B* **109**(1), 312–320 (2005).
22. T. Szymborski, E. Witkowska, and W. Adamkiewicz, "Electrospun polymer mat as a SERS platform for the immobilization and detection of bacteria from fluids," *Analyst* **139**, 5061–5064 (2014).
23. Y. Liu et al., "Potential of surface-enhanced Raman spectroscopy for the rapid identification of Escherichia coli and Listeria monocytogenes cultures on silver colloidal nanoparticles," *Appl. Spectrosc.* **61**(8), 824–831 (2007).
24. J. Chen et al., "Fabrication of large-area, high-enhancement SERS substrates with tunable interparticle spacing and application in identifying microorganisms at the single cell level," *J. Phys. Chem. C* **116**(5), 3320–3328 (2012).
25. H. Zhou et al., "SERS detection of bacteria in water by in situ coating with Ag nanoparticles," *Anal. Chem.* **86**(3), 1525–1533 (2014).
26. M. Çulha and M. Kahraman, "Surface-enhanced Raman scattering of bacteria in microwells constructed from silver nanoparticles," *J. Phys. Chem. C* **112**(28), 10338–10343 (2008).
27. A. Sengupta, M. Mujacic, and E. J. Davis, "Detection of bacteria by surface-enhanced Raman spectroscopy," *Anal. Bioanal. Chem.* **386**(5), 1379–1386 (2006).
28. I. Sayin et al., "Characterization of yeast species using surface-enhanced Raman scattering," *Appl. Spectrosc.* **63**(11), 1276–1282 (2009).
29. .B. Luo and M. Lin, "A portable Raman system for the identification of foodborne pathogenic bacteria," *J. Rapid Methods Autom. Microbiol.* **16**(3), 238–255 (2008).
30. .S. Efrima and L. Zeiri, "Understanding SERS of bacteria," *J. Raman Spectrosc.* **40**(3), 277–288 (2009).
31. K. Kneipp et al., "Single molecule detection using surface-enhanced Raman scattering (SERS)," *Phys. Rev. Lett.* **78**(9), 1667–1670 (1997).
32. J. Kneipp, H. Kneipp, and K. Kneipp, "SERS—a single-molecule and nanoscale tool for bioanalytics," *Chem. Soc. Rev.* **37**(5), 1052 (2008).
33. M. Li et al., "Three-dimensional hierarchical plasmonic nano-architecture enhanced surface-enhanced Raman scattering immunosensor for cancer biomarker detection in blood plasma," *ACS Nano* **7**(6), 4967–4976 (2013).
34. L. He, B. Deen, and T. Rodda, "Rapid detection of ricin in milk using immunomagnetic separation combined with surface enhanced Raman spectroscopy," *J. Food Sci.* **76**(5), N49–N53 (2011).
35. L. He et al., "Rapid detection of a foreign protein in milk using IMS-SERS," *J. Raman Spectrosc.* **42**(6), 1428–1434 (2011).
36. Y. Wang, S. Ravindranath, and J. Irudayaraj, "Separation and detection of multiple pathogens in a food matrix by magnetic SERS nanoprobes," *Anal. Bioanal. Chem.* **399**(3), 1271–1278 (2011).
37. U. Tamer et al., "Fabrication of magnetic gold nanorod particles for immunomagnetic separation and SERS application," *J. Nanopart. Res.* **13**(8), 3167–3176 (2011).
38. K. Bantz, A. Meyer, and N. Wittenberg, "Recent progress in SERS biosensing," *Phys. Chem. Chem. Phys.* **13**, 11551–11567 (2011).
39. S. Nie, "Probing single molecules and single nanoparticles by surface-enhanced Raman scattering," *Science* **275**(5303), 1102–1106 (1997).
40. M. Li et al., "Stamping surface-enhanced Raman spectroscopy for label-free, multiplexed, molecular sensing and imaging," *J. Biomed. Opt.* **19**(5), 050501 (2014).
41. T.-S. Wong et al., "Nanochromatography driven by the coffee ring effect," *Anal. Chem.* **83**(6), 1871–1873 (2011).
42. G. Frens, "Controlled nucleation for the regulation of the particle size in monodisperse gold suspensions," *Nature* **241**(105), 20–22 (1973).
43. S. Z. Oo et al., "Disposable plasmonic plastic SERS sensor," *Opt. Express* **21**(15), 18484–18491 (2013).

Sanna Uusitalo received her master's degree in biophysics from the University of Oulu, Finland, in 2004. Currently, she is preparing her doctoral degree in electrical engineering while working as a research scientist at Technical Research Centre of Finland. Her research interests include identification of biological cells and small molecules with surface enhanced Raman spectroscopy and integration of microfluidic circuits into photonic sensing platforms.

Martin Kögler received his diploma degree in IT information systems at the Technical University of Ilmenau, Germany, in 2006. He worked at the Telebitcom GmbH sensor-engineering company in Germany and continued his research at the Bioprocess Engineering Laboratory (University of Oulu) in Finland. Before continuing his PhD project at TU-Berlin (Germany) and University of Helsinki in January 2015, he worked for VTT (Technical Research Centre of Finland), mainly on the technical development of Raman spectrometers.

Anna-Liisa Välimaa received her MSc degree in nutrition and food biotechnology from the University of Eastern Finland, Kuopio, Finland, in 2004 and her PhD in biotechnology and toxicology from Tampere University of Technology, Tampere, Finland, in 2010, with research titled "*In vitro* bioassays in bioactivity and residue assessments." She is currently working as a principal research scientist at Natural Resources Institute, Finland. Her research interests include biotechnology and food research: nutrition, food safety, and value-added products.

Jarno Petäjä received his MSc degree in physics from the University of Oulu, Finland, in 2003. He is currently working as a research scientist at Technical Research Centre of Finland. His latest research activities are in printed electronics and nanoimprint lithography of photonic structures.

Ville Kontturi received his MSc and PhD degrees in measurements technology from the University of Joensuu/Eastern Finland in 2007 and 2011 with research titled "Optical measurements of complex liquids." His research interests are measurements and fabrication technologies for photonics applications.

Samuli Siitonen is CTO at Nanocomp Oy Ltd. He joined the Nanocomp team in 2001, while he was simultaneously conducting scientific research in physics at the University of Eastern Finland, Department of Physics and Mathematics, Micro and Nanophotonics group. He received his PhD in diffractive optics for light guide applications. He applies wide-ranging knowledge gained from experimental research and industry-related cooperation in multiple areas of manufacturing technology in the field of nano- and micro-photonics components.

Riitta Laitinen received her MSc and PhD degrees in chemistry from the University of Oulu Finland in 1991 and 1999 with research titled "New heterodonor phosphine and bipyridine ligands." She is currently working as a group manager at Natural Resources Institute of Finland. Her research interests include biotechnology and food research.

Matti Kinnunen received his MSc (Tech) and DSc (Tech) degrees in electrical engineering from the University of Oulu, Finland, in 2002 and 2006, respectively. His research interests include light–matter interactions in tissues and at the single cell level, sensors and measurement techniques, as well as optical noninvasive measurement

techniques for biomedical applications. He is currently working as a senior research fellow at the University of Oulu.

Tapani Viitala received his PhD in physical chemistry in 1999. His current research focuses on developing novel real-time label-free in vitro measuring platforms for existing biological assays and animal tests. He aims to gain a better understanding of the kinetics and intermolecular interactions involved in drug action and delivery. He is currently working as a researcher and cogroup leader of the Pharmaceutical Biophysics research group at the faculty of Pharmacy at the University of Helsinki.

Jussi Hiltunen received his doctoral degree in electrical engineering from the University of Oulu, Finland, in 2008. His research interests include photonics materials and fabrication technologies for sensor applications.

PAPER IV

Surface-enhanced Raman spectroscopy for identification and discrimination of beverage spoilage yeasts using patterned substrates and gold nanoparticles

Journal of Food Engineering, 212, 47–54,
DOI information: 10.1016/j.jfoodeng.2017. 05.007.

Journal of Food Engineering 212 (2017) 47–54

Contents lists available at ScienceDirect

Journal of Food Engineering

journal homepage: www.elsevier.com/locate/jfoodeng

Surface-enhanced Raman spectroscopy for identification and discrimination of beverage spoilage yeasts using patterned substrates and gold nanoparticles

Sanna Uusitalo [a, *], Alexey Popov [b, g, i], Yury V. Ryabchikov [c, d], Olga Bibikova [b], Hanna-Leena Alakomi [a], Riikka Juvonen [a], Ville Kontturi [e], Samuli Siitonen [e], Andrei Kabashin [c], Igor Meglinski [b, f, g, h, i], Jussi Hiltunen [a, 1], Arja Laitila [a, 1]

[a] VTT Technical Research Centre of Finland, Kaitoväylä 1, Oulu, 90590, Finland
[b] Optoelectronics and Measurement Techniques, Faculty of Information Technology and Electrical Engineering, University of Oulu, Erkki-Koiso Kanttilan katu 3, Oulu, 90570 Finland
[c] Aix-Marseille University, CNRS, UMR 7341 CNRS, LP3, Campus de Luminy, Case 917, F-13288, Marseille Cedex 9, France
[d] P.N. Lebedev Physical Institute of Russian Academy of Sciences, 53 Leninskii Prospekt, Moscow 199 991, Russia
[e] Nanocomp Oy Ltd, Ensolantie 6, Lehmo, 80710, Finland
[f] National Research Nuclear University "MEPhI", Institute of Engineering Physics for Biomedicine (PhysBio), 115409 Moscow, Russia
[g] Terahertz Biomedicine Laboratory, ITMO University, 49 Kronverksky Prospekt, St. Petersburg, 197101, Russia
[h] Laboratory of Biosensorics and Eco-Photonics, Irkutsk State University, Irkutsk, 664003, Russia
[i] Interdisciplinary Laboratory of Biophotonics, Tomsk National Research State University, 634050 Tomsk, Russia

ARTICLE INFO

Article history:
Received 3 January 2017
Received in revised form
28 April 2017
Accepted 9 May 2017
Available online 18 May 2017

Keywords:
Beverage
Yeast
Raman spectroscopy
SERS
Nanoparticles

ABSTRACT

In the beverage industry, the detection of spoilage yeasts such as *Wickerhamomyces anomalus* and *Brettanomyces bruxellensis* can be labourious and time-consuming. In the present study, a simple and repeatable technique was developed for rapid yeast detection using a combination of patterned gold-coated surface-enhanced Raman spectroscopy (SERS) substrates and gold nanoparticles. *W. anomalus* and *B. bruxellensis* showed several characteristic peaks, enabling the discrimination of these yeasts without chemometric analysis. The control yeast used as an indicator yeast, *Rhodotorula mucilaginosa*, showed 7 cell wall-related peaks originating from lipids and haemoproteins. Analysing *W. anomalus* SERS spectra with differently sized and shaped gold nanoparticles revealed the benefit of using either large, spherical, chemically synthesised gold nanoparticles or small, laser-synthesised, gold-silicon nanoparticles for yeast detection. Additionally, the spectra showed differences in SERS signal construction for small molecules and biological cells, as the nanoparticles with best response in biological cell detection did not excel in small molecule detection. The use of small composite gold-silicon nanoparticles in combination with the SERS substrate gave distinctive spectra for all detected yeast species.

1. Introduction

Yeast spoilage in the beverage industry is a costly problem arising from off-flavours caused by the metabolic end products of the yeast cells (Loureiro and Querol, 1999; Loureiro, 2000). Although yeasts are essential for making beer and wine and are often vital for forming the specific taste of the beverage (Stratford, 2006; Amorim et al., 2016), some yeasts can spoil the final products. In the worst cases, yeast spoilage can lead to exploded cans of soft drinks and cloudy re-fermented products with unwanted off-flavour in beverages (Rodriguez et al., 2013; Stratford, 2006). The presence of a few cells of a specific spoilage yeast at any stage of the manufacturing process may result in quality defects that are perceptible by the consumer. Despite many advances in controlling microbiological risks in beverage production, the globalisation of trade, use of exotic raw materials and novel processing technologies and the growing demand for minimally processed fresh-tasting products create new challenges for manufacturers to ensure product safety and stability. Thus, there is a need to develop

* Corresponding author.
E-mail address: sanna.uusitalo@vtt.fi (S. Uusitalo).
[1] Equally shared supervision.

http://dx.doi.org/10.1016/j.jfoodeng.2017.05.007
0260-8774/

effective control and detection tools for harmful microbes, including spoilage yeasts.

Beverages containing spoilage yeasts are difficult to detect by the naked eye. As many as 10,000 cells/ml are required to change the appearance of a drink. In the beverage industry, microbiological quality control mainly relies on the use of plate cultivation techniques, which are often labourious and time-consuming. The detection of spoilage fungi typically requires at least 5–7 days, and these methods rarely distinguish between spoilage and harmless microbes. After detection, the identification of yeasts often requires slow, labourious DNA sequencing or morphological and physiological testing to identify the organisms (Loureiro and Malfeito-Ferreira, 2003; Loureiro and Querol, 1999; Loureiro, 2000; Pitt and Hocking, 2009).

Recently, surface-enhanced Raman spectroscopy (SERS) has been demonstrated for the identification of yeasts by several research groups (Chen et al., 2012; Chrimes et al., 2013; Gessner et al., 2002; Sayin et al., 2009; Sujith et al., 2008; Sujith et al., 2009; Syamala et al., 2012). SERS detection is based on vibrational spectroscopy, where the signal intensity of Raman scattering is enhanced by localised or propagating plasmon resonance in noble metals (Anker et al., 2008). Thus, bonds to biomolecules such as proteins, lipids, carbohydrates, and nucleic acids on the cell wall of yeast cells create a specific Raman spectrum, enabling identification of different yeast species. SERS is promising for molecular and microbial detection, with advantages such as analyte identification, speed and the possibility for multiple simultaneous analyses. The presence of other microbes or DNA in the laboratory is not a concern in SERS (Rodriguez et al., 2013). Yeast detection by SERS has mainly focused on characterisation of different yeasts with colloidal suspensions of silver nanoparticles (Ag NPs) incubated with the cells, and by focussing on single cells or small clusters of cells in combination with highly magnifying optics (Chrimes et al., 2013; Culha et al., 2010; Sayin et al., 2009; Sujith et al., 2008; Syamala et al., 2012). Syamala et al. revealed the difficulty in obtaining reproducible SERS spectra from yeast cells with Ag NP incubation, as there are various factors affecting the adsorption of Ag NPs to the proteins, including flexibility/mobility, accessibility, polarity and the exposed surface (Syamala et al., 2012). Silver nanoparticles are advantageous for SERS, as silver has a higher SERS enhancement factor than other metals such as gold (Schwartzberg et al., 2004). However, there are reasons to consider the latter for SERS. AgNPs are prone to oxidation and release toxic silver ions; although surface stabilisation is applied, it can make the nanoparticles bio-incompatible and inappropriate for longer storage (Greulich et al., 2012). Gold is stable and non-toxic, and does not harm the yeast cells under inspection (Alkilany and Murphy, 2010); (Shukla et al., 2005). Additionally, gold-initiated SERS can be excited with near-infrared (NIR) wavelengths, thus reducing thermal damage due to longer wavelengths with lower energy (Notingher et al., 2002).

Very little research has been performed using Raman or SERS detection of beverage yeasts other than *Saccharomyces cerevisiae*. Rodriguez et al. measured the Raman spectra of wine spoilage yeasts including *Saccharomyces cerevisiae*, *Zygosaccharomyces bailii*, and *Brettanomyces bruxellensis (B. bruxellensis)*, but specific Raman spectra with several peaks for *Brettanomyces bruxellensis* or other yeasts used in the study were not observed. The study was executed using microscope-assisted Raman without SERS enhancement, and relatively high excitation laser power (30 mW) was used (Rodriguez et al., 2013). In the present study, yeast detection by SERS was developed using NIR excitation, reduced laser power and thermally dried yeast cells on top of a SERS substrate with gold nanoparticles (AuNPs) to achieve characteristic Raman spectra, which can be used for straightforward, simple discrimination of the beverage yeast species. Incubation of nanoparticles with yeast cells prior to detection was avoided to obtain spectra with less variance due to various colloid adsorption factors. Raman spectra for two beverage spoilage yeasts, *Wickerhamomyces anomalus* (*W. anomalus)* and *B. bruxellensis*, and a reference yeast, *Rhodotorula mucilaginosa (R. mucilaginosa)* were successfully detected. Different AuNPs for the detection of *W. anomalus* were analysed to determine the optimal combination of SERS substrate and NPs, producing high SERS enhancement with low background signal. The SERS substrates were used as an analysis chip basis to increase the electromagnetic field (Li et al., 2013; Uusitalo et al., 2016) with the combination of nanoparticles. They were fabricated with roll-to-roll UV-nanoimprint lithography, allowing for high-throughput manufacturing of the SERS chips (Oo et al., 2013).

2. Materials and methods

2.1. Gold nanoparticles

2.1.1. Star nanoparticles (star AuNPs)

Nanostars were fabricated using a seed-mediated growth method (Yuan et al., 2012) with slight modifications (Bibikova and Popov, 2015; Bibikova et al., 2016). Gold nanospheres (NSps) with 15 nm diameter were used as seeds. In detail, 10 μL of 1 M HCl and 100 μL of the NSps solution were added to 10 mL of 0.25 mM $HAuCl_4$ aqueous solution at room temperature under vigorous stirring. Then, 100 μL of 2 mM $AgNO_3$ and 50 μL of 0.1 M ascorbic acid were added to the solution with 30 s stirring as the colour changed to dark grey. Next, 250 μL of 0.36 mM poly(vinyl pyrrolidone) was added under gentle stirring for 15 min. The solution was centrifuged twice at 7500 relative centrifugal force in terms of acceleration for 10 min. The 15 nm sized star AuNPs were synthesised by the reduction of $HAuCl_4$ with sodium citrate using Grabar's method: 4.5 mL of 1% sodium citrate was added quickly to boiling 0.03% $HAuCl_4$ (50 mL), resulting in a change in solution colour to deep orange-red. The original star AuNP concentration was diluted in a ratio of 1:4 into deionised (DI) water to better match the optical density (OD) of spherical particles.

2.1.2. Ultrapure nanoparticles

Synthesis of gold-silicon nanocomposite particles (AuSi NCs) was performed using the pulsed laser ablation method described previously (Blandin et al., 2013; Kabashin and Meunier, 2003; Maximova et al., 2015; Rioux et al., 2009; Ryabchikov et al., 2016). In brief, a gold target was ablated in a previously prepared solution of silicon NPs. Laser ablation was performed by Ti:Sapphire laser (Hurricane Spectra Physics Laser) operated at 800 nm and a 1000-Hz repetition rate, with a 110-fs pulse duration. Laser energy fluence was fixed at 150 μJ/pulse. For fabrication of a colloidal solution of silicon NPs (Blandin et al., 2013; Rioux et al., 2009) a silicon target was immersed in 18-MΩ deionised water and exposed to fs-pulsed laser radiation. The Si target was replaced by an Au target, and laser ablation was applied in the presence of Si nanoparticles (Kabashin and Meunier, 2003). The dual ablation leads to the formation of composite AuSi composite nanoparticles (AuSi NC) (Ryabchikov et al., 2016). The advantage of laser-assisted synthesis is in the absence of ligands on the nanoparticle surface, which guarantees a strong response for the formed nanoparticles (Angelov et al., 2016; Hebié et al., 2015). Despite the presence of protective ligands, AuSi NCs are extremely stable, due to the strong negative charge of colloids, which leads to an electric repulsion effect. The AuSi NC suspension was diluted in a ratio of 1:1 into DI water to better match the OD of the spherical particles.

2.1.3. Chemically synthesised spherical nanoparticles

Spherical NPs of different sizes were purchased from Sigma-Aldrich (CytoDiagnostics, Inc., Burlington, Ontario, Canada). NPs 10 nm, 80 nm, 150 nm and 200 nm in diameter were acquired in 0.1 mg/mL citrate buffer. According to the CytoDiagnostics product description, the nanoparticles in citrate buffer have a high salt stability (30 mM NaCl, 30 min). The optical density (OD) of particles was set to 1. The concentrations of the 200-nm, 150-nm, 80-nm and 10-nm particles in citrate buffer were $1.9 \cdot 10^9$ particles/mL, $3.6 \cdot 10^9$ particles/mL, $7.8 \cdot 10^9$ particles/mL and $6.0 \cdot 10^{12}$ particles/mL, respectively. The 150-nm diameter particles were also acquired in phosphate buffered saline (PBS) buffer. The concentration of the particles was $3.6 \cdot 10^9$ particles/mL, the OD was 1 and the solution was 99% free of residual reactants from manufacturing.

2.2. SERS substrate and PDMS sample well

SERS substrate fabrication and PDMS well integration were described previously (Oo et al., 2013; Uusitalo et al., 2016). In short, the SERS substrates were fabricated using UV-nanoimprint lithography and roll-to-roll (R2R) equipment. UV-curable lacquer was applied with reverse gravure and patterned with an embossing reel, and the structures were cured through UV exposure. The web was die-cut and coated with a 240-nm gold layer by vapour deposition. The 2-mm diameter hydrophobic sample wells were integrated into the gold layer of the SERS substrates by physical adsorption. The developed R2R fabrication is capable of high-throughput volumes with low cost per chip, which simplifies the detection as the chips can be disposed after use and do not require extra cleaning steps.

2.3. VIS-NIR spectroscopy and TEM imaging

VIS-NIR spectroscopy was performed using a spectrophotometer (Optronic Laboratories, USA) from 350 to 1050-nm. The original measured collimated transmittance was recalculated into OD. The maximum signal absorbance of different AuNPs was tuned to a similar range by diluting the AuSi NCs in a 1:1 ratio and the Star AuNPs in a 1:4 ratio. The diluted samples were used in the SERS detection of *W. anomalus*. TEM imaging was performed with LEO 912 Ω EFTEM (Zeiss, Germany) by drop-casting NP suspensions onto carbon-coated copper grids.

2.4. Raman spectroscopy of small molecules and yeast cultures

A 785-nm excitation laser was used in a Raman system coupled with an optical Olympus Microscope (Olympus BX-51, Japan), in combination with 50 × magnifying optics. Spectra were acquired over a Raman shift range of 400–2100 cm^{-1} with 1.076 cm^{-1} resolution. The 100 μM Rhodamine 6G (R6G) in the study was mixed with 0.1% non-ionic detergent TWEEN in a volume ratio of 70:30 and dried on top of a hot plate (40 °C) inside 1.5-mm diameter PDMS that was well integrated on the SERS substrate. Subsequently, AuNP solutions were dried on top of the R6G samples (40 °C). The integration times were 1 s for diluted star AuNPs, AuSi NCs and 150 nm AuNPs in PBS Otherwise, the integration time was 2 s. 15 points were recorded per sample, and results were normalised with the integration time. Yeast strains *Wickerhamomyces anomalus* VTT C-02470 (C470), *Brettanomyces bruxellensis* VTT C-05796 (C796) and *Rhodotorula mucilaginosa* VTT C-89179 (C179), isolated from beverage production, were obtained from the VTT Culture Collection (http://culturecollection.vtt.fi). Yeast strains were grown on yeast-malt extract agar, (YM-agar, Difco Laboratories, Detroit, USA) at 25 °C for 2–4 days. Yeast samples in 0.9% physiological saline buffer were prepared using a precision scale to measure the ratio of inoculating loop-inserted yeast mass and saline. *W. anomalus* concentration for the nanoparticle analysis was $8 \cdot 10^7$ cells/ml, prepared by adding 0.015 g of yeast to 2 mL of saline. The *W. anomalus, B. bruxellensis* and *R. mucilaginosa* concentrations for gold-silicon composite nanoparticle (AuSi NC) detection was $4 \cdot 10^7$ cells/ml. The yeast buffer solutions with 4-μl volume were pipetted inside PDMS wells integrated onto the SERS substrates and dried at 30 °C. Drying caused the salts of the buffer to crystallise locally. Raman detection was conducted over areas free of the crystallised salt. AuNP solutions with 4-μl were dried on top of the yeast samples (at 30 °C). Yeast response results were averaged from three collected spectra, with three averaged 5-s integration times each. Each yeast species was measured in triplicate with PDMS wells 2 mm in diameter, and 10 measurement points with approximately 30 μm spacing were recorded per well (30 measurement points/sample).

3. Results and discussion

Two spoilage yeasts, *Wickerhamomyces anomalus* and *Brettanomyces bruxellensis*, and an additional control yeast, *Rhodotorula mucilaginosa,* were chosen for this study to develop a new method for beverage yeast detection by SERS. *W. anomalus* and *B. bruxellensis* are often related to the production of volatile compounds causing off-flavours in wines, beers and soft drinks (Martin et al., 2016). *Brettanomyces bruxellensis*, also known as *Dekkera bruxellensis*, can produce an acetic taste in beers and undesirable flavours in soft drinks due to acetate-ester production (Hayashi et al., 2007). *Rhodotorula mucilaginosa* is a soil yeast that produces red/pink coloured carotenoids (Aksu and Eren, 2005). In the beverage industry, *Rhodotorula* yeasts are often considered hygiene indicators at manufacturing plants but are not normally associated with spoilage of the final product (Laitila et al., 2011). Detection of yeast cells on SERS substrates can be difficult, as the yeasts are relatively large species (diameter 4–10 μm). When the size of the yeast cells is compared to the size of the SERS excitation patterns on the substrates (diameter nanometre to 1 μm), it is evident that SERS signal acquisition is limited to the area of the yeast near the substrate, thus covering only one side of the yeast cell. It follows that the yeast cells have been commonly detected using metal nanoparticles (NPs) adsorbed around the yeast cell. Although this enhances the signal, in the case of nanoparticles, the highest SERS enhancement factor may be missing because the yeast cells are too large to fit into the small hotspot pockets of the aggregated NPs. In SERS, the metal used, composition, size and shape of the NPs affect the field enhancement factor and the resonance excitation wavelength. In this study, the compatibility of a new hybrid detection method, joining a gold-plated SERS substrate patterned with UV-nano imprinting and nanoparticles of differing composition, size and shape, was analysed for yeast cell detection. The method benefits from the overlapping local surface plasmon resonance fields, which can lead to the growth of the total field, as shown in the case of protein biomarkers (Li et al., 2013b) and bacteria detection (Uusitalo et al., 2016). The effect of size, shape and buffer of NPs on Raman spectra was studied with light spectroscopy, Transmission electron microscopy (TEM) imaging and hybrid SERS detection using the model analyte Rhodamine 6G (R6G) and the chosen beverage yeast strains. TEM imaging was used to compare the shapes and reveal the NP size distribution. All NPs had spherical shapes, as shown in Fig. 1 a) -g). The star AuNPs shown in Fig. 1 a) have additional sharp spikes, affecting their VIS-NIR absorbance and creating SERS hotspots. According to the images, the size ranges of the commercial particles and star AuNPs are consistent, but the AuSi NCs, as shown in Fig. 1 b), have some larger particles amid the small ones.

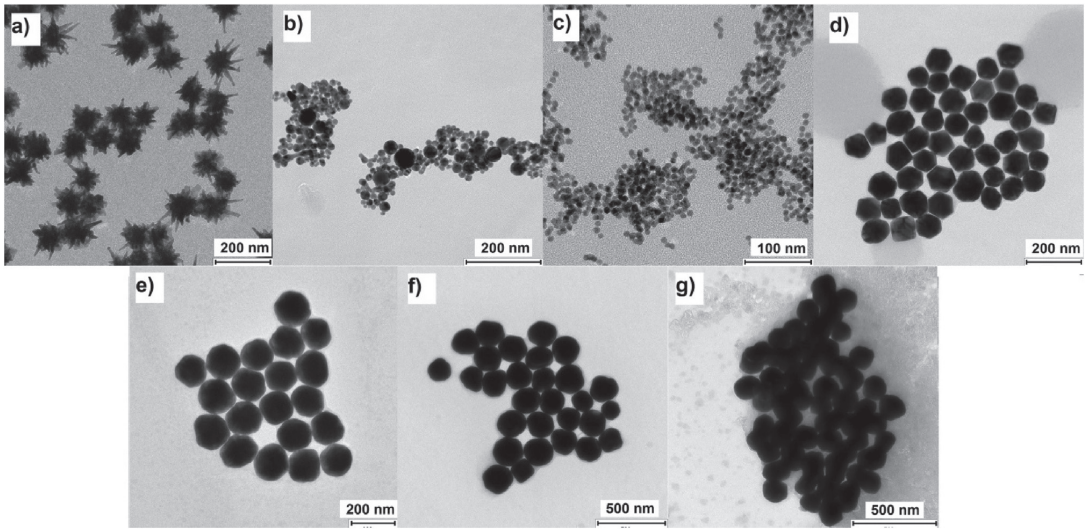

Fig. 1. TEM images of the analysed AuNPs. a) Star AuNPs with an average diameter of 79 nm, with spikes excluded, b) AuSi NCs with an average diameter of 16 nm, c) 10-nm AuNPs in citrate buffer, c) 80-nm AuNPs in citrate buffer, d) 150-nm AuNPs in citrate buffer, e) 200-nm AuNPs in citrate buffer and f) 150-nm AuNPs in PBS buffer. The size histograms for the calculation of average NP diameters are presented in Supplementary Material Fig. S1.

As the absorbance of the nanoparticles indicated the best excitation wavelength band for SERS via the connection to the resonance wavelength of the particles, VIS-NIR spectra for the chosen nanoparticles were recorded (Fig. 2). According to the VIS-NIR spectra, star AuNPs and 200-nm AuNPs in citrate buffer showed the highest absorbance at 785 nm, while 10-nm and 80-nm spherical NPs and AuSi NCs showed the lowest. The 10-nm and 80-nm spherical nanoparticles and AuSi NCs showed the lowest absorbance at 785 nm. Thus, it was assumed that the 200 nm particles and star AuNPs would show the highest SERS enhancement factors.

The relative SERS enhancement of AuNPs was further studied by recording the SERS spectra for Raman active R6G, which is commonly used as a reference sample in Raman detection. As follows from Fig. 3, the large spherical AuNPs showed the highest R6G peaks. The strongest spectrum was achieved with 150-nm AuNPs in PBS, but the peaks had a large fluorescence background originating

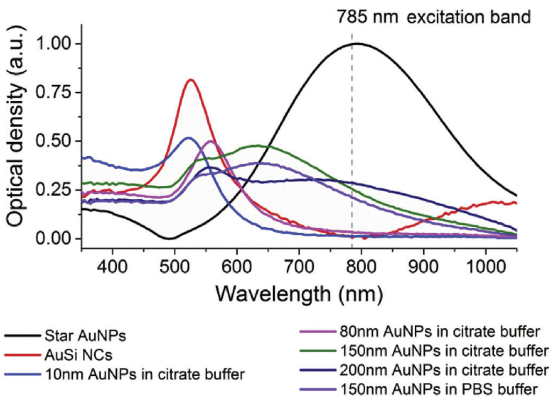

Fig. 2. VIS-NIR absorbance spectrum (optical density) for the analysed AuNPs.

from the PBS buffer. This background can pose a problem in handling biological samples and mask Raman signals less intense than the R6G sample. Interestingly, the star AuNPs showing the best absorbance at 785 nm showed lower enhancement. The signal intensity of R6G with star AuNPs was in the same range achieved with similarly sized 80-nm AuNPs. Thus, although a SERS signal was detected, the spike-shaped stars did not show an additional advantage, possibly due to presence of ligands on their surface. Also observed was the peak intensity of R6G with bare AuSi NCs. The 16 nm AuSi NCs showed similar enhancement as the 80-nm particles, possibly due to better adsorption of R6G molecules to the bare surface of the AuSi NCs. This ensures excellent contact of R6G molecules with metal, providing higher SERS enhancement. The 10-nm particles did not show additional enhancement with the SERS substrate.

From the results of the R6G detection, we conclude that the citrate buffer is preferential to the PBS buffer, as it shows lower fluorescent background signal. The largest particles, 150-nm and 200-nm diameter AuNPs, exhibited the highest peak intensity. A combination of 80-nm particles, star AuNPs or the AuSi NCs with SERS substrate showed lower enhancement, but with 10-fold higher signal than the SERS substrate alone.

As shown in the literature, excitation laser power can damage biological cells during measurement (Gessner et al., 2002; Rösch et al., 2003). Appropriate laser power also depends on whether the cells are measured in solution or dried on top of the SERS substrate. Syamala et al. reported that the detection of yeast cells incubated with silver colloids had problems in terms of repeatability, the aim of the present study was to detect cells in a thermally dried state using an NIR excitation wavelength and low excitation power that causes less thermal damage to the cells. Optimal power for the dried yeast cells was studied by recording the SERS spectrum for *W. anomalus* as a function of laser power. The change in the average intensity of the main Raman peak 738 cm^{-1} relative to power is presented in Fig. 4 a). An excitation power of 2 mW requires more than 60 s integration times to show several distinctive peaks for the yeast cells. However, a laser power above

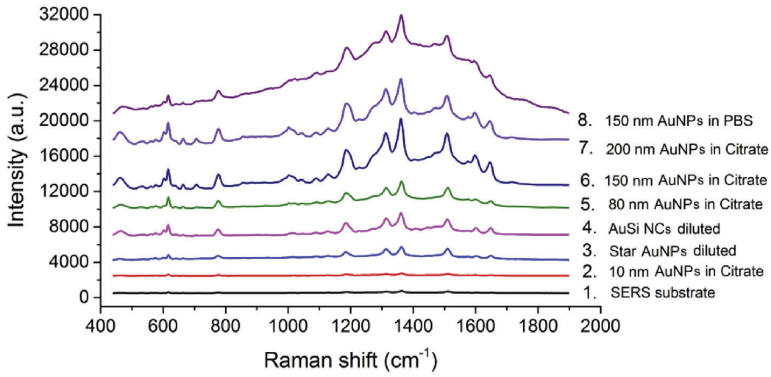

Fig. 3. SERS spectra of R6G detected with different AuNPs on top of a SERS substrate. The average SERS spectra were calculated from 30 points measured in duplicate. Curves are separated for clarity with arbitrary constant values.

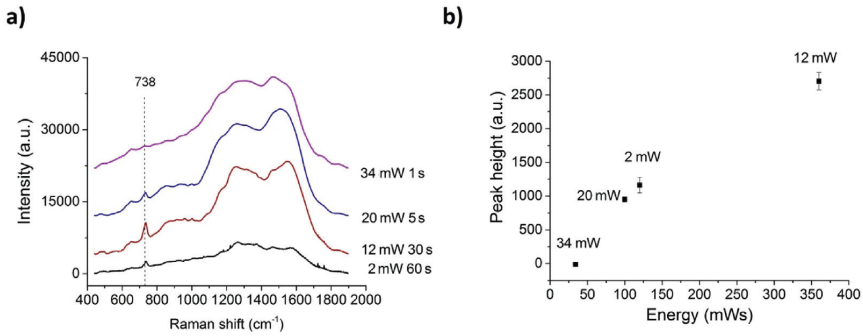

Fig. 4. a) SERS spectra of *W. anomalus* detected using four laser powers and varying integration times. b) The baseline corrected peak height for the 738 cm^{-1} Raman peak as a function of energy calculated from the laser power and integration time. The average SERS spectra were detected using 150-nm AuNPs in citrate buffer on top of SERS substrate and calculated from 15 points measured for each laser power.

20 mW destroys the characteristic Raman peaks, such as 738 cm^{-1} and 967 cm^{-1}, seen in Fig. 4 b). The main Raman peak is no longer visible with 34 mW power. Clearly, high laser power can damage the cells under inspection, although it does not destroy the buffer-derived fluorescence signal. With 12 mW power, the 738 cm^{-1} Raman peak has the highest intensity after background reduction, and the integration time could be shortened by half from 2 mW excitation laser power. To ensure that the detected *W. anomalus* signal originates from the yeast cells, the effect of yeast cell concentration on SERS signal was detected with 150 nm AuNPs in citrate buffer, showing how the Raman peak intensity increases with sample concentration. The results are presented in Supplementary Material Fig. S3.

The chosen AuNPs were applied to measure the spectrum for *W. anomalus* using a slightly lower 10 mW excitation laser power and reduced total integration time of 15 s to ensure minimal thermal damage. This study included triplicate samples with 10 measurement points per sample to demonstrate the repeatability of the detection method. The SERS response of the hybrid detection method with differently shaped NPs is shown in Fig. 5. The SERS

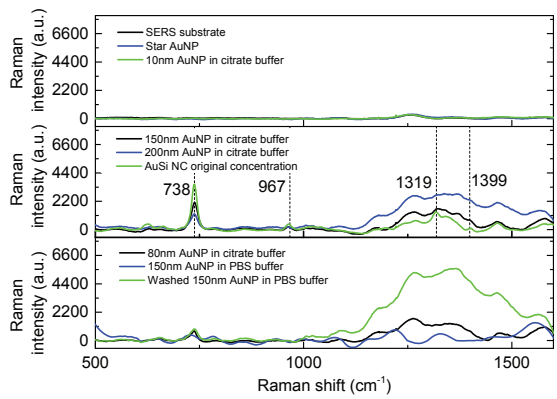

Fig. 5. SERS spectra of *W. anomalus* detected using different AuNPs with similar optical density (Fig. 2) on top of SERS substrate. The average SERS spectra were calculated from 10 points measured in triplicate.

substrate alone without AuNPs does not show characteristic peaks, such as the 738 cm^{-1} for *W. anomalus*, and the signal intensity for the entire spectrum remains low. The star AuNPs and 10-nm spherical AuNPs show similarly low signal intensity, without characteristic peaks. The star AuNPs showed a clear signal with the R6G sample (Fig. 3) which invites speculation about whether the coverage of the star AuNPs with PVP has a stronger influence on biological cells than the small molecules entirely inhibiting the contact of the gold surface with yeast cells, suppressing the Raman signal. The larger spherical AuNPs in citrate buffer show the characteristic peak 738 cm^{-1}, although for the 150-nm AuNPs spectrum it is more distinct than for 80-nm or 200 nm-AuNPs. The good suitability indicated for 200-nm particles by the VIS-NIR absorbance spectrum (Fig. 2), does not exhibit higher Raman signals with the actual yeast samples. Additionally, the difference in AuNP buffer can significantly affect yeast detection, as the 150-nm AuNPs in PBS do not show any characteristic yeast peaks, unlike the 150-nm AuNPs in citrate buffer. This could be due to the Raman signal and the fluorescence background of the PBS buffer. After washing AuNPs and replacing the buffer with DI water (Raman neutral medium) the background signal was diminished and the main Raman peak was detected, but the intensity was lower than acquired with similar AuNPs in citrate buffer. The results obtained with the ultra-pure composite AuSi NCs showed better compatibility of nanocomposites for biological cell detection than for small molecule detection. They produced the lowest background signal for the *W. anomalus*, and in this respect are optimal for yeast detection. The deviation of the SERS signals in Fig. 5 is presented in the Supplementary Material (Fig. S2) showing that the detected Raman peaks do not shift in wavenumber between detection points and parallel samples.

AuSi NCs were used to detect the SERS spectrum for *W. anomalus*, *B. bruxellensis* and *R. mucilaginosa.* The NP concentration was increased by half, and the effect of the higher NP concentration on the SERS signal construction is shown in Supplementary Material Fig. S4. The samples were dried on top of the SERS substrate, with subsequent addition of AuSi NC. The recorded yeast SERS spectra are shown in Fig. 6, where several Raman bands for the yeast strains are clearly distinguishable. The pink-pigmented *R. mucilaginosa* showed seven characteristic peaks, while the spoilage yeasts *W. anomalus* and *B. bruxellensis* showed four peaks. The background SERS spectrum for physiological saline was subtracted from the spectra of the yeasts. The original raw data without background reduction is presented in Supplementary Material (Fig. S5).

The detected Raman bands, with preliminary band assignments, are presented in Table 1. Typically, the yeast cell wall is composed of 25% helical b(1–3) and b(1–6)-D-glucans, 25% oligomannans, 20% protein, 10% lipids, and some chitin. The proteins present are predominantly mannoprotein complexes (Sayin et al., 2009). To our knowledge, this is the first study showing the Raman spectra for *W. anomalus*. Four characteristics peaks were detected at 738 cm^{-1}, 967 cm^{-1}, 1322 cm^{-1} and 1399 cm^{-1}. Possible assignments for the detected bands are related to the C-S bond and C-N stretch and to protein and lipid bands. The recorded *W. anomalus* spectra has similar features to previously published *Candida albicans* spectra (Sayin et al., 2009). *B. bruxellensis* showed four characteristics peaks situated at 735 cm^{-1}, 920 cm^{-1}, 1319 cm^{-1} and 1472 cm^{-1} Raman shifts. Although the peaks for the spoilage yeasts were in similar regions, they were slightly shifted allowing easy discrimination. When comparing the *B. bruxellensis* result to the study conducted by S. B. Rodriguez et al., the detected spectrum had more distinctive Raman lines (Rodriguez et al., 2013). This could be related to the use of NIR excitation and lower excitation laser power, as the cells do not endure strong thermal damage. This shows how the use of thermally dried cells can be beneficial in detecting cell wall

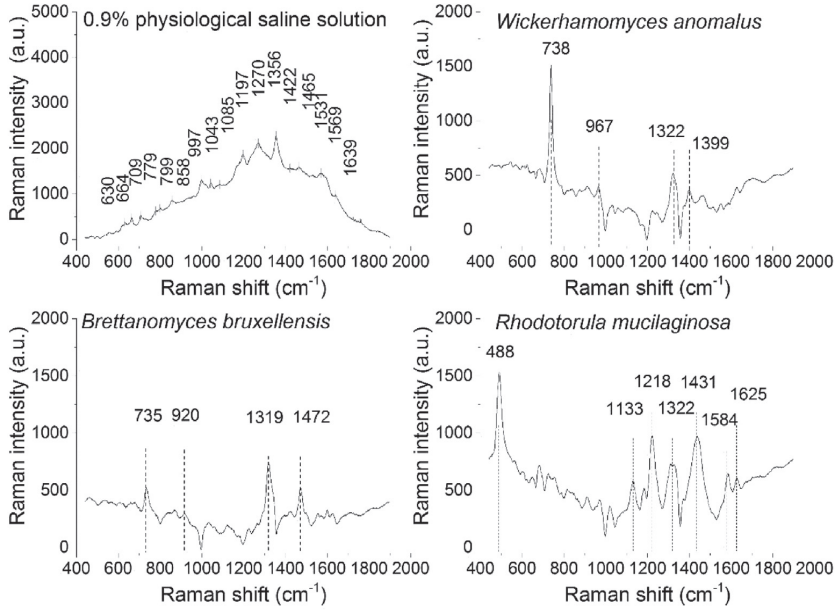

Fig. 6. a) SERS spectra of 0.9% physiological saline. SERS spectra of b) *W. anomalus*, c) *B. bruxellensis* and d) *R. mucilaginosa* detected on top of SERS substrate with AuSi NCs. The average SERS spectra were recorded in triplicate using total 15 s integration time. Origin Pro user defined baseline reduction was utilised to remove fluorescence background (shown for *W. anomalus* in Fig. 6).

Table 1
Raman band assignments (Sayin et al., 2009) for the spectra of *W. anomalus, B. bruxellensis and R. mucilaginosa* and a reference biomolecule listing for *R. mucilaginosa.*

Raman band	*W. anomalus*	*B. bruxellensis*	*R. mucilaginosa*	*Study by* M. Z. Pacia et al. (Pacia et al., 2015)
488			Polysaccharides	Outside detection range
735/738	Adenine from flavin, C–S, N-acetyl-D-glucosamine	Adenine from flavin, C–S, N-acetyl-D-glucosamine		
920		Glucose		
967	C-N stretch			
1133			Lipid	Haemoprotein, cell wall
1218			Amide III	Haemoprotein, cell wall
1319/1322	C-H bend protein	C-H bend protein	C-H bend protein	Lipid or haemoprotein, cell wall
1399	CH_2 bend (protein, lipid)			
1431			CH_2 bend (protein, lipid)	Lipid, cell wall
1472		CH_2 bend (protein, lipid)		
1584			N-H, C-H bend, C=C stretch	Lipid, cell wall
1625			Tyrosine, tryptophan	Haemoprotein, cell wall

features. The *B. bruxellensis* peaks appear to originate from sugars, proteins and lipids. The *R. mucilaginosa* Raman spectrum was previously studied using Raman microimaging (Pacia et al., 2015) (Rösch et al., 2003); and by SERS with active silver-coated glass fibre tips (Gessner et al., 2002). The detection method here revealed several Raman bands for *R. mucilaginosa*, originating from polysaccharides, lipids and haemoproteins. The features of the cell responsible for the detected peaks are listed next to the band assignments (Pacia et al., 2015). Contrary to studies conducted by R. Gessner et al., the characteristic peaks for carotenoids (Gessner et al., 2002) at Raman shifts of 1001 cm^{-1}, 1151 cm^{-1} and 1508 cm^{-1} are missing. The absence of these peaks can likely be attributed to the fact that the excitation light (785 nm) does not match the carotenoid absorption spectrum. Although this wavelength is preferable to non-pigmented yeasts due to reduced fluorescence, the carotenoid peaks are suppressed with NIR wavelengths as seen in the study by P. Rösch et al., in the case of *Micrococcus luteus* (Rösch et al., 2003). However, the spectrum detected here showed several characteristic peaks for *R. mucilaginosa* that can be used for yeast discrimination.

The developed SERS detection method makes discrimination of yeast cells of *W. anomalus*, *B. bruxellensis* and *R. mucilaginosa* very straightforward, as the detected Raman peaks of different yeasts are clearly shifted from each other. There is thus no need for chemometric calculations such as multivariate principal components analysis (PCA) (Guicheteau et al., 2010) or unsupervised hierarchical cluster analysis (HCA) (Meisel et al., 2014) to separate the samples using peak intensities of similar spectrums to distinguish yeasts from each other. In this study, yeast was cultivated on plates in rich culture medium and harvested at relatively high concentrations (10^7 cells/ml) into physiological saline. The method can be implemented for the detection of lower cell counts and discrimination of yeasts at the strain level, utilising improved data analysis and additional cell accumulation methods such as filtration (Lemma et al., 2015).

4. Conclusions

We recorded characteristic Raman spectra for yeast strains of *W. anomalus, B. bruxellensis and R. mucilaginosa* using a hybrid detection method with gold nanoparticles on top of a structured SERS substrate. Our study revealed that thermally dried yeast cells of different species could be clearly discriminated with near-infrared excitation without chemometric calculations. The analysis of different AuNPs showed that the effect of the buffer of the gold nanoparticle suspensions on the acquired spectra could overflow the spectra and hide the Raman lines of the yeast. Care must be taken to avoid buffers incompatible with the nanoparticles and yeast solutions when analysing yeast strains using Raman spectroscopy. Additionally, the PVP cover of the gold star-like nanoparticles substantially decreased particle Raman enhancement efficacy. The large spherical gold nanoparticles (150 nm) in citrate buffer and the ultrapure composite nanoparticles showed promising SERS enhancement capability for yeast detection. Bare AuSi composite nanoparticles were used to detect *W. anomalus, B. bruxellensis and R. mucilaginosa*, and distinctive spectra were recorded for all yeast species. The developed SERS detection method provides a simple and straightforward yeast discrimination tool for the food and beverage industry.

Acknowledgements

This project was funded by a VTT government grant through the SENSFOOD-project and by the Academy of Finland through an M-SPEC project (284907); it was also partially funded by projects 260321 and 290596. The authors are thankful for support from Infotech Oulu Graduate School. O. Bibikova acknowledges support from the International Graduate School in Molecular Medicine Ulm. This work was partially supported by the Government of Russian Federation (Grant 074-U01). Yu. Ryabchikov and A. V. Kabashin acknowledge support from LASERNANOCANCER (No. PC201420) and GRAVITY projects of the ITMO “Plan Cancer 2014–2019” of INSERM and the AMIDEX project (No ANR-11-IDEX-0001-02) funded by the French Government.

Appendix A. Supplementary data

Supplementary data related to this article can be found at http://dx.doi.org/10.1016/j.jfoodeng.2017.05.007.

References

Aksu, Z., Eren, A.T., 2005. Carotenoids production by the yeast Rhodotorula mucilaginosa: use of agricultural wastes as a carbon source. Process Biochem. 40 (9), 2985–2991. In: https://doi.org/10.1016/j.procbio.2005.01.011.

Alkilany, A.M., Murphy, C.J., 2010. Toxicity and cellular uptake of gold nanoparticles: what we have learned so far? J. Nanoparticle Res. 12 (7), 2313–2333. https://doi.org/10.1007/s11051-010-9911-8.

Amorim, M., Pereira, J.O., Gomes, D., Pereira, C.D., Pinheiro, H., Pintado, M., 2016. Nutritional ingredients from spent brewer's yeast obtained by hydrolysis and selective membrane filtration integrated in a pilot process. J. Food Eng. 185, 42–47. https://doi.org/10.1016/j.jfoodeng.2016.03.032.

Angelov, S.D., Koenen, S., Jakobi, J., Heissler, H.E., Alam, M., Schwabe, K., et al., 2016. Electrophoretic deposition of ligand-free platinum nanoparticles on neural electrodes affects their impedance in vitro and in vivo with no negative effect on reactive gliosis. J. Nanobiotechnology 14 (1), 3. https://doi.org/10.1186/s12951-015-0154-9.

Anker, J.N., Hall, W.P., Lyandres, O., Shah, N.C., Zhao, J., Van Duyne, R.P., 2008. Biosensing with plasmonic nanosensors. Nat. Mater. 7 (6), 442–453. https://doi.org/10.1038/nmat2162.

Bibikova, O., Popov, A., 2015. Optical properties of plasmon-resonant bare and silica-coated nanostars used for cell imaging. J. Biomed. Opt. 20(7) (76017). https://doi.org/doi:10.1117/1.JBO.20.7.076017.

Bibikova, O., Popov, A., Bykov, A., Fales, A., Yuan, H., Skovorodkin, I., et al., 2016. Plasmon-Resonant gold nanostars with variable size as contrast agents for imaging applications. IEEE J. Sel. Top. Quantum Electron. 22 (3), 13–20. https://doi.org/10.1109/JSTQE.2016.2526602.

Blandin, P., Maximova, K.A., Gongalsky, M.B., Sanchez-Royo, J.F., Chirvony, V.S., Sentis, M., et al., 2013. Femtosecond laser fragmentation from water-dispersed microcolloids: toward fast controllable growth of ultrapure Si-based nanomaterials for biological applications. J. Mater. Chem. B 1(19) (2489). https://doi.org/10.1039/c3tb20285b.

Chen, J., Shen, B., Qin, G., Hu, X., Qian, L., Wang, Z., et al., 2012. Fabrication of large-area, high-enhancement SERS substrates with tunable interparticle spacing and application in identifying microorganisms at the single cell level. J. Phys. Chem. C 116 (5), 3320–3328. https://doi.org/10.1021/jp210147c.

Chrimes, A.F., Khoshmanesh, K., Tang, S.-Y., Wood, B.R., Stoddart, P.R., Collins, S.S.E., et al., 2013. In situ SERS probing of nano-silver coated individual yeast cells. Biosens. Bioelectron. 49, 536–541. https://doi.org/10.1016/j.bios.2013.05.053.

Culha, M., Kahraman, M., Çam, D., Sayın, I., Keseroğlu, K., 2010. Rapid identification of bacteria and yeast using surface-enhanced Raman scattering. Surf. Interface Analysis 42 (6–7), 462–465. https://doi.org/10.1002/sia.3256.

Gessner, R., Rösch, P., Kiefer, W., Popp, J., 2002. Raman spectroscopy investigation of biological materials by use of etched and silver coated glass fiber tips. Biopolymers 67 (4–5), 327–330. https://doi.org/10.1002/bip.10090.

Greulich, C., Braun, D., Peetsch, A., Diendorf, J., Siebers, B., Epple, M., Köller, M., 2012. The toxic effect of silver ions and silver nanoparticles towards bacteria and human cells occurs in the same concentration range. RSC Adv. 2(17) (6981). https://doi.org/10.1039/c2ra20684f.

Guicheteau, J., Christesen, S., Emge, D., Tripathi, A., 2010. Bacterial mixture identification using Raman and surface-enhanced Raman chemical imaging. J. Raman Spectrosc. 41 (12), 1632–1637. https://doi.org/10.1002/jrs.2601.

Hayashi, N., Arai, R., Tada, S., Taguchi, H., Ogawa, Y., 2007. Detection and identification of Brettanomyces/Dekkera sp. yeasts with a loop-mediated isothermal amplification method. Food Microbiol. 24 (7), 778–785. https://doi.org/10.1016/j.fm.2007.01.007.

Hebié, S., Holade, Y., Maximova, K., Sentis, M., Delaporte, P., Kokoh, K.B., et al., 2015. Adv. Electrocatalysts Basis Bare Au Nanomater. Biofuel Cell Appl. 5 (11), 6489–6496. https://doi.org/10.1021/acscatal.5b01478.

Kabashin, A.V., Meunier, M., 2003. Synthesis of colloidal nanoparticles during femtosecond laser ablation of gold in water. J. Appl. Phys. 94 (12). https://doi.org/. http://dx.doi.org/10.1063/1.1626793.

Laitila, A., Sarlin, T., Raulio, M., Wilhelmson, A., Kotaviita, E., Huttunen, T., Juvonen, R., 2011. Yeasts in malting, with special emphasis on Wickerhamomyces anomalus (synonym Pichia anomala). Antonie Leeuwenhoek 99 (1), 75–84. https://doi.org/10.1007/s10482-010-9511-8.

Lemma, S.M., Esposito, A., Mason, M., Brusetti, L., Cesco, S., Scampicchio, M., 2015. Removal of bacteria and yeast in water and beer by nylon nanofibrous membranes. J. Food Eng. 157, 1–6. https://doi.org/10.1016/j.jfoodeng.2015.02.005.

Li, M., Cushing, S.K., Zhang, J., Suri, S., Evans, R., Petros, W.P., et al., 2013. Three-dimensional hierarchical plasmonic nano-architecture enhanced surface-enhanced raman scattering immunosensor for cancer biomarker detection in blood plasma. ACS Nano 7 (6), 4967–4976. https://doi.org/https://doi.org/10.1021/nn4018284.

Loureiro, V., 2000. Spoilage yeasts in foods and beverages: characterisation and ecology for improved diagnosis and control. Food Res. Int. 33 (3), 247–256. https://doi.org/10.1016/S0963-9969(00)00044-2.

Loureiro, V., Malfeito-Ferreira, M., 2003. Spoilage yeasts in the wine industry. Int. J. Food Microbiol. 86 (1), 23–50. https://doi.org/10.1016/S0168-1605(03)00246-0.

Loureiro, V., Querol, A., 1999. The prevalence and control of spoilage yeasts in foods and beverages. Trends Food Sci. Technol. 10 (11), 356–365. https://doi.org/10.1016/S0924-2244(00)00021-2.

Martin, E., Bongiorno, G., Giovati, L., Montagna, M., Crotti, E., Damiani, C., et al., 2016. Isolation of a Wickerhamomyces anomalus yeast strain from the sandfly Phlebotomus perniciosus, displaying the killer phenotype. Med. Veterinary Entomology 30 (1), 101–106. https://doi.org/10.1111/mve.12149.

Maximova, K., Aristov, A., Sentis, M., Kabashin, A., 2015. Size-controllable synthesis of bare gold nanoparticles by femtosecond laser fragmentation in water. Nanotechnology 26(6) (65601). https://doi.org/10.1088/0957-4484/26/6/065601.

Meisel, S., Stöckel, S., Rösch, P., Popp, J., April 2014. Identification of meat-associated pathogens via Raman microspectroscopy. Food Microbiology 38, 36–43. https://doi.org/. http://dx.doi.org/10.1016/j.fm.2013.08.007.

Notingher, I., Verrier, S., Romanska, H., Bishop, A.E., Polak, J.M., Hench, L.L., 2002. *In situ* characterisation of living cells by raman spectroscopy. Spectroscopy 16 (2), 43–51. https://doi.org/10.1155/2002/408381.

Oo, S.Z., Chen, R.Y., Siitonen, S., Kontturi, V., Eustace, D.A., Tuominen, J., et al., 2013. Disposable plasmonic plastic SERS sensor. Opt. Express 21 (15), 18484–18491. https://doi.org/10.1364/OE.21.018484.

Pacia, M.Z., Turnau, K., Baranska, M., Kaczor, A., Huang, Y.S., Karashima, T., et al., 2015. Interplay between carotenoids, hemoproteins and the "life band" origin studied in live Rhodotorula mucilaginosa cells by means of Raman microimaging. Analyst 140 (6), 1809–1813. https://doi.org/10.1039/C4AN01787K.

Pitt, J.I., Hocking, A.D., 2009. Methods for isolation, enumeration and identification. In: Fungi and Food Spoilage. Springer US, Boston, MA, pp. 19–52. https://doi.org/10.1007/978-0-387-92207-2_4.

Rioux, D., Laferriere, M., Douplik, A., Shah, D., Lilge, L., Kabashin, A.V., Meunier, M.M., 2009. Silicon nanoparticles produced by femtosecond laser ablation in water as novel contamination-free photosensitizers. J. Biomed. Opt. 14(2) (21010). https://doi.org/10.1117/1.3086608.

Rodriguez, S.B., Thornton, M.A., Thornton, R.J., 2013. Raman spectroscopy and chemometrics for identification and strain discrimination of the wine spoilage yeasts Saccharomyces cerevisiae, Zygosaccharomyces bailii, and Brettanomyces bruxellensis. Appl. Environ. Microbiol. 79 (20), 6264–6270. https://doi.org/10.1128/AEM.01886-13.

Ryabchikov, Y.V., Popov, A.A., Sentis, M., Timoshenko, V.Y., Kabashin, A.V., 2016. Structural properties of gold-silicon nanohybrids formed by femtosecond laser ablation in water at different fluences. In: Kabashin, A.V., Geohegan, D.B., Dubowski, J.J. (Eds.), International Society for Optics and Photonics, p. 97370F. https://doi.org/10.1117/12.2217777.

Rösch, P., Schmitt, M., Kiefer, W., Popp, J., 2003. The identification of microorganisms by micro-Raman spectroscopy. J. Mol. Struct. 661, 363–369. https://doi.org/10.1016/j.molstruc.2003.06.004.

Sayin, I., Kahraman, M., Sahin, F., Yurdakul, D., Culha, M., 2009. Characterization of yeast species using surface-enhanced raman scattering. Appl. Spectrosc. 63 (11), 1276–1282.

Schwartzberg, A.M., Grant, C.D., Wolcott, A., Talley, C.E., Thomas, R. Huser, And, R.B., Zhang, J.Z., 2004. Unique Gold Nanoparticle Aggregates as a Highly Act. Surface-Enhanced Raman Scatt. Substrate 108 (50), 19191–19197. https://doi.org/https://doi.org/10.1021/jp048430p.

Shukla, R., Bansal, V., Chaudhary, M., Basu, A., And, R.R.B., Sastry, M., 2005. Biocompatibility of gold nanoparticles and their endocytotic fate inside the cellular compartment: a microscopic overview. Langmuir 21 (23), 10644–10654. https://doi.org/https://doi.org/10.1021/la0513712.

Stratford, M., 2006. Food and Beverage Spoilage Yeasts. Yeasts in Food and Beverages. Springer Berlin Heidelberg.

Sujith, A., Itoh, T., Abe, H., Anas, A.A., Yoshida, K., Biju, V., Ishikawa, M., 2008. Surface enhanced Raman scattering analyses of individual silver nanoaggregates on living single yeast cell wall. Appl. Phys. Lett. 92(10) (103901). https://doi.org/10.1063/1.2891086.

Sujith, A., Itoh, T., Abe, H., Yoshida, K., Kiran, M.S., Biju, V., Ishikawa, M., 2009. Imaging the cell wall of living single yeast cells using surface-enhanced Raman spectroscopy. Anal. Bioanal. Chem. 394 (7), 1803–1809. https://doi.org/10.1007/s00216-009-2883-9.

Syamala, K.M., Abe, H., Fujita, Y., Tomimoto, K., Biju, V., Ishikawa, M., et al., 2012. Inhibition assay of yeast cell walls by plasmon resonance rayleigh scattering and surface-enhanced raman scattering imaging. Langmuir 28 (24), 8952–8958. https://doi.org/https://doi.org/10.1021/la3004245.

Uusitalo, S., Kögler, M., Välimaa, A.-L., Popov, A., Ryabchikov, Y., Kontturi, V., et al., 2016. Detection of Listeria innocua on roll-to-roll produced SERS substrates with gold nanoparticles. RSC Adv. 6 (67), 62981–62989. https://doi.org/10.1039/C6RA08313G.

Yuan, H., Khoury, C.G., Hwang, H., Wilson, C.M., Grant, G.A., Vo-Dinh, T., 2012. Gold nanostars: surfactant-free synthesis, 3D modelling, and two-photon photoluminescence imaging. Nanotechnology 23(7) (75102). https://doi.org/10.1088/0957-4484/23/7/075102.

Series title and number

VTT Science 165

Title	**Detection of small molecules and microbial cells by surface-enhanced Raman spectroscopy using roll-to-roll produced substrates**
Author(s)	Sanna Uusitalo
Abstract	The objective of this thesis was to study patterned substrates and gold nanoparticles as surface-enhanced Raman spectroscopy tools for label-free detection of biological analytes with high sensitivity and easy sample handling. There are many fields, such as environmental monitoring, medical analysis, food safety and national security, which currently lack a rapid analysis tool for bioanalyte recognition. This thesis concentrated on applying disposable single-use surface-enhanced Raman scattering (SERS) substrates for the detection of microbial cells and small molecules. The substrates were patterned with roll-to-roll (R2R) UV replication. R2R fabrication of the SERS substrates enables industrial scale manufacturing of large sensor areas in a repeatable manner. SERS detection is based on the recording of inelastically scattered photons. The scattering is enhanced locally by a resonance effect of the surface plasmons of noble metal surfaces. SERS can achieve sensitive detection of low analyte volumes, even in the range of a few particles. In addition, it has the advantage of label-free detection due to the fingerprint spectrum, in which the signal reveals information concerning the composition of the molecules forming the analyte. In this study the SERS substrates were combined with metal nanoparticles and the samples were concentrated with hydrophobic materials. The sample intake to the chip was developed for the detection of rhodamine 6G inside an optofluidic SERS chip. The behaviour of small molecules in the flow was studied through a polymer lid with microfluidic circuits attached to SERS substrates. The second topic concentrated on detection of Listeria innocua ATCC 33090 bacterial cells with SERS substrates and gold nanoparticles. The limit of detection (LOD) was found to be approx. 2·104 CFU/ml. In the third topic, the effect of the shape and composition of the nanoparticles on the SERS detection of yeast was studied with three yeast strains originating from the beverage industry: Wickerhamomyces anomalus, Brettanomyces bruxellensis and Rhodotorula mucilaginous. A specific Raman spectrum was detected for all of the strains.
ISBN, ISSN, URN	ISBN 978-951-38-8577-9 (Soft back ed.) ISBN 978-951-38-8576-2 (URL: http://www.vttresearch.com/impact/publications) ISSN-L 2242-119X ISSN 2242-119X (Print) ISSN 2242-1203 (Online) http://urn.fi/URN:ISBN:978-951-38-8576-2
Date	November 2017
Language	English, Finnish abstract
Pages	88 p. + app. 42 p.
Name of the project	
Commissioned by	
Keywords	SERS substrate, nanoimprint lithography, disposability, microbial cells, nanoparticles
Publisher	VTT Technical Research Centre of Finland Ltd P.O. Box 1000, FI-02044 VTT, Finland, Tel. 020 722 111

Julkaisun sarja ja numero

VTT Science 165

Nimeke	**Rullalta rullalle valmistettujen SERS-pintojen käyttö pienmolekyylien ja mikrobisolujen määritykseen**
Tekijä(t)	Sanna Uusitalo
Tiivistelmä	Tämän väitöksen tavoitteena on tutkia kuvioitujen substraattien ja kulta-nanopartikkeleiden käyttöä signaalin vahvistuksessa pinta-aktivoidulla Raman -spektroskopialla. Tarkoituksena on kehittää edullinen ja helppokäyttöinen leimaton mittausmenetelmä, jota voitaisiin hyödyntää ympäristön valvonnassa, lääketieteessä, elintarviketurvallisuudessa sekä turvallisuusalalla. Tutkimuksessa keskitytään kertakäyttöisten polymeeripohjaisten sensoripintojen käyttöön pienmolekyylien ja mikrobien havainnoinnissa. Kertakäyttöiset sensoripinnat valmistetaan rullalta rullalle -laitteistolla siirtämällä muotin kuviot polymeerin pinnalle UV-kovetettavalle lakalle. Tämä kuviointitekniikka soveltuu suurien sensorimäärien edulliseen tuottamiseen. Tutkimuksessa käytetty mittausmenetelmä pohjautuu valon epäelastisen Raman -sironnan mittaukseen. Sironta vahvistetaan jalometallien paikallisilla pintaplasmoneilla, jolloin voidaan saavuttaa jopa muutamien partikkeleiden mittausherkkyys. Tutkimuksessa kuvioitu SERS -pinta yhdistettiin metallisten nanopartikkeleiden käyttöön ja näytteen konsentrointiin hydrofobisten materiaalien avulla. Yhdistelmällä mitattiin biomolekyylien ja mikrobien spektrejä näytteistä, joissa analyyttien määrä on alhainen. Koska Raman -spektri kuvastaa näytteen molekyylisidoksia, SERS:llä mitattavat kohteet voidaan tunnistaa leimattomasti. Tässä tutkimuksessa kehitettiin näytteen tuontia SERS -alustalle, bakteerisolujen mittausta sekä hiivasolujen tunnistusta. Työn ensimmäinen tutkimuskohde keskittyy SERS -alustan käytön kehittämiseen integroimalla mikronestekanava alustan pinnalle. Toinen tutkimuskohde keskittyy Listeria innocua ATCC 33090 -bakteerisolujen mittaamiseen SERS:llä. Mittauksen määritysmenetelmän osoitusrajaksi (LOD) tutkimuksessa saatiin 104 pmy/ml. SERS -alustaan yhdistettyjen kulta -nanopartikkeleiden muodon, koon sekä rakenteen vaikutusta hiivasoluihin tutkittiin mittaamalla kolmea juomateollisuutta kiinnostavaa kantaa: Wickerhamomyces anomalus:sta, Brettanomyces bruxellensis:stä ja Rhodotorula mucilaginosa:a. Tutkimuksessa W. anomalus, B. bruxellensis ja R. mucilaginosa -kannoille mitattiin spektrit, joiden avulla hiivat on mahdollista erotella toisistaan.
ISBN, ISSN, URN	ISBN 978-951-38-8577-9 (nid.) ISBN 978-951-38-8576-2 (URL: http://www.vtt.fi/julkaisut) ISSN-L 2242-119X ISSN 2242-119X (Painettu) ISSN 2242-1203 (Verkkojulkaisu) http://urn.fi/URN:ISBN:978-951-38-8576-2
Julkaisuaika	Marraskuu 2017
Kieli	Englanti, suomenkielinen tiivistelmä
Sivumäärä	88 s. + liitt. 42 s.
Projektin nimi	
Rahoittajat	
Avainsanat	SERS-mittauspinnat, nanolitografia, kertakäyttöisyys, mikrobi, nanopartikkeli
Julkaisija	Teknologian tutkimuskeskus VTT Oy PL 1000, 02044 VTT, puh. 020 722 111

Detection of small molecules and microbial cells by surface-enhanced Raman spectroscopy using roll-to-roll produced substrates

In this thesis disposable single-use surface-enhanced Raman scattering (SERS) substrates and gold nanoparticles were used for label-free detection of biological analytes and small molecules. The SERS substrates were patterned with roll-to-roll (R2R) UV replication, which enables industrial scale manufacturing with large sensor volumes. These SERS sensors are based on the recording of inelastically scattered Raman photons with enhanced efficiency. The signal is enhanced by a local resonance effect of the surface plasmons of noble metal surfaces. SERS can achieve sensitive detection of low analyte volumes and it has the advantage of label-free detection.

The SERS substrates of the study were combined with metal nanoparticles and the samples were concentrated with hydrophobic materials. Rhodamine 6G samples were detected inside an optofluidic SERS chip. The Raman spectrum of Listeria innocua ATCC 33090 bacterial cells were recorded inside a hydrophobic sample chamber with the limit of detection (LOD) of approx. 2·104 CFU/ml. Additionally the effect of the shape and composition of the nanoparticles on the SERS detection of yeast was studied with three yeast strains: Wickerhamomyces anomalus, Brettanomyces bruxellensis and Rhodotorula mucilaginous.

ISBN 978-951-38-8577-9 (Soft back ed.)
ISBN 978-951-38-8576-2 (URL: http://www.vttresearch.com/impact/publications)
ISSN-L 2242-119X
ISSN 2242-119X (Print)
ISSN 2242-1203 (Online)
http://urn.fi/URN:ISBN:978-951-38-8576-2